CHARACTERIZATION AND INTERWELL CONNECTIVITY EVALUATION OF GREEN RIVER RESERVOIRS, WELLS DRAW STUDY AREA, UINTA BASIN, UTAH

A Thesis

by

JOSEPH UCHECHUKWU ABIAZIE

Submitted to the Office of Graduate Studies of
Texas A&M University
in partial fulfillment of the requirements for the degree of

MASTER OF SCIENCE

May 2008

Major Subject: Petroleum Engineering

CHARACTERIZATION AND INTERWELL CONNECTIVITY EVALUATION OF GREEN RIVER RESERVOIRS, WELLS DRAW STUDY AREA, UINTA BASIN, UTAH

A Thesis

by

JOSEPH UCHECHUKWU ABIAZIE

Submitted to the Office of Graduate Studies of
Texas A&M University
in partial fulfillment of the requirements for the degree of

MASTER OF SCIENCE

Approved by:

Chair of Committee,	Duane A. McVay
Committee Members,	Walter B. Ayers
	Wayne M. Ahr
Head of Department,	Stephen A. Holditch

May 2008

Major Subject: Petroleum Engineering

ABSTRACT

Characterization and Interwell Connectivity Evaluation of Green River Reservoirs, Wells Draw Study Area, Uinta Basin, Utah. (May 2008)

Joseph Uchechukwu Abiazie, B. Tech.,

Federal University of Technology; Owerri, Nigeria

Chair of Advisory Committee: Dr. Duane A. McVay

Recent efforts to optimize oil recovery from Green River reservoirs, Uinta Basin, have stimulated the need for better understanding of the reservoir connectivity at the scale of the operational unit. This study focuses on Green River reservoirs in the Wells Draw study area where oil production response to implemented waterflood is poor and a better understanding of the reservoir connectivity is required to enhance future secondary oil recovery. Correlating the sand bodies between well locations in the area remains difficult at 40-acre well spacing. Thus, interwell connectivity of the reservoirs is uncertain. Understanding the reservoir connectivity in the Wells Draw study area requires integration of all static and dynamic data for generation of probabilistic models of the reservoir at the interwell locations.

The objective of this study is two-fold. The first objective was to determine reservoir connectivity at the interwell scale in the Wells Draw study area. To achieve this goal, I used well log and perforation data in the Wells Draw study area to produce

probabilistic models of net-porosity for four producing intervals: (1) Castle Peak, (2) Lower Douglas Creek, (3) Upper Douglas Creek, and (4) Garden Gulch.

The second objective was to find readily applicable methods for determining interwell connectivity. To achieve this goal, I used sandstone net thickness and perforation data to evaluate interwell connectivity in the Wells Draw study area. This evaluation was done to: (1) assess and visualize connectivity, (2) provide an assessment of connectivity for validating / calibrating percolation and capacitance based methods, and (3) determine flow barriers for simulation.

The probabilistic models encompass the four producing intervals with a gross thickness of 1,900 ft and enable simulation assessments of different development strategies for optimization of oil recovery in the Wells Draw study area. The method developed for determining interwell connectivity in Wells Draw study area is reliable and suited to the four producing intervals. Also, this study shows that the percolation based method is reliable for determining interwell connectivity in the four producing intervals.

DEDICATION

Firstly, I dedicate this work to him who began a good work in me and is faithful to its completion—Christ Jesus.

I dedicate it to my parents for their guidance and my wife, Doris Ebere, for her trust, patience and love. I also dedicate this work to the many people who have provided me encouragement or advice at one point or the other in my life.

ACKNOWLEDGEMENTS

I would like to thank my committee chair, Dr. Duane McVay and my committee members, Dr. Walter Ayers and Dr. Wayne Ahr for their guidance and support throughout the course of this research. I also remember Dr. Jerry Jensen who also participated in this research at one time.

I would also like to thank my research colleagues, Jianwei Wang, Weiqiang Li and Danial Kaviani, and friends, Nduonyi Moses and Syihab Zuher, to mention a few for their constructive discussions, time and effort during the course of this research.

Thanks also go to the department faculty and staff for making my time at Texas A&M University a great experience. I also want to extend my gratitude to the Newfield Exploration Company, which provided the data for this study.

Finally, thanks to my parents for their encouragement and to my wife, Doris Ebere, for her patience and love.

TABLE OF CONTENTS

CHAPTER Page

Page

LIST OF FIGURES

FIGURE Page

FIGURE Page

FIGURE Page

LIST OF TABLES

CHAPTER I

INTRODUCTION

Overview

The Green River reservoirs, Uinta Basin has been the focus of many reservoir characterization studies aimed at delineating the reservoir connectivity to optimize enhanced oil recovery efforts.[1-17] These studies show the difficulty of transferring the reservoir connectivity characteristics even at the scale of an operational unit. Thus, they suggest the need to address reservoir connectivity on an operational-unit basis to enhance secondary oil recovery.

This study focuses on Green River reservoirs in the Wells Draw study area where oil production response to implemented waterflood is poor and a better understanding of the reservoir connectivity is required to enhance future secondary oil recovery.

Reservoir Development History

Wells Draw study area is in Monument Butte area, Uinta Basin (**Fig. 1**).[18] It lies in a 6-section area west of the Monument Butte Unit—a focus of previous reservoir characterization studies (**Fig. 2**).[1-3] The northern half of the Wells Draw study area is in sections 32 to 34 of township 8S and range 16 E, while its southern half is in sections 3 to 5 of township 9S and range 16 E. The Wells Draw study area covers 1362 acres (5.5 sq. km) mainly in Wells Draw Unit and parts of the South Wells Draw and Travis units. Presently, there are 18 oil wells and 17 water injector wells spaced at 40 acres (**Fig. 3**).

This thesis follows the style of *SPE Reservoir Evaluation & Engineering Journal*.

Reservoirs in the Castle Peak, Lower and Upper Douglas Creek, and Garden Gulch intervals have been perforated between 4412 ft and 6277 ft (1345 m and 1913 m) measured depths. The main pay consists of the D1 and C sands of the Upper Douglas Creek interval. The oil has 33^{o}API gravity. Primary production commenced on June 1, 1982 and lasted until January 1, 1995 when water injection was introduced (**Fig. 4**). Monthly production on August 1, 1982, from the four producing intervals was 5144 STB of oil with solution gas-oil ratio (GOR) of 625 SCF/STB and 178 STB of water. As of January 1, 1995, oil production had dropped to 3166 STB/mon with a GOR of 7524 SCF/STB and 384 STB/mon of water

Problem Statement

Secondary oil production in the Wells Draw study area responded poorly to implemented waterflood (**Fig. 4**). Thus, better understanding of the reservoir connectivity in the Wells Draw study area is needed to improve future waterflood performance. Correlating the sand bodies between well locations remains difficult at 40-acre well spacing. Thus, interwell connectivity of the reservoirs is uncertain. Understanding the reservoir connectivity in the Wells Draw study area requires integration of all static and dynamic data for generation of probabilistic models of the reservoir at the interwell locations.

Objectives

The objective of this study is two-fold. The first objective was to determine reservoir connectivity at the interwell scale in the Wells Draw study area. To achieve this goal, I used well log and perforation data in the Wells Draw study area to produce probabilistic models of net-porosity for four producing intervals: (1) Castle Peak, (2) Lower Douglas Creek, (3) Upper Douglas Creek, and (4) Garden Gulch. The probabilistic models will enable reservoir simulation assessments of different development strategies for optimization of oil and gas recovery in the Wells Draw study area.

The second objective was to find readily applicable methods for determining interwell connectivity. To achieve this goal, I used sandstone net thickness and perforation data to evaluate interwell connectivity in the Wells Draw study area. This evaluation was done to: (1) assess and visualize connectivity, (2) provide an assessment of connectivity for validating / calibrating percolation and capacitance based methods, and (3) determine flow barriers for simulation. The models developed in this study encompass the four producing intervals with a gross thickness of approximately 1,900 ft (**Fig. 5**).

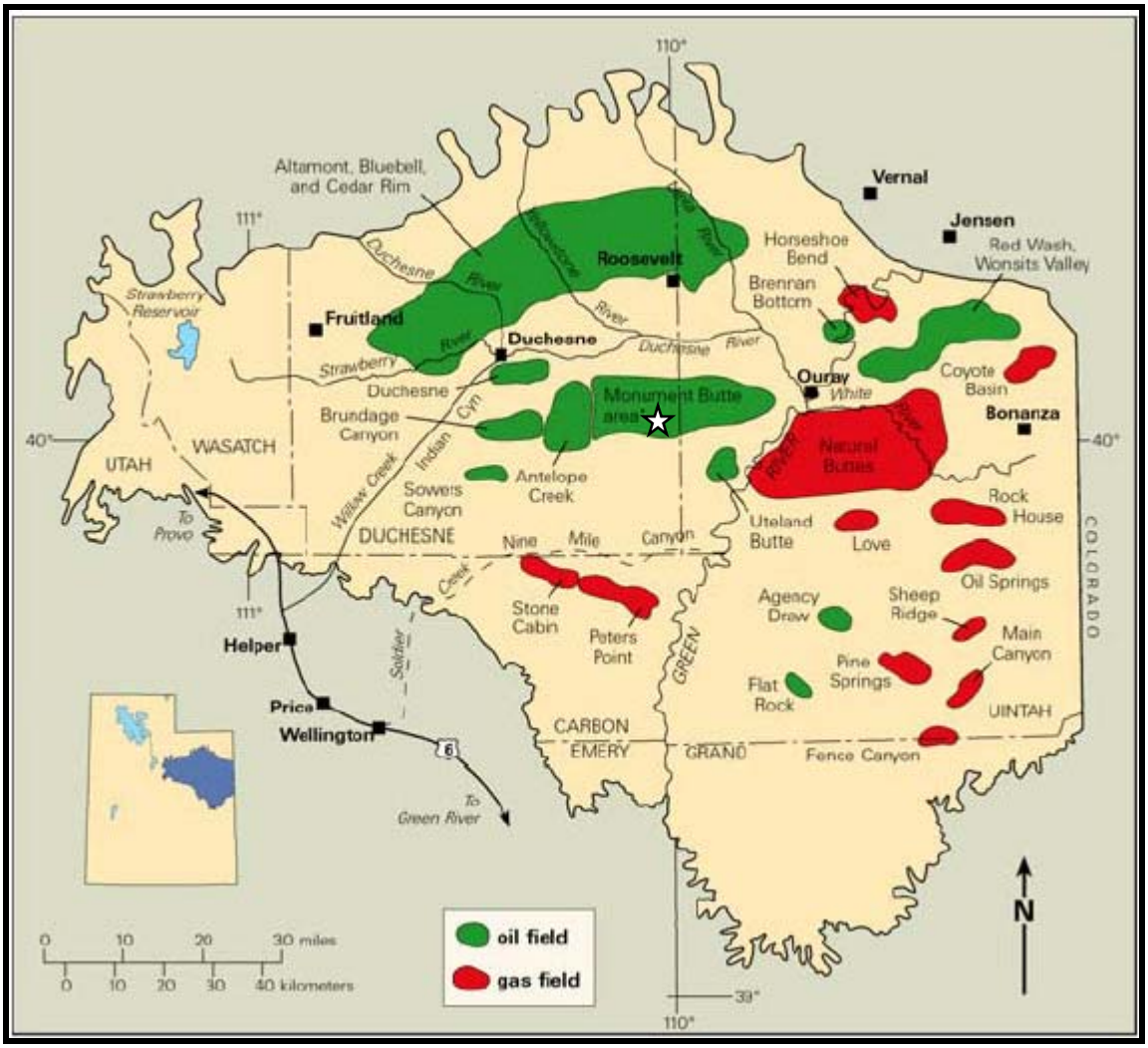

Fig. 1—Location of the Wells Draw study area in Monument Butte area, Uinta Basin (star symbol).[18]

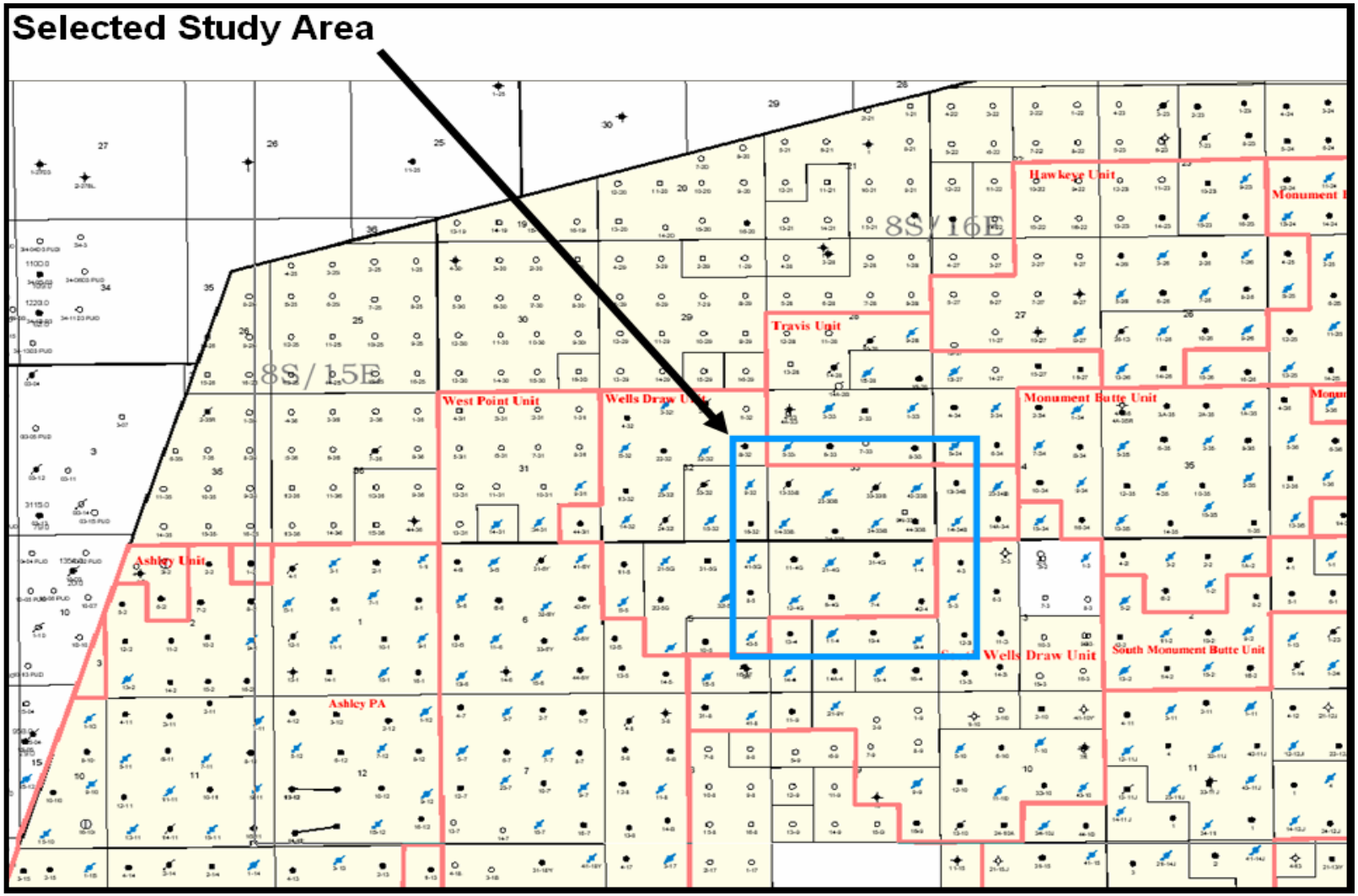

Fig. 2—Wells Draw study area is located west of the Monument Butte Unit. It covers mainly the Wells Draw Unit and parts of the Travis and South Wells Draw units.

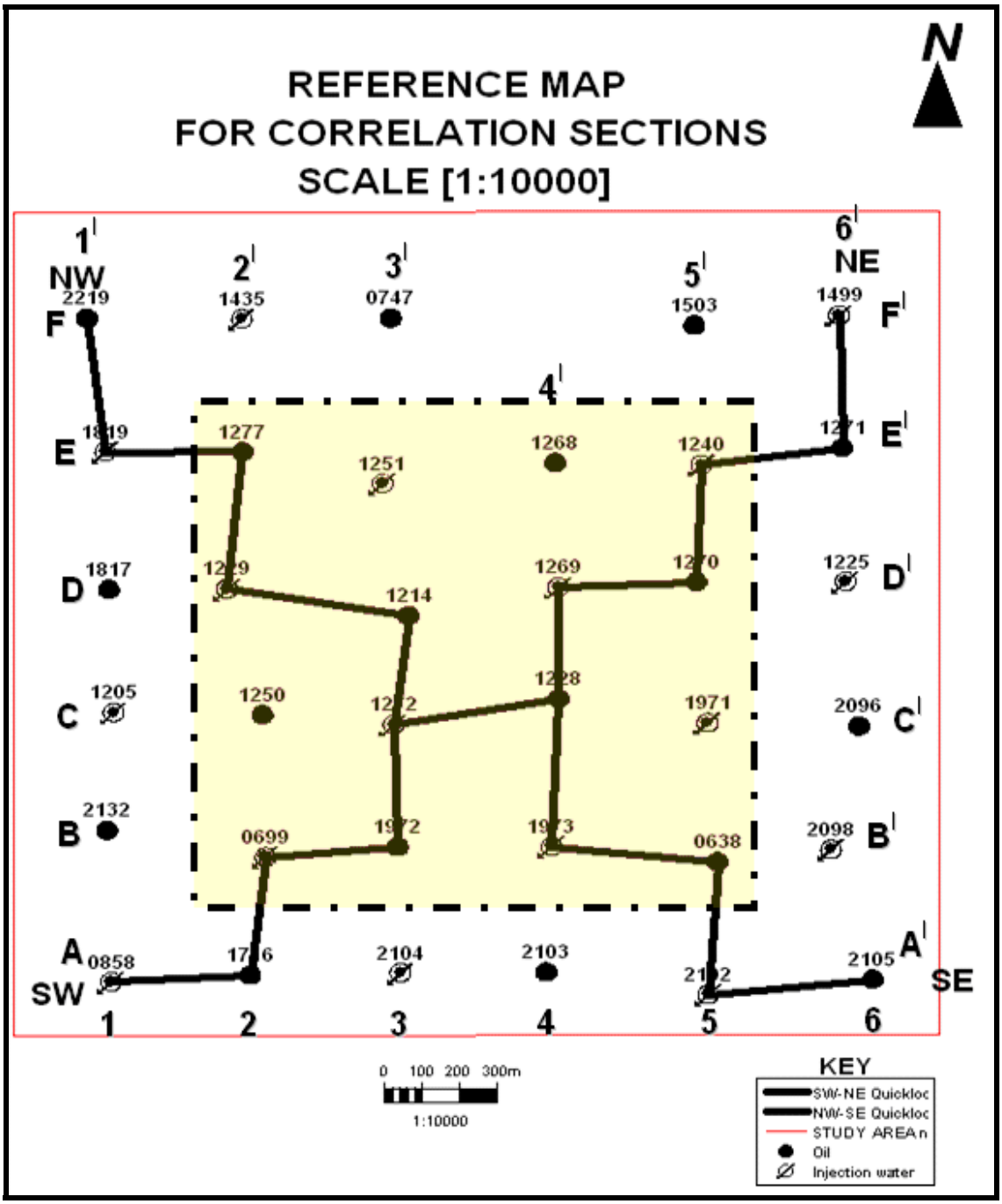

Fig. 3—Details of the Wells Draw study area. Well density is 40 acres. Reference axes of correlation sections are shown.

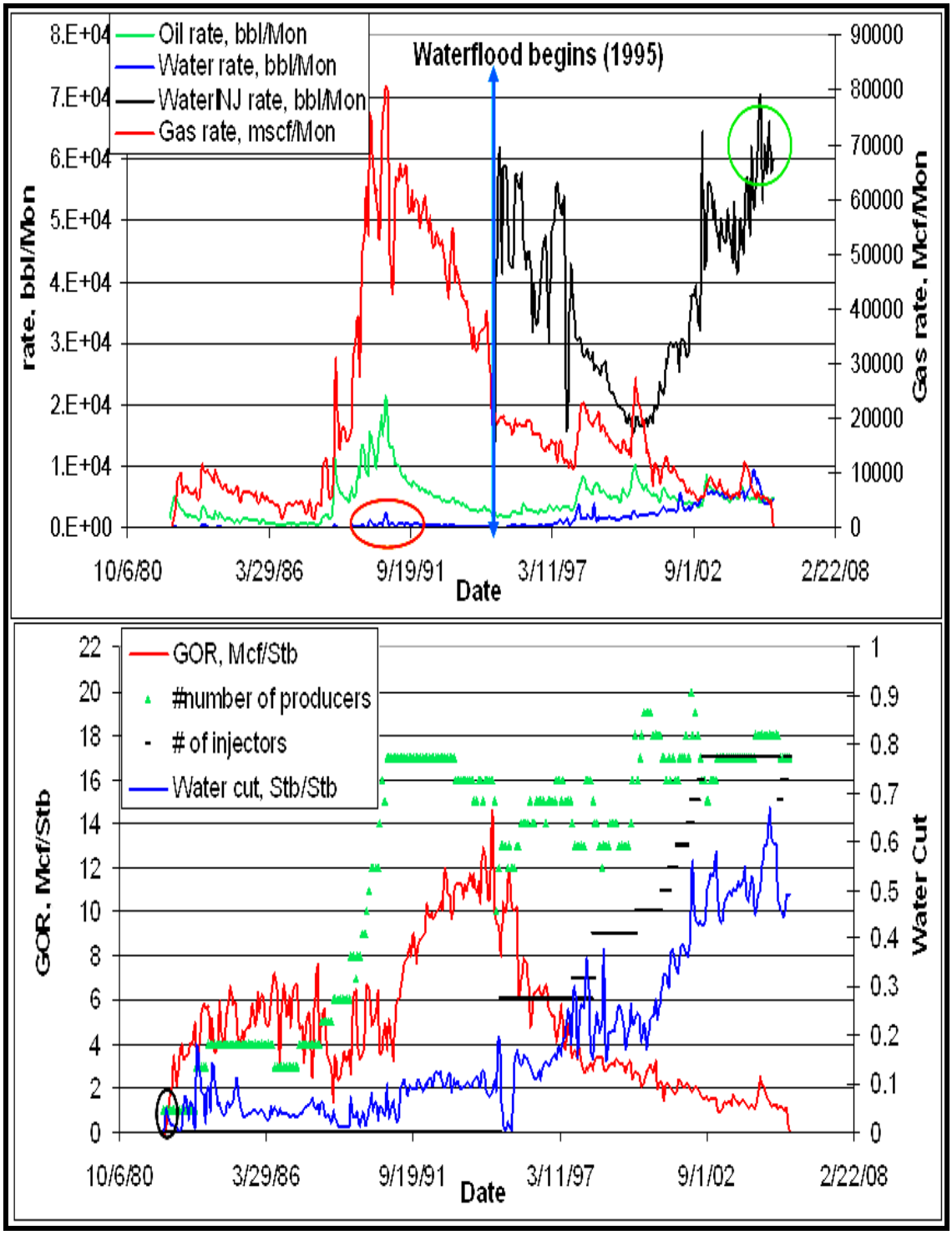

Fig. 4—Production and injection data from the 35 wells studied.

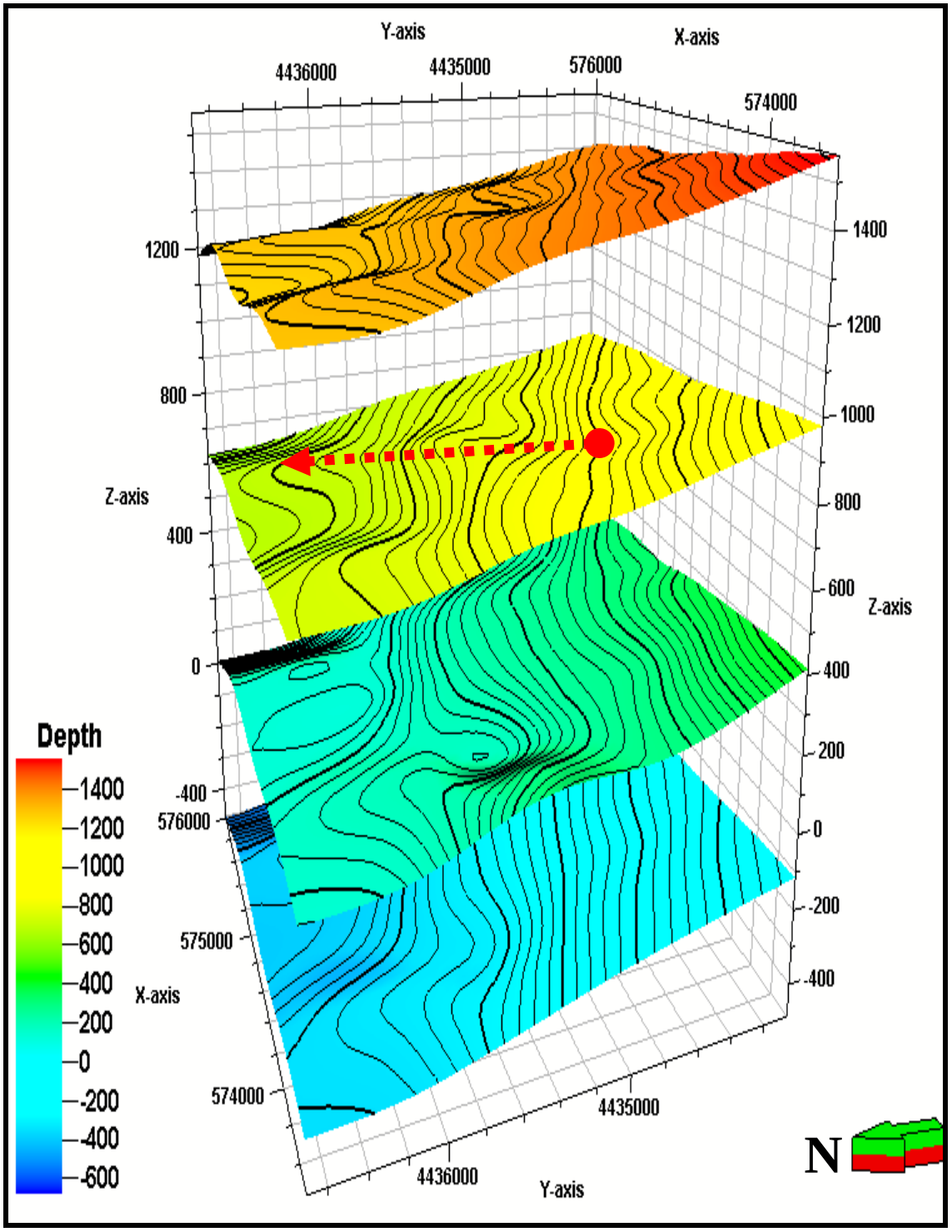

Fig. 5—3D framework shows four major structural horizons. The gross thickness is about 1,900 ft. Dashed lined arrow shows southwest-northeast dip direction seen on all four major horizons. X and Y axes are in meters. Z axis is in feet.

Research Background

The goal of reservoir characterization is to create predictive models of the distribution and flow properties of reservoir rocks in oil and gas fields.[19-21] One of the goals of reservoir characterization is to determine continuity or connectivity of reservoirs, usually from subsurface data acquired from oil and gas fields, often by indirect methods of measurement.[22]

Reservoir connectivity is a key subsurface uncertainty in the evaluation and development of many oil fields. It is a complex uncertainty that is a product of the interaction of several variables that Ainsworth[23] grouped into three categories: (1) primary or depositional connectivity, (2) secondary or structural connectivity, and (3) tertiary or dynamic connectivity. **Fig. 6** shows a summary chart of the variables that make up each category of reservoir connectivity. Several authors have proposed different methods for analyzing reservoir connectivity.[24-28] However, reservoir connectivity is by nature a complex, 3D problem.[29]

3D geostatistical characterization techniques [30-35] have an advantage over other methods for predicting reservoir connectivity. They enable the integration of multidisciplinary data at different scales for the generation of probabilistic 3D models of reservoir connectivity that are consistent with all available data. In addition, geostatistical characterization techniques allow for uncertainty in reservoir connectivity to be incorporated into reservoir simulation assessments of different development strategies for optimization of oil and gas recovery (**Fig. 7**).[32,36-39] For the above reasons, 3D geostatistical characterization techniques were applied in this research to generate

probabilistic 3D models that reflect the uncertainty in reservoir connectivity at the interwell scale. Since geostatistical characterization is never an end goal on its own, the characterization procedures designed for this research are tailored to the particular reservoir engineering question to be addressed.

The probabilistic 3D models made in this study represent different scenarios of reservoir connectivity at the interwell scale that are all equally possible for the same data set and connectivity constraints in the Wells Draw study area. In other words, the models represent equiprobable images or realizations of the true reservoir away from well locations where it is partially known. It is often not feasible to performance full scale simulation assessments on all the realizations due to technical and time constraint. A more practical approach is to arrange the realizations in an order that reflects the relative position of each realization with respect to a selected measure or index. This process is known as ranking.[40] The idea of ranking a suite of geological realizations is to exploit a fit-for-purpose measure for reliable selection of the low-side, expected, and high-side realizations.[40] In other words, ranking realizations allows bounding of the uncertainty without performing full scale simulation assessments for all the realizations. Several ranking parameters are available and are broadly classified as static or dynamic ranking.[41] Extensive investigations show that no ranking parameter is unique or perfect.[40-43] In line with the above, a static ranking measure was used to select the models that represent the bounding cases of uncertainty in reservoir connectivity. The models thus selected were recommended for full scale simulation assessments.

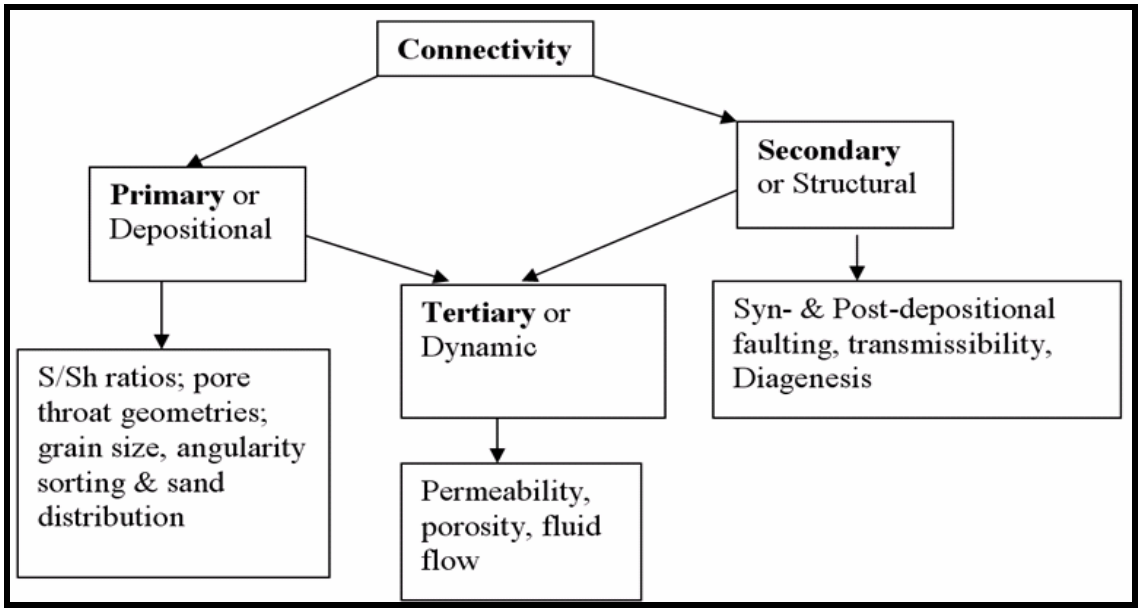

Fig. 6—Summary chart of the three categories of reservoir connectivity variables and their relationship as classified by Ainsworth.[23]

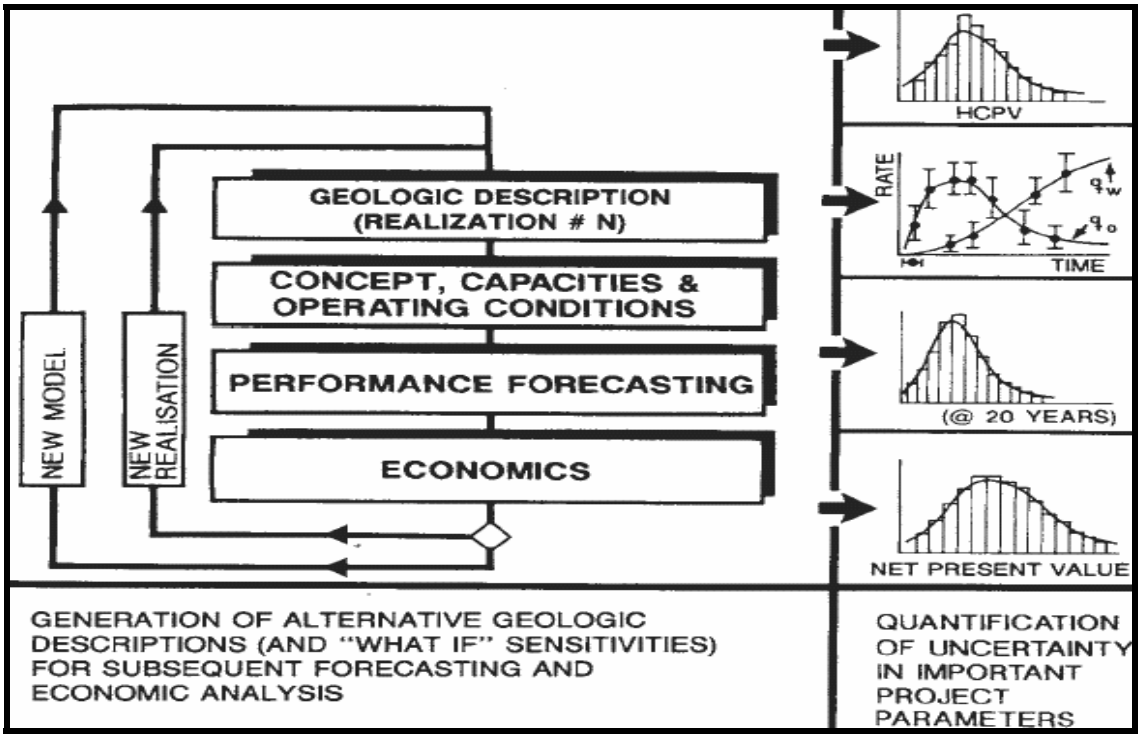

Fig. 7—Process of incorporating the uncertainty in reservoir connectivity into simulation assessments.[32]

Database

Several data types were available for characterization of the sandstone reservoirs in the Wells Draw study area (Fig. 2). The significance of each data type to this characterization and its associated uncertainty were evaluated in **Table 1**.

Well data were integrated in a commercial database to determine the spatial distribution of reservoir quality sandstones within the Wells Draw study area (Fig. 2). The first step involved constructions of several cross-sections linking the well locations along different axes for visualization and correlation purposes. Then, marker horizons were used to indicate intervals of reservoir quality sandstones as well as important stratigraphic marker beds and carbonate units in the Castle Peak to Garden Gulch stratigraphic interval. A total of 68 marker horizons were identified.

Several gamma-ray and density-porosity well log cutoffs were investigated to identify which best matched the perforation data. Gamma ray logs were observed to be less effective compared to density-porosity logs. This observation is consistent with those of Morgan *et.al.*[12] A density-porosity cut-off ($\geq$ 8%) was observed to match best with the perforation data. Thus, it was considered a more appropriate cut-off for identifying potential zones for future perforation at well locations and estimating reservoir quality at unobserved locations. Further attempts to discriminate between facies using density-porosity cut-offs proved difficult, especially since the density-porosity log is not a lithology log. The density-porosity range (0-21%) also compares well with the porosity range from core analysis (**Fig. 8**).

Core analysis data of 12 out of the 32 sidewall and conventional cores published by Morgan *et.al.*[6] were used (**Table 2**). Although these data come directly from core samples of the reservoir, they are assigned a high level of uncertainty in Table 1 for the following reasons:

i. Only 2 out of the 12 cores are located in the Wells Draw study area (Fig. 2), though, the other 10 cores are nearby;

ii. core analysis for porosity, permeability and other properties will differ from reservoir conditions because the core sample are no longer in the original state; and

iii. 12 cores samples represent a smaller sampled volume compared to available well logs.

However, the core analysis data remains significant because it provides a correlation between porosity and permeability (**Fig. 8**). For the 12 core samples, the porosity range is 1-20.5% while the permeability range is 0.01-170 md. The higher core permeability values may be the result of natural fractures in the core samples or dislocation and twisting, which occurs with sidewall cores.

Production data (Fig. 4) in the Wells Draw study area are available from June 1, 1982 to December 31, 2006. Water injection data (Fig. 4) are available from January 1, 1995 to December 31, 2006. These data are mainly of 8 types including q_o, q_w & I_w (Stb/mon), q_g (Mscf/mon), GOR (Mscf/Stb), water-cut (Stb/Stb), and number of producers and injectors.

Because production data is commingled it is not feasible to determine oil and water production allocations for the several contributing flow units. Thus, a performance assessment via simulation studies requires a stacked 3D model of the flow zones.

Table 1—Data types listed in approximate order of increasing uncertainty (1 to 8).

#	Data Type	Quantity	Description	Significance	Comments
1	**Well headers**	35 wells (18 oil producers & 17 water injectors).	Well surface/ bottom coordinates showed that all wells were verticals and spaced at 40acres/well.	All data at these locations are honored in the characterization.	A few wells penetrated the sandstones of the Castle Peak reservoir, which is the deepest in this study.
2	**Marker horizons**	68 levels identified and correlated across 35 wells.	68 marker horizons from Castle Peak base to Garden Gulch top are used in the model.	They delineate the reservoir geometry and architecture for defining the model framework. Guide zonation of the sandstones for computing the petrophysical properties.	Some marker horizons were redefined and new ones were created where the DPHI log cutoff and/or perforation data indicated the presence of reservoir quality sandstones.
3	**Perforation data**	380 perforations in Wells Draw study area (Jun-1-1982 to Aug-1-2005).	A significant portion of the perforation data is found in the interval between the D1 and CP5 sandstones.	Perforation data helps indicate the appropriate cut-off previously used to select layers of reservoir quality sandstones.	The perforation data were also used in computing the interwell connectivity in this study.

Table 1 Continued

#	Data Type	Quantity	Description	Significance	Comments
4	**Well logs**	5 log types	Logs sampled at 0.5ft: gamma ray GR; density-porosity DPHI (0–16% for sandstones); neutron-porosity NPHI; laterolog-deep LLD; laterolog-shallow LLS.	Most populous form of data available. Used for estimation of reservoir properties at the unobserved interwell locations.	Comparison of log cutoffs (GR $\geq$75API and DPHI $\geq$8%) showed the DPHI log to identify layers of reservoir quality sandstones better than the GR log.
5	**Core analysis data**	Sidewall and whole cores were taken from 12 wells. Table 3 shows well numbers and cored intervals.	Porosity range (1-20.5%). Permeability range (0.01-170md). High core permeability may due to fractures or twisting in sidewall cores.	Provides por-perm correlation for creating 3D model of permeability.	The use of one porosity-permeability correlation in the 3D model is one simplification in this study.
6	**Net perforated sand map**	One	This map shows the net perforated thickness in the area.	Provide visual guide in the initial task of selecting the study area.	None.
7	**Production data**	8 types. 13 years of production data.11 years of injection data.	q_o, q_w & I_w (bbl/mon.), q_g (Mscf/mon.); GOR (Mscf/Stb); water-cut (Stb/Stb); number of producers and injectors.	Commingled production data requires a stacked 3D model of the flow zones for simulation assessments.	Production period (Jun-1-1982 to Dec-31-2006). Injection period (Jan-1-1995 to Dec-31-2006).
8	**Published outcrop studies**	Several	Morgan and others.[14] Taylor and Ritts.[17]	Provide outcrop analogs of the sandstone facies geometries & width-thickness statistics.	The width thickness statistics are useful for estimating aspect ratios.

Table 2—List of sidewall and whole cores taken from 12 wells (Morgan *et.al.*[6]).

#	Well Number	Section, Township, Range	API Number	Cored Interval (feet)	Inside Study Area?
1	33-8	Sec. 8, T. 9 S., R. 17 E.	43-013-31427	4632-4660 5440-5470	No
2	41-8	Sec. 8, T. 9 S., R. 17 E.	43-013-30741	4105-4156 4993-5052	No
3	9-34	Sec. 34, T. 8 S., R. 16 E.	43-013-31407	15 rotaries	No
4	10-34	Sec. 34, T. 8 S., R. 16 E.	43-013-31371	rotaries	No
5	12-35	Sec. 35, T. 8 S., R. 16 E.	43-013-30744	5021-5033	No
6	12-4	Sec. 4, T. 9 S., R. 16 E.	43-013-30699	4878-4933	Yes
7	33-11J	Sec. 11, T. 9 S., R. 16 E.	43-013-31451	4840-4870 5158-5207 5370-5424	No
8	3A-35	Sec. 35, T. 8 S., R. 16 E.	43-013-30608	4993-5022	No
9	5-33	Sec. 33, T. 8 S., R. 16 E.	43-013-31435	24 rotaries	Yes
10	6-35	Sec. 35, T. 8 S., R. 16 E.	43-013-30751	5026-5033 5042-5048	No
11	13-32	Sec. 32, T. 8 S., R. 16 E.	43-013-31112	7 rotaries	No
12	14A-28	Sec. 28, T. 8 S., R. 16 E.	43-013-30792	5550-5646	No

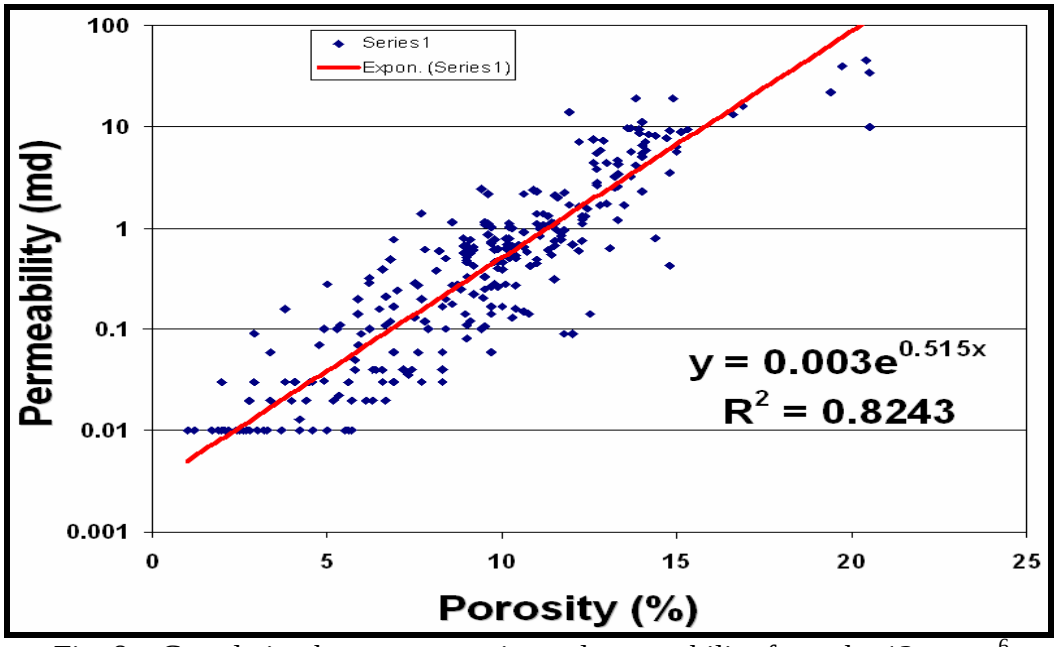

Fig. 8—Correlation between porosity and permeability from the 12 cores.[6] Porosity range (1-20.5%). Permeability range (0.01-170md).

Procedures

The procedures used are discussed under 3 major tasks below.

Characterizing Static Reservoir Properties

Both deterministic and geostatistical techniques were combined in the procedures for static reservoir characterization. Deterministic techniques have become less preferred in reservoir characterization practice mainly because they return one estimate for the same sample data and cannot convey the uncertainty of the outcome.[34,38] However, they still find use for cases where the well data density is considered sufficient for estimations at interwell locations.[21] On the other hand, geostatistical techniques simulate several equally possible outcomes for the same sample data by combining a random seed with the sample data and variogram constraints.[21,31,32] Thus, they provide a means of quantifying uncertainty in simulations by generating different possible outcomes that all honor the sample data variability.[32] To simplify the characterization task, a deterministic net-to-gross ratio model was used in this study while a geostatistical technique was used to quantify the uncertainty in porosity distribution at interwell locations. This approach was used because I focused on the uncertainty in porosity distribution and assumed that the 40-acre well spacing was adequate to model the net-to-gross ratio deterministically. Following is the procedure I used for characterizing the static reservoir properties from well and perforation data in the Wells Draw study area.

1. Define the major geometry and architecture of the reservoirs by correlation of stratigraphic markers in all wells. This constitutes the model framework.

2. Apply density porosity log cutoff (≥8%) to identify net sandstones within the reservoirs.
3. Display the perforation data on well logs and compare perforations with occurrences of pay sand. A good match was obtained with the density porosity log cutoff (≥8%).
4. Group the reservoirs into units separated by significant shale intervals.
5. Calculate the following properties for each unit:
    - Net sand thickness,
    - Net-to-gross ratio (NTG) ratio, and
    - Average porosity of net sandstone.
6. Transfer properties into 3D framework.
7. Build one deterministic NTG distribution using the moving average algorithm.
8. Build 21 geostatistical porosity realizations using sequential Gaussian simulation with collocated cokriging, conditioning each realization with the NTG property. The relationship between NTG and porosity is established by step 2.
9. Assign permeability using the porosity and permeability relationship determined from the available core data.

Static Ranking

The purpose of ranking a suite of geological realizations is to exploit a fit-for-purpose measure for reliable selection of the low-side, expected, and high-side realizations.[40] In other words, ranking realizations allows bounding the uncertainty without performing full scale simulation assessments for all realizations. Several ranking parameters are available and are broadly classified as static or dynamic ranking

parameters.[41] Extensive investigations show that no ranking parameter is unique or perfect.[40-43] Deutsch and Srinivasan[40] have performed extensive assessments on the applicability of the pore volume ranking index as a statistical ranking measure. In line with the above, I selected the mean pore volume ranking parameter to weight the net-porosity with the product of net-to-gross ratio and cell bulk volume models. Firstly, pore volume is calculated for each grid cell in the reservoir model from a product of cell bulk volume, net-to-gross ratio ratio, and net-porosity. Since, we have one bulk volume model, one deterministic net-to-gross ratio model and 21 porosity realizations, the resulting pore volume models reflect only the uncertainty in porosity distribution. Then, I calculated the average pore volume of the sand zones to get the mean pore volume for each realization which I used it to construct a cumulative relative frequency curve. Below is the static ranking procedure I used to select the models that represent the bounding cases of uncertainty in reservoir connectivity.

1. Choose an appropriate measure to rank the 21 porosity realizations. I selected the mean pore volume.
2. Compute the mean pore volume for each of the 21 porosity realizations.
3. Create a table listing the names of the 21 realizations of mean pore volume in column-one and their corresponding values in the second column.
4. Sort the mean pore volume values from highest to lowest in column-two.
5. Make a second table containing a representative number of class boundaries, corresponding class mark, and frequency values for the ranking measure.
6. Compute the interval and boundary for each class boundary.

7. Plot a curve of the cumulative distribution frequency (CDF) of the 21 realizations of mean pore volume that shows the upper class boundaries on the x-axis and the cumulative relative frequency on the y-axis.
8. Select the low, base, and high cases of mean pore volume distribution from the plot. I selected P25, P50 and P75 respectively.

Evaluating Interwell Connectivity

An evaluation of interwell connectivity was conducted from analysis of well data. Sandstone net thickness and perforation data were analyzed for more than 33 sandstone reservoirs to quantify interwell connectivity as a function of well spacing. “Static connectivity” is assumed to exist between two adjacent wells in a layer if sandstone net thickness is identified in both wells. “Hydraulic connectivity” is assumed to exist between two adjacent wells in a layer if net thickness and perforations are present in both wells. Thus, a condition for the presence of hydraulic connectivity is that static connectivity has been identified. Other results of the interwell connectivity evaluation are visualizations of interwell connectivity at the model zone level. Following are procedure I used for evaluating static and hydraulic interwell connectivity.

1. Create a spreadsheet containing all 35 study wells in column-one and the adjacent wells in subsequent columns.
2. Create a second spreadsheet containing all 35 study wells and the corresponding net sand thickness calculated for each correlated sand layer, grouped into 13 zones separated by 9 significant shale zones. This will provide the input data for assessing interwell static connectivity.

3. Create a third spreadsheet containing all 35 study wells and the corresponding net perforated thickness calculated for each correlated sand layer, grouped into 13 zones separated by 9 significant shale zones. This will provide the input data for assessing interwell hydraulic connectivity.
4. Link the three input spreadsheets with a program that returns a numeric value of unity to indicate the presence of static or hydraulic connectivity between each well pair penetrating a gross unit and zero where static or hydraulic connectivity is absent.
5. Generate the interwell connectivity results and visualizations for each of the 13 zones.

Further details of the interwell connectivity evaluation are presented in Chapter IV.

CHAPTER II

GEOLOGIC SETTING

A brief discussion of the geologic setting is provided in the context of the Uinta Basin and the Green River petroleum system.

Uinta Basin

The Uinta Basin is defined as a topographic and structural trough covering an area greater than 9,300 sq. miles (14,900 km^2). It is sharply asymmetrical with a steep north flank and a gently dipping south flank. The Uinta basin is bounded on the north by the east-trending Uinta Mountains, on the east by the Douglas Creek Arch, on the southeast by the Uncompahgre uplift, on the southwest by the San Rafael uplift, and on the west by the Wasatch Mountain Range.[44] **Fig. 9** shows the major structural features, surface faults, and gilsonite veins in and around the Uinta Basin.[44] Within the Monument Butte area, the two major structural features are the gilsonite veins and the Duchesne fault zone.

The regional fracture systems are aligned north-northwestward. They are tens of miles long and are genetically related to major structural features that border or extend into the basin.[45] Some authors have suggested the presence of the fracture systems have greatly increased permeability of reservoirs in the Uinta Basin.[46,47] The structural development of the Uinta Basin began in Late Cretaceous (Maastrichtian) time with the withdrawal of the Cretaceous inland sea and the onset of the Laramide orogeny, creating a large area of internal drainage, that was filled by ancestral Lake Uinta during the

Paleocene and Eocene.[48] Thus, Lake Uinta became the site for the deposition of open- to marginal-lacustrine sediments of the prolific Green River petroleum system in northeastern Utah.

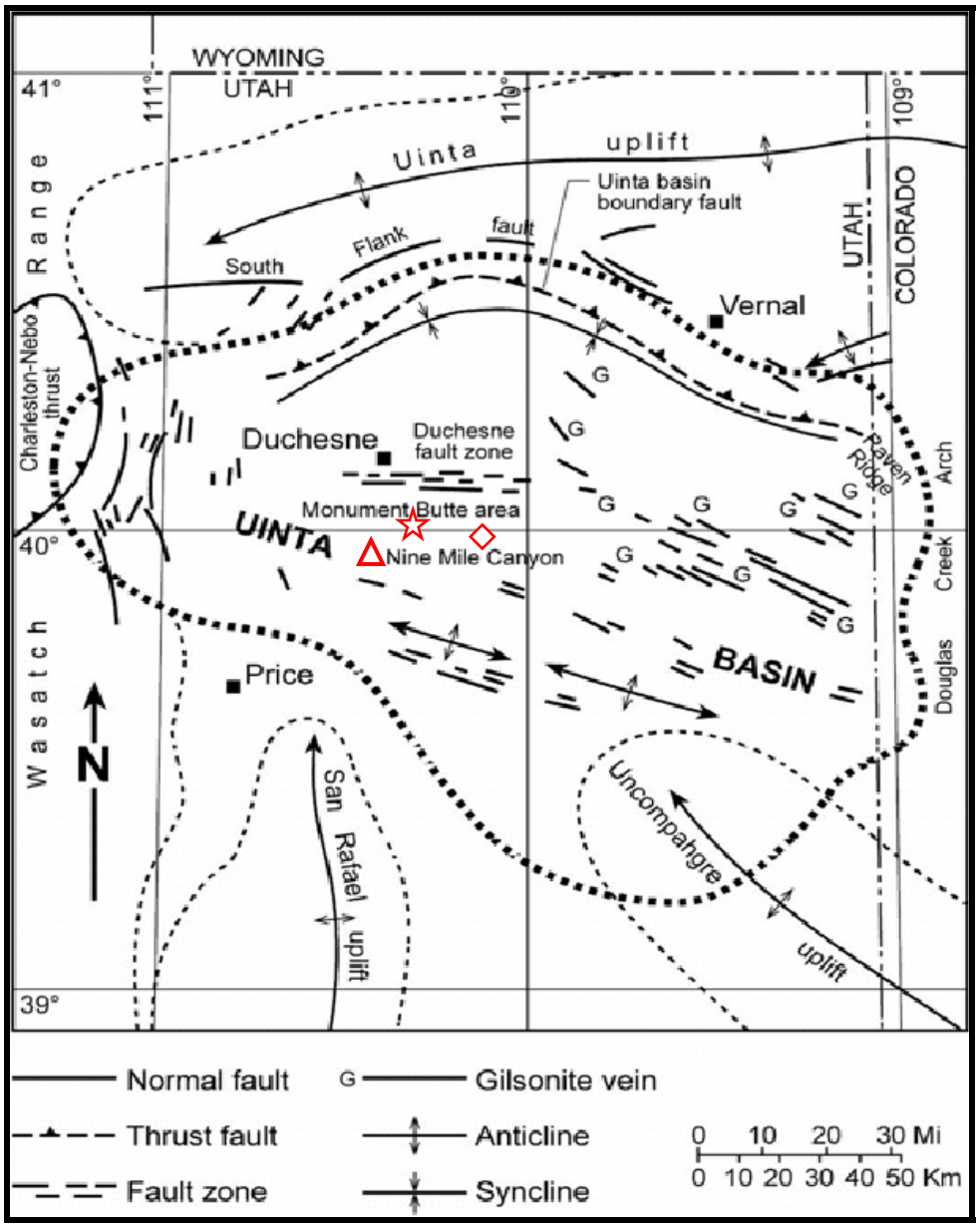

Fig. 9—Major structural features, surface faults, and gilsonite veins in and around the Uinta Basin.[44] Shape symbols indicate different outcrop locations reviewed in this thesis.

Green River Petroleum System

The Wells Draw study area is located in the Green River petroleum system.[49] This petroleum system has produced more than 450 MMBO mainly from two formations, the Green River and Colton Formations.[7] The Green River Formation contains the source rock and most of the reservoir and seal rocks (**Fig. 10**).[49] Most of the kerogen-rich oil shale source rocks formed in an open lacustrine environment with abundant type I and some type II kerogens. The reservoir and seal rocks of the Green River Formation are mixed fluvial and lakes rocks (marginal lacustrine facies) and contain types I, II, and III kerogens. The Colton (Wasatch) Formation consists of alluvial red-bed deposits and contains mostly type III kerogen. It is laterally equivalent to, and intertongues with, the Green River formation (Fig. 10). Most of the commercial oil accumulations in the Green River petroleum system are associated with source rock and reservoir rock that have a vitrinite reflectance greater than 0.5 % (**Fig. 11**).[49]

The Green River and Colton Formations have differences in depositional and reservoir characteristics in the northern and southern parts of the Green River petroleum system as a result of two dominant sources of sediment supply that existed to the north and south of Lake Uinta. **Fig. 12** is a schematic of the depositional setting for Lake Uinta during high lake and low lake levels.[15] The Uinta Mountains were the source for the northern shoreline deposits of Lake Uinta, which produce oil in the Altamont, Bluebell, Cedar Rim, and Red Wash fields.[50-52] In contrast, the southern shore deposits of Lake Uinta are sourced from the highlands further south. Because the southern shore of Lake Uinta was broad and flat, the frequent rise and fall of the lake level induced by climatic

and tectonic changes caused large transgressive and regressive shifts of the shoreline.[16] In the Monument Butte area, the cyclic deposition of the Green River Formation created several stacked deltaic deposits that included distributary-mouth bar, distributary channels and nearshore bar lithofacies assemblages, which are the primary oil producing sandstone reservoirs.[16] **Fig. 13** shows the facies complexity of the Green River Formation in the Parley Canyon, southwest Uinta Basin.[17] Bounding surfaces and complex stacking patterns illustrate the complex sandstone architecture. This outcrop, located about 21 miles (34 km) south of the Monument Butte area, is excellent analog for the Lower and Middle members of the Green River Formation, which are the focus of this study. The complex architecture and stacking patterns at the Parley Canyon supports the need for better understanding of reservoir connectivity to improve oil recovery in the Monument Butte area.

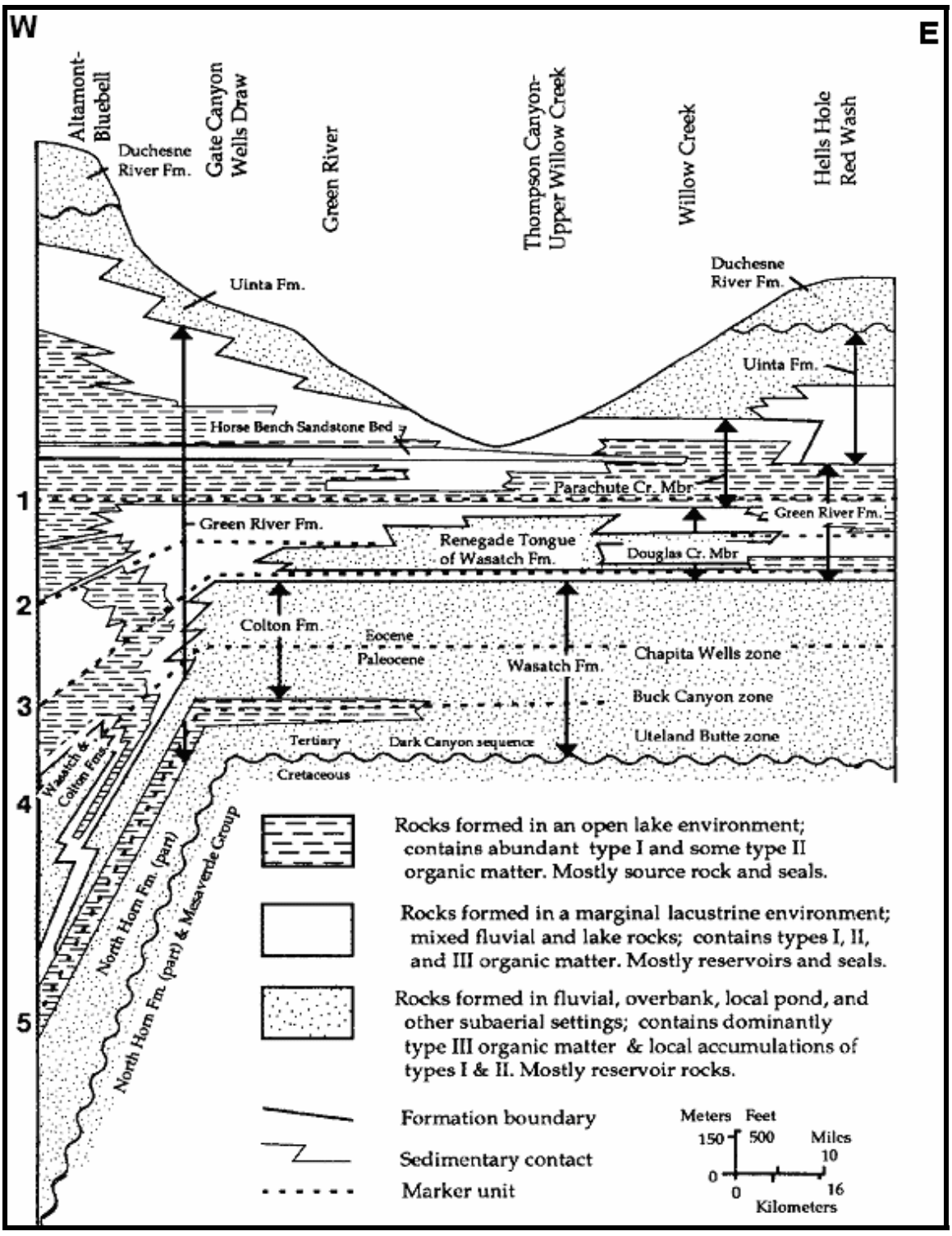

Fig. 10—Stratigraphic section of source rocks, reservoir rocks and seal rocks of the Green River petroleum system. Datum is Mahoganey oil shale bed (1).[49]

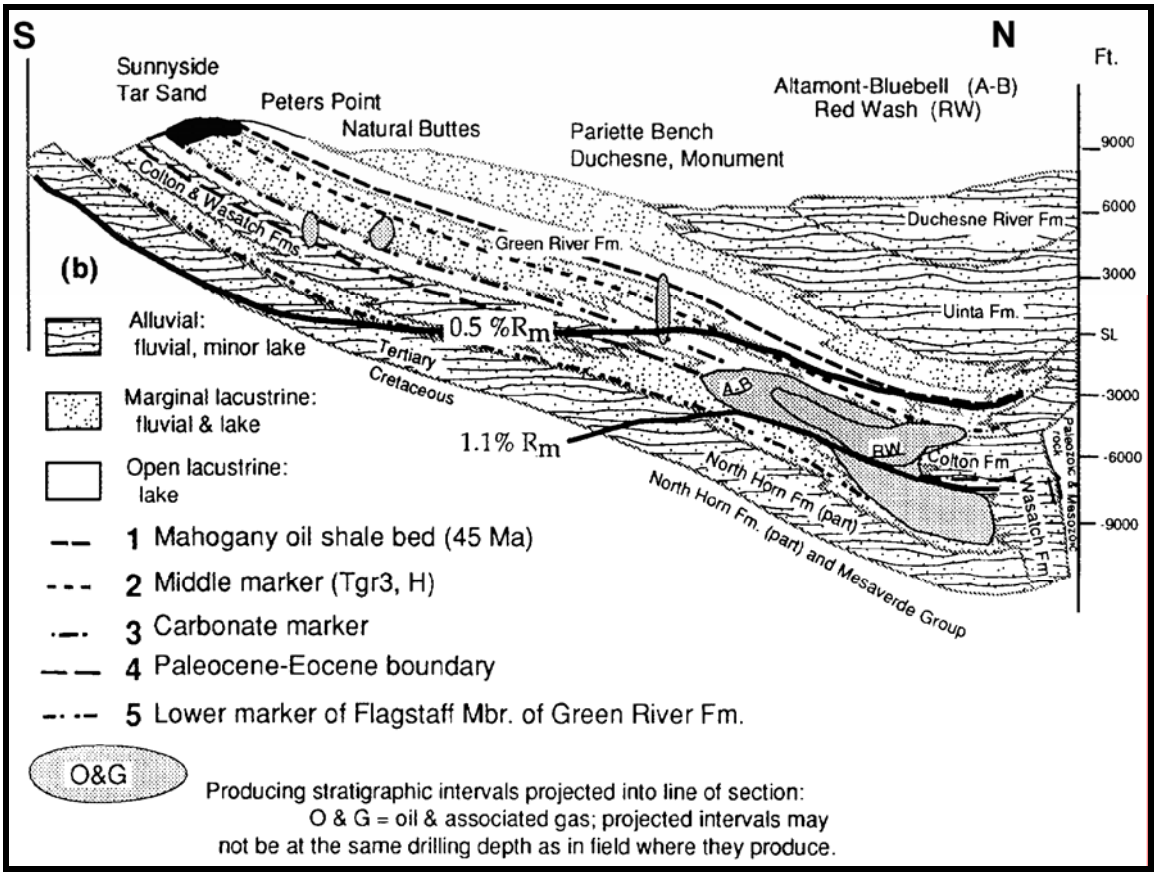

Fig. 11—Cross-section of thermal maturity of oil accumulations in the Green River petroleum system.[49]

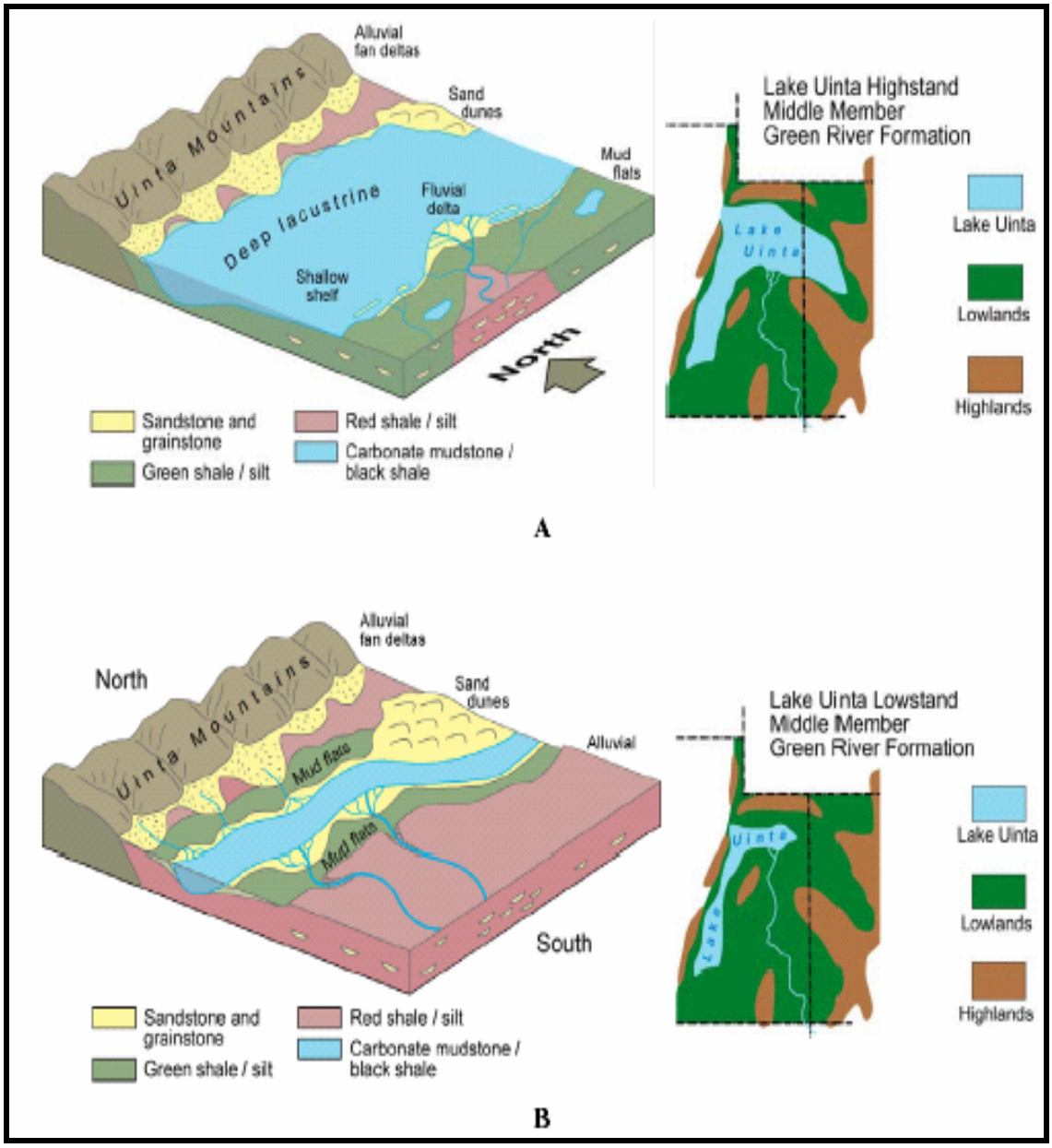

Fig. 12— Lake Uinta depositional setting during high and low lake levels.[15]

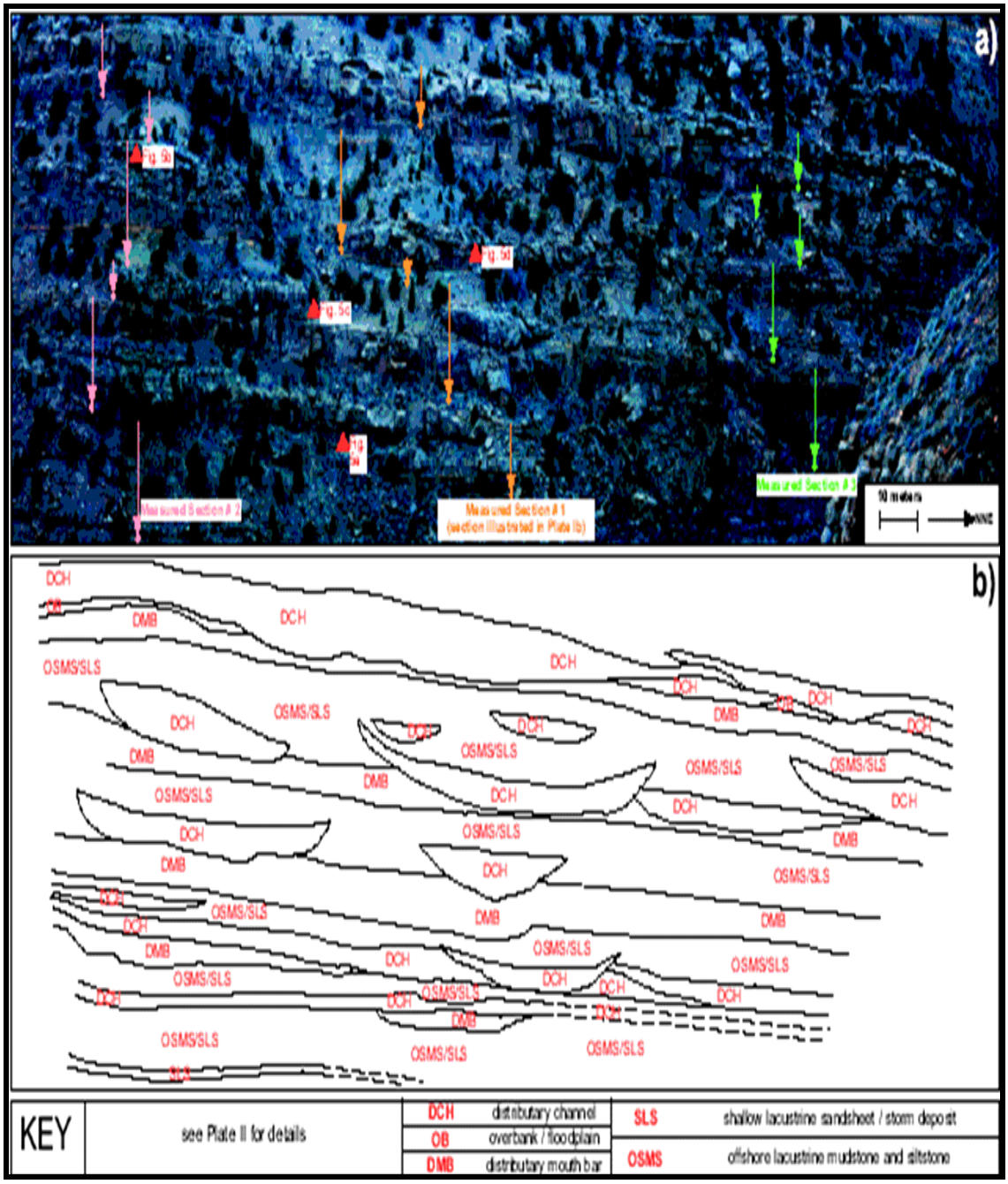

Fig. 13—Facies complexity of the Green River formation in Parley Canyon, Uinta Basin.[17] (a) Outcrop photograph. (b) Surface tracing of the geometry. See **Fig. 8** for location of outcrop in Parley Canyon (star symbol).

Green River Formation

Several authors have proposed different stratigraphic nomenclature for the Eocene Green River formation in efforts to group its lithofacies into distinct intervals having common reservoir characteristics (**Fig. 14**).[53-57] This study follows the stratigraphic nomenclature of Morgan and others (2003).[4-12] They correlated more than 1,300 well logs, examined 32 cores, and described outcrops in Willow Creek, Nine Mile and Desolation Canyons and their tributaries. Their study is significant, because it presents in one project a detailed comprehensive account of the tectonic and paleodepositional history, petrology and, regional trends of the five distinct reservoirs that make up the Green River formation.

The Green River formation is divided into the Lower and Middle members which are separated by a carbonate marker bed.[4-12] The two members are further sub-divided into five distinct intervals. **Fig. 15** is a type log from well Federal 2-35 in Monument Butte field that shows the five oil producing intervals of the Eocene Green River formation.[15] In ascending order, the Lower member of the Green River Formation is divided into the Uteland Butte and Castle Peak intervals, the Middle member is divided into the Lower Douglas Creek (Travis interval), Upper Douglas Creek (Monument Butte interval) and Garden Gulch (Beluga interval). These intervals include several sandstone reservoirs identified by detailed correlation. This study is restricted to reservoir characterization of only four of the intervals: (1) Castle Peak, (2) Lower Douglas Creek, (3) Upper Douglas Creek, and (4) Garden Gulch intervals. However, the representative reservoir characteristics of the five distinct intervals are discussed below.

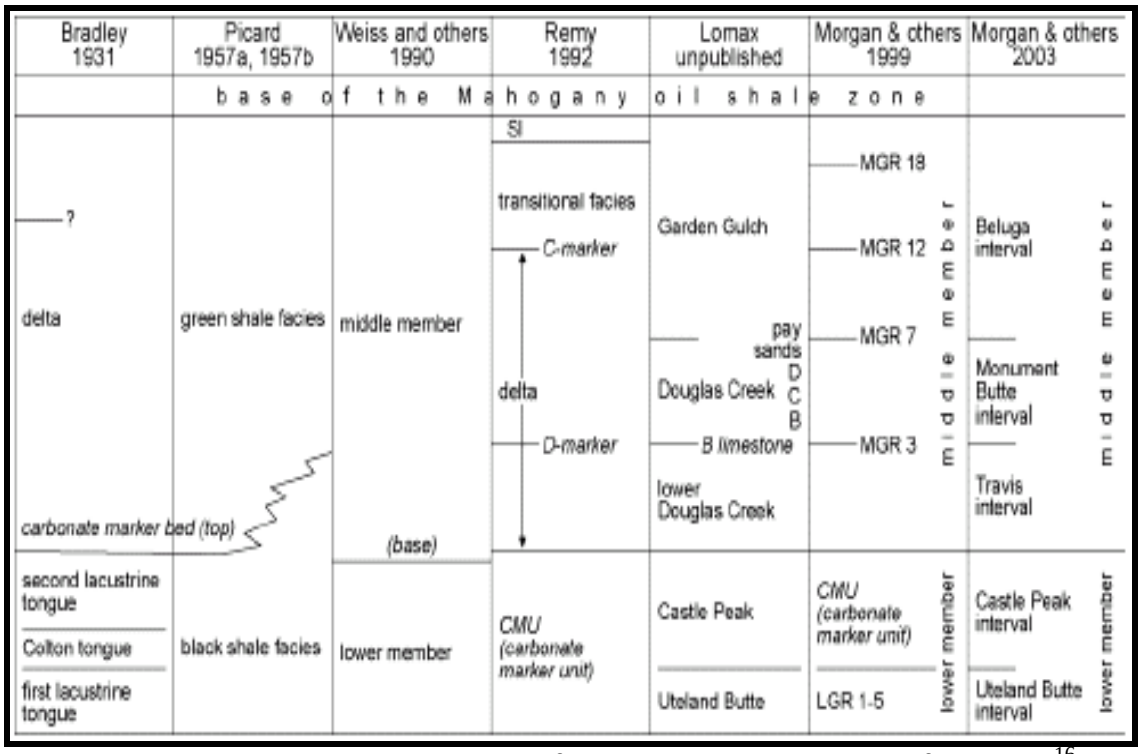

Fig. 14—Stratigraphic nomenclature used for the Eocene Green River formation.[16] This study follows the stratigraphic nomenclature of Morgan and others (2003).[4-12]

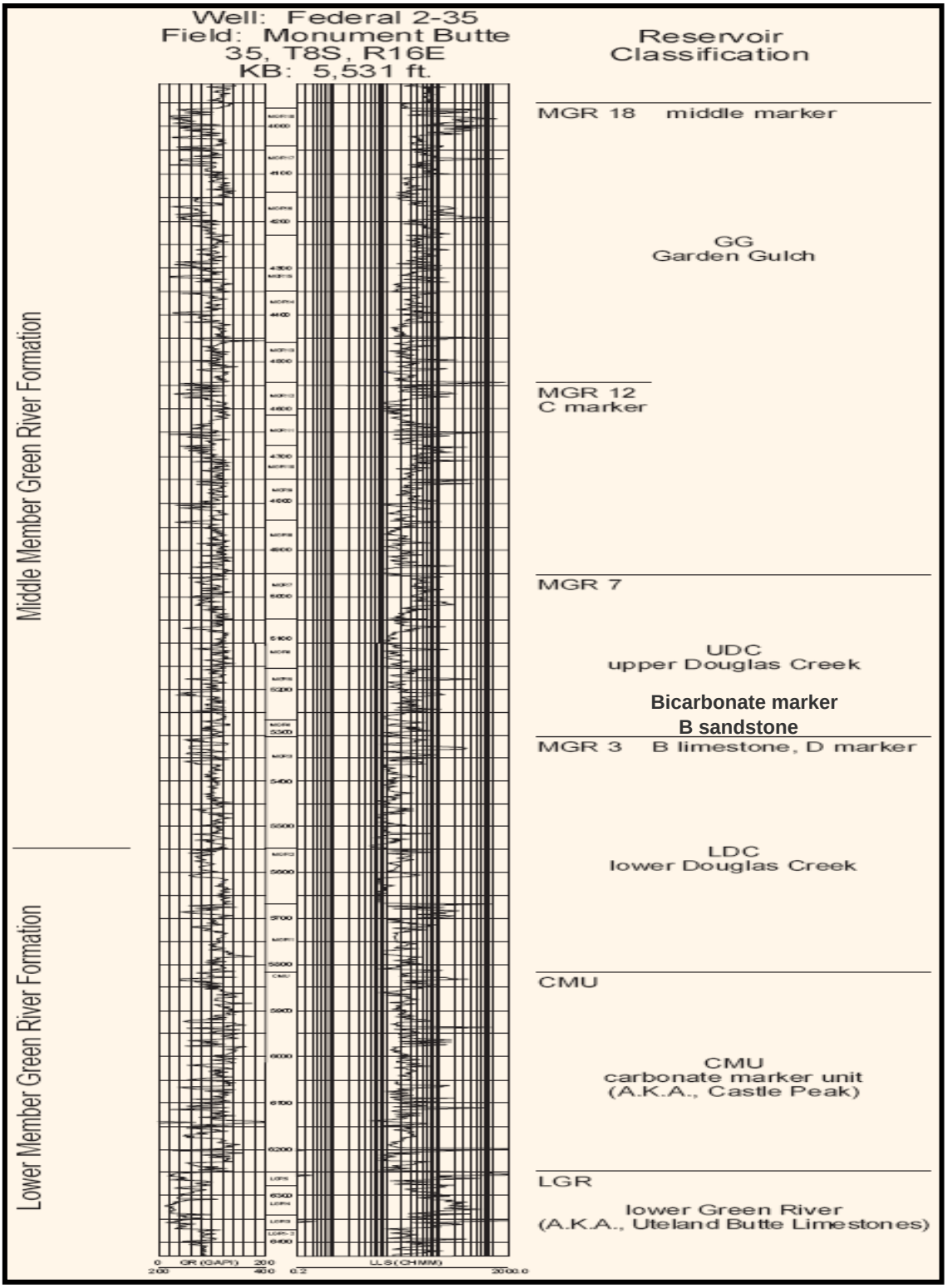

Fig. 15—Type log from well Federal 2-35 in Monument Butte field showing five distinct intervals of the Eocene Green River Formation.[15]

Uteland Butte Interval

The Uteland Butte interval is the deepest of the five distinct Green River intervals and overlies the alluvial Colton Formation. Morgan and others[4-11] characterized the reservoir rocks as predominantly low-permeability carbonates with presence of thin, shallow, bar sandstones (**Fig. 16**). Within Uteland Butte field, they observed very little siliciclastic sediment and suggested sediment entrapment in the proximal channels due to rising lake levels or remoteness of the sediment source far south of the San Rafael Swell as two possible isolated or combined causes. They reported the characteristics of the Uteland Butte reservoir as follows: bed thickness (8-22 ft.); porosity (5-15%); permeability (<1 md.); oil saturation (40-80%); oil-in-place (572 BO/ac.ft); and oil recovery factor (2.68%).

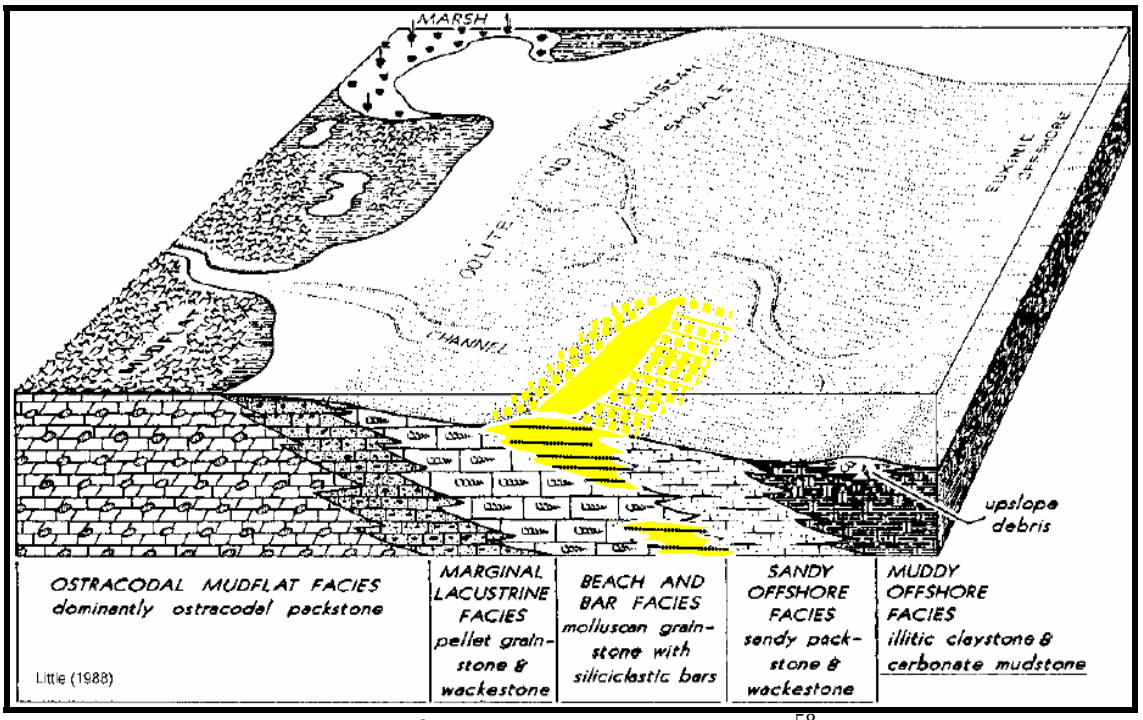

Fig. 16—Depositional model of the Uteland Butte interval.[58] The reservoir rocks are predominantly low-permeability carbonates with presence of thin, shallow, bar sandstones.

Castle Peak Interval

The Castle Peak interval overlies the Uteland Butte interval. The upper boundary of Castle Peak is recognizable on well logs by the presence of a wide-spread carbonate marker bed. Morgan and others[4-11] characterized the reservoir rocks as highly compacted, medium-grained, isolated channel sandstone beds encased in carbonate and shale. The following range of values were reported as characteristic of the Castle Peak reservoir: sandstone thickness (4-16 ft.); porosity (8-12%); permeability (0.5-3 md); oil saturation (30-50%); oil-in-place (428 BO/ac.ft.); and oil recovery factor (4%). **Fig. 17** is an outcrop analog of the Green River formation that shows the Castle Peak interval (interbedded shale and channel sandstone with some carbonate) and Uteland Butte interval (dominantly lacustrine carbonate) which overlie and intertongue with the alluvial Colton formation.[14]

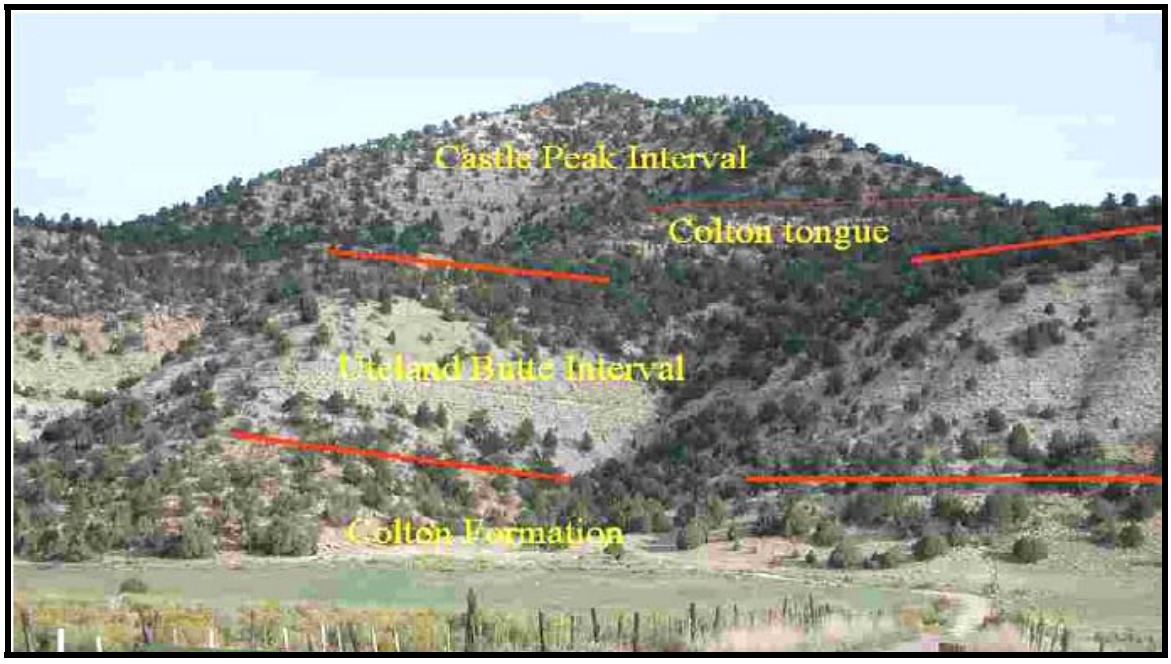

Fig. 17—Outcrop of Castle Peak and Uteland Butte intervals.[14] See **Fig. 8** for location of outcrop near Nine Mile Canyon (triangle symbol).

Travis Interval (Lower Douglas Creek)

The Lower Douglas Creek is the basal unit of the Green River middle member. It overlies the Castle Peak interval and is capped by the B limestone. Morgan and others[4-11] characterized this interval as turbidite channel, debris and gravity flow deposits. They reported that the sandstone texture was fine-grained with clay coats and noted that these characteristics made a gamma-ray log cut-off inadequate for proper definition and mapping of the Lower Douglas Creek reservoir sandstone thicknesses. The following values were reported as characteristic of the Lower Douglas Creek reservoir in the Monument Butte Northeast Unit: sandstone thickness (10-64 ft); porosity (9-17%); permeability (0.4-13 md); and oil saturation (40-70%). Also, they state that the wide range of reservoir properties results from the high degree of sandstone heterogeneity and makes these reservoirs good candidates for horizontal drilling.

Deo *et al.*[1-3] investigated the effect of reservoir connectivity of the Lower Douglas Creek reservoir on the performance of a water flood project in the Monument Butte unit (Fig. 2). By using a gamma-ray log cut-off for sandstone reservoir definition and mapping reservoir facies, they found the Lower Douglas Creek sandstone to be oriented east-west and showed that the thickest sections of the Lower Douglas Creek reservoir exceed 100 ft in the west part of the Greater monument Butte area (**Fig. 18**). Deo *et al.*[1-3] reported that the sandstones have a funnel-shaped profile on gamma ray logs and exhibit an erosive base that cuts into relatively flat, underlying units. This down-cutting implies a lacustrine low-stand. Vertical stacking of channels implies a lacustrine high-stand and backfilling of the channel scour during subsequent rise in lake

level. The deposition of the sediment gravity flows (slumps, turbidites and sandy debris flows) in sub-lacustrine fans probably occurred during a wet climatic cycle, when both water and sediment inflow was high and the lake was deep. The occurrence of these fans appears to have been controlled by the location of deep incised channels which were produced during a previous lake low-stand. These channel incisions into marginal lacustrine deposits occurred along an east-west trending zone that may be related to the Duchesne fault zone.

A southwest-northeast well log section of the Lower Douglas Creek sandstone in the Travis unit (**Fig. 19**) shows the turbiditic and debris flow sands in the upper section to be relatively flat-lying and uniform in thickness in contrast with the channel-fill sands lower in the section. Deo *et al.*[2] noted that the planar-laminated sandstones in the upper turbidite unit are the most strongly oil-stained sandstones with oil saturation of 67-70.7%; horizontal permeability of 2.5-13 md; and porosity of 14.8-16.6%. The lower turbidite channel sequence sandstones were observed to be moderately stained, with oil saturation of 49.6-40.5%; horizontal permeability of 0.46-0.77 md; vertical permeability of 0.50-0.99 md; and porosities of 9-11.7%. They concluded that the Lower Douglas Creek reservoir was a less than ideal candidate for the water flood demonstration because of its lithologic heterogeneity, complex reservoir architecture, and pervasive fracturing. Also, they concluded that the Lower Douglas Creek reservoir was a difficult exploration target because of its local occurrence.

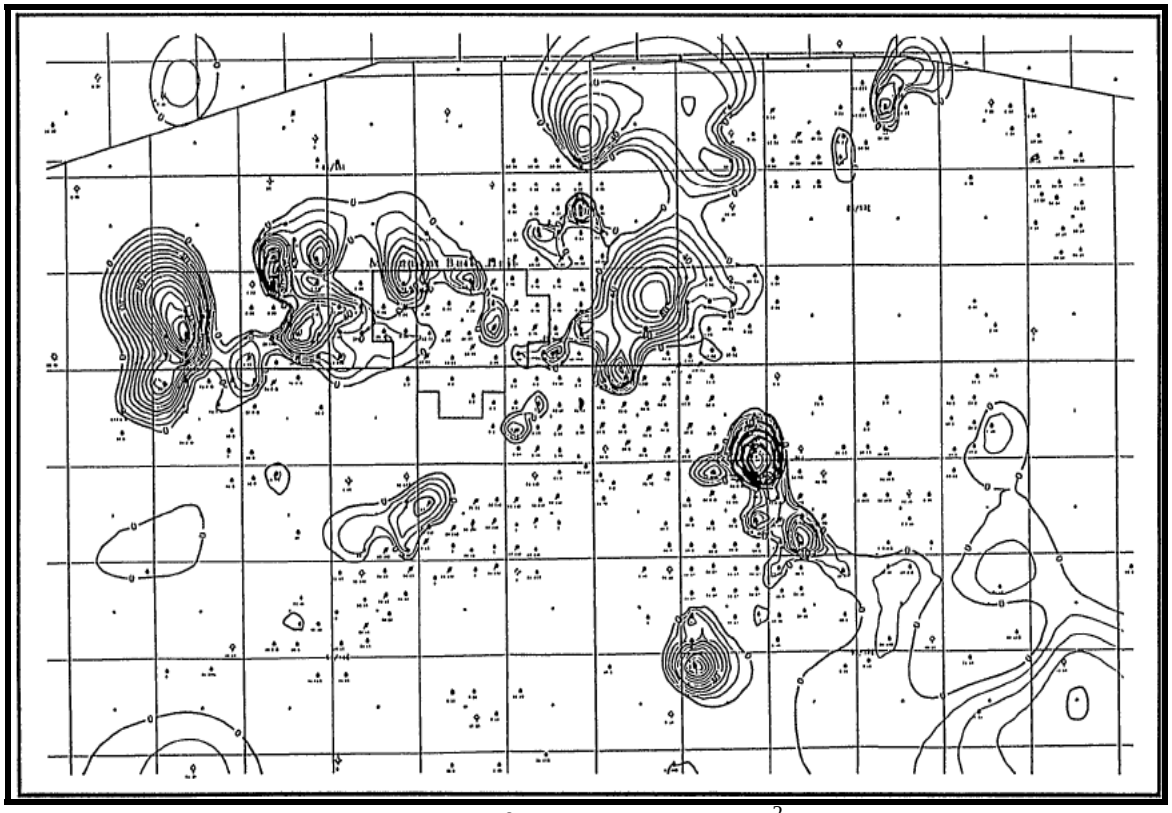

Fig. 18—Net sandstone isopach map of the Lower Douglas.[2]

"A" Sandstone

Deo *et al.*[2] designated the sandstone between the Lower Douglas Creek sandstone and the B limestone marker bed as the "A" sandstone (**Fig. 19**). This sandstone is probably a channel-fill deposit and represents a fall in base level and superposition of a fluvial section above the deepwater turbidites of the Lower Douglas Creek. They concluded that the discontinuous nature of the "A" sandstone makes it unsuitable for water flooding.

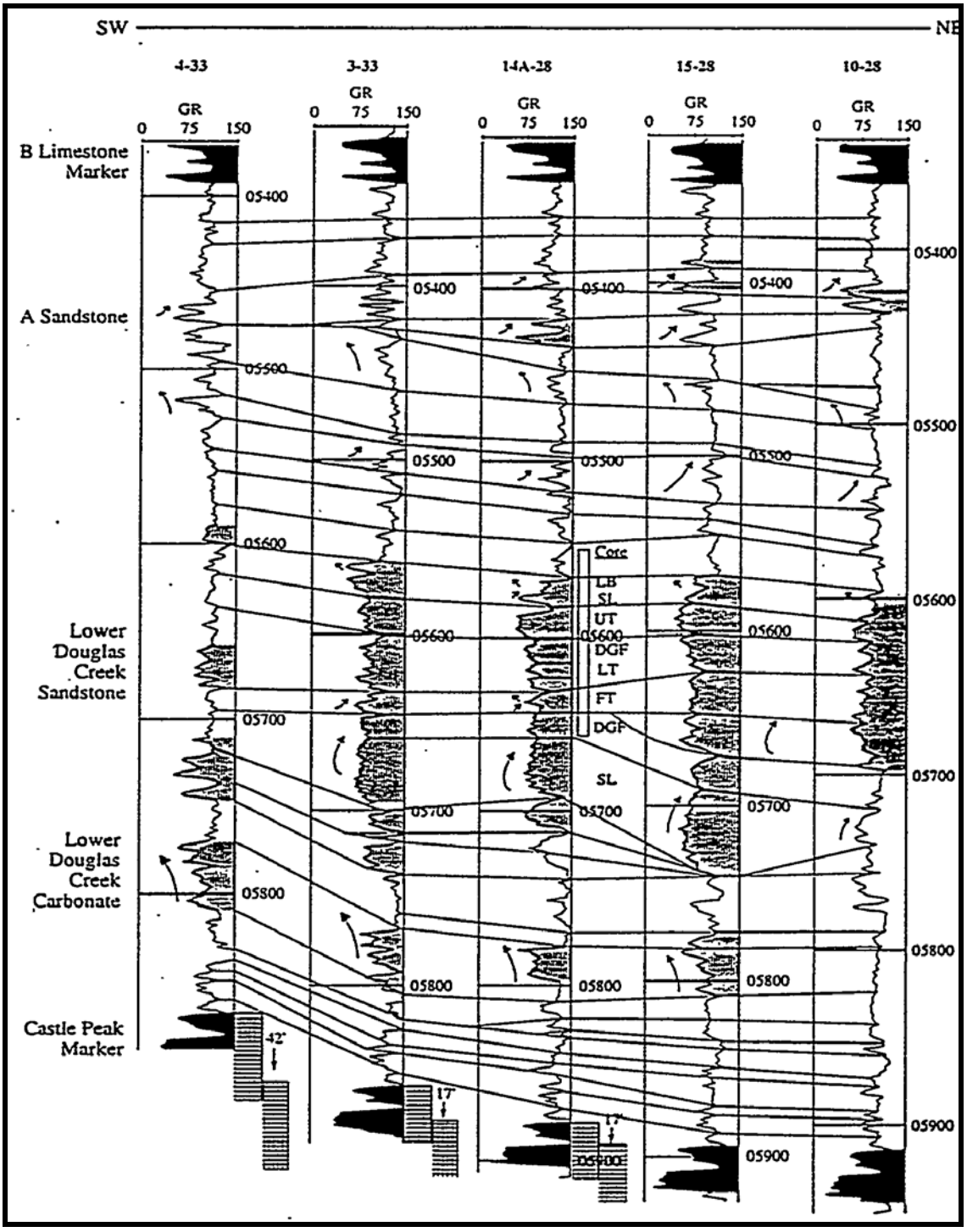

Fig.19—Southwest-northeast well log section of the Lower Douglas Creek reservoir in Travis unit.[2] A general fining-upward well log pattern (indicated by arrows to right) represents channel-fill sands. A coarsening-upward well log pattern (indicated by arrows to left) represents wave worked sub-lacustrine bars. SL=slump, FT=fluxoturbidite, DGF=debris and grain flows, UT=upper turbidite, LB=lacustrine bar

Monument Butte Interval (Upper Douglas Creek)

The Upper Douglas Creek (Fig. 15) is the primary pay zone in the greater Monument Butte area and for most of the southwest Uinta Basin. Morgan and others[4-11] characterized reservoirs in this interval as distributary channel and mouth bar sandstone beds deposited on a lower delta plain. The sandstone beds are usually vertically amalgamated. Sandstone grain sizes range from very fine to fine grained. **Fig. 20** is an outcrop photograph of Green River formation distributary channel sandstone deposits interbedded with carbonate grainstone, marlstone and shale. This exposure represents a deepening of the lake that resulted in the deposition of the Mahogany shale at the cliff top. Exposed lake cycles range from 90 to 110 ft thick. The lower part of the exposure is a good analog for the Upper Douglas Creek reservoir (Monument Butte interval), whereas the upper deepening section is a good analog for the Garden Gulch reservoir (Beluga interval).[14] The following range of values was reported as characteristic of the Upper Douglas Creek reservoir sandstone in the Monument Butte Northeast Unit: porosity (10-15%); permeability (1-10 md); oil saturation (36-45%); oil-in-place (660 BO/ac.ft.); and oil recovery factor (1.4%). The reservoir characterization study conducted by Deo *et al.*[2] further subdivided the Upper Douglas Creek reservoir into the D, C and B sandstones in descending order.

Fig. 20—Outcrop analog of the Monument Butte and Beluga intervals.[14] This exposure represents a deepening of the lake that resulted in the deposition of the Mahogany shale at the cliff top. Exposed lake cycles range from 90 to 110 ft thick. The lower part of the exposure is a good analog for the Upper Douglas Creek reservoir (Monument Butte interval), whereas the upper deepening section is a good analog for the Garden Gulch reservoir (Beluga interval).[14] See Fig. 9 for location of outcrop at junction of Gate and Nine Mile Canyons (diamond symbol).

D Sandstone

The D sandstone interval lies between the C sandstone and the Douglas Creek marker bed. Deo *et al.*[2] identified three distinct sands in this unit denoted as D1, D2 and D3 in descending order (**Fig. 21**). Fig. 21 is a west-east gamma ray well log section of the D sandstone interval in the Monument Butte Unit. The D1 sandstone is intercalated by thin shales that may act as baffles hence, reduce the vertical permeability in the D1 sandstone. Deo *et al.*[2] interpreted the D1 sandstone as marginal lacustrine facies because

of its fine grain size and the absence of strong normal grading. **Fig. 22** is a net sandstone isopach map that shows the thick, widespread and continuous accumulations of the D1 sandstone.[2] Deo *et al.*[2] concluded that the D1 sandstone was an excellent waterflood sweep candidate, because of its lateral continuity and homogeneous lithology. The D2 and D3 sandstones were not considered for waterflood.

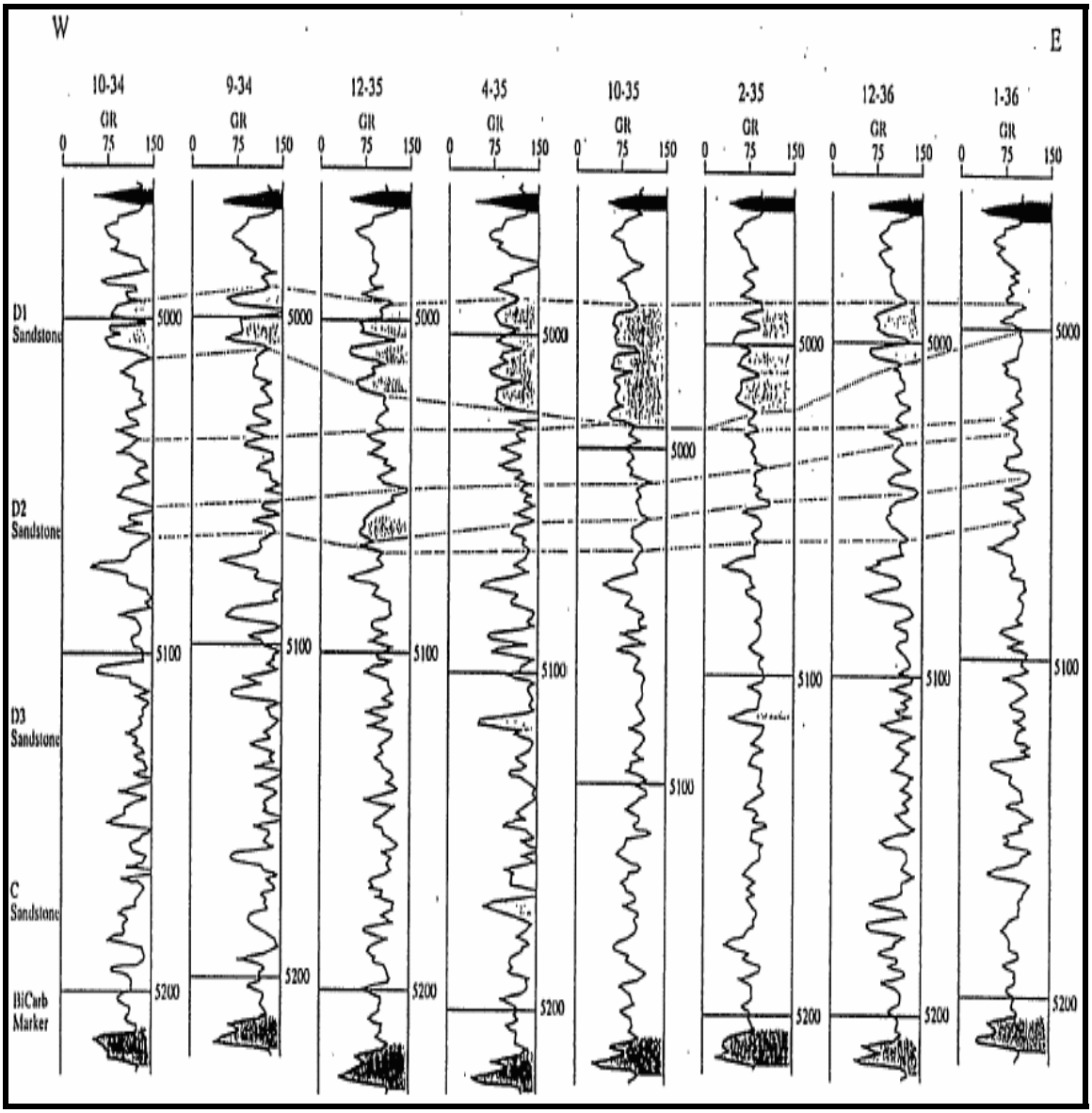

Fig. 21—West-east gamma-ray well log section of the D sandstone interval in the Monument Butte Unit.[2]

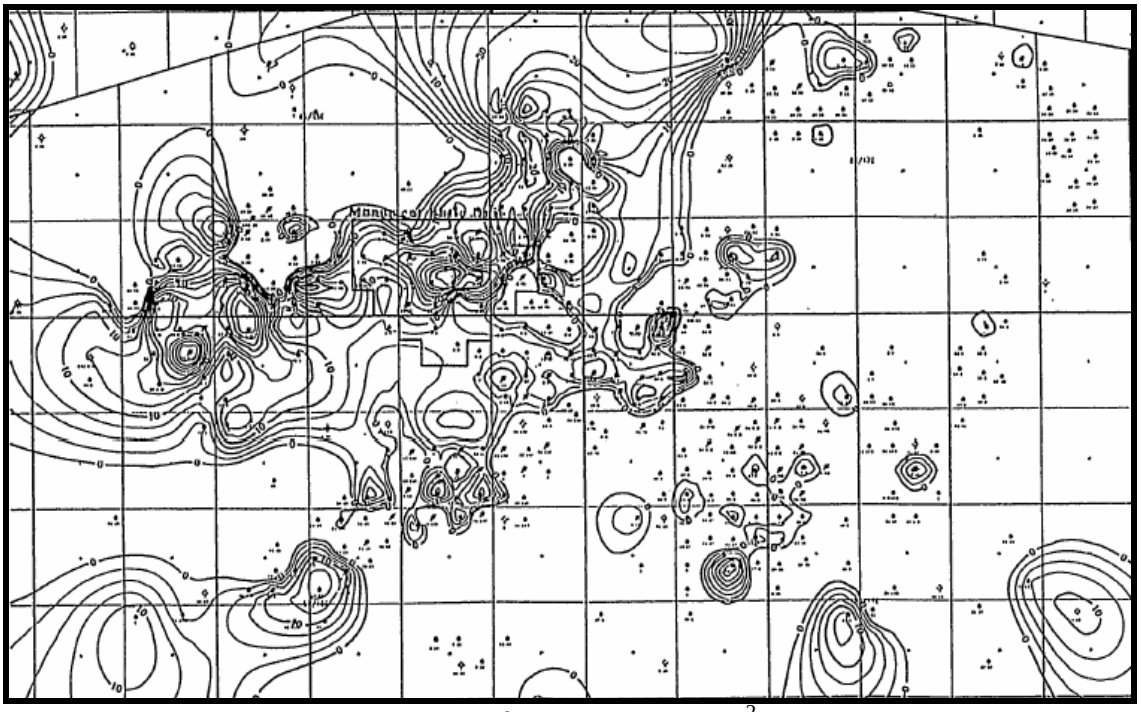

Fig. 22—Net sandstone isopach map of the D1 sandstone.[2]

C Sandstone

Deo *et al.*[2] identified the "C" sandstone (Fig. 21) in nearly 50% of the wells in the project area. Though the "C" sandstone is characteristically thin, it is greater than 30 feet in some wells.[2] The net sandstone isopach map of the "C" sandstone (**Fig. 23**) shows a strong northeast trend southeast of the Monument Butte Unit.[2]

B Sandstone

The "B" sandstone lies between the "B" limestone and the Bicarbonate marker (Fig. 15). **Fig. 24** is a net sandstone isopach map of the "B2" sandstone.[2] Deo *et al.*[2] reported that the "B" sandstone is part of a distributary channel system in a lower delta plain environment. They inferred that it has good geometry for water flood sweep, because it is most likely well confined by shales.

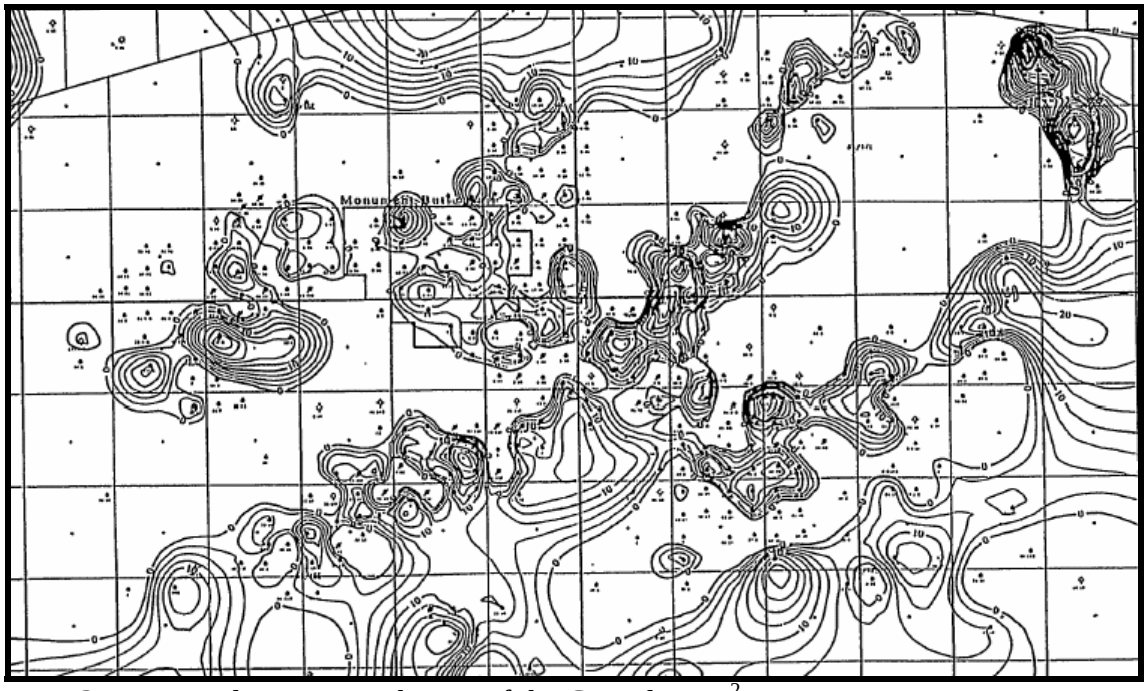

Fig. 23—Net sandstone isopach map of the C sandstone.[2]

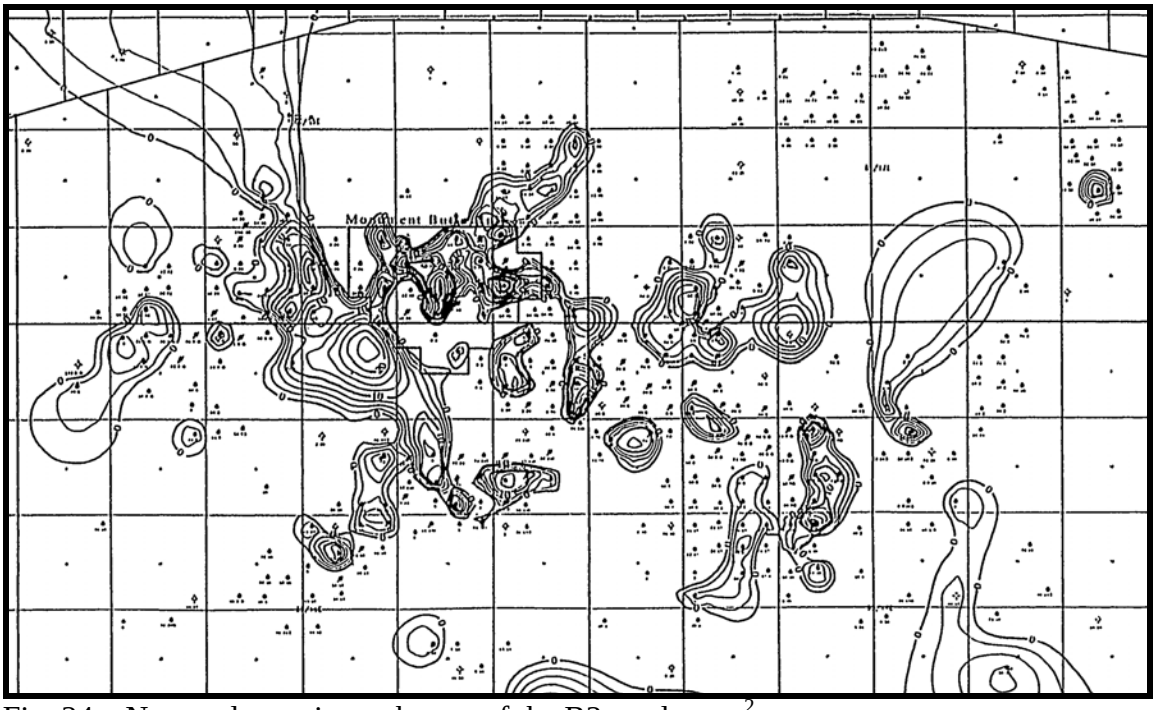

Fig. 24—Net sandstone isopach map of the B2 sandstone.[2]

Beluga Interval (Garden Gulch)

The Garden Gulch or Beluga interval (Figs.15 and 20) is the youngest of the five, distinctive Green River intervals and also the least exploited. Morgan and others[4-11] characterized this interval as a transitional unit from delta to deep lake. It occurs at drill depths of 4,200 to 5,000 ft in Monument Butte Northeast Unit. The sandstones in this interval are encased in carbonate and shale units. The following values were reported as characteristic of the Garden Gulch interval in Monument Butte Northeast: porosity (9-15%); permeability (0.5-5 md); and oil saturation (35-60%).

Geometry and Aspect Ratio of Green River Sandstone

At Parley Canyon (Fig. 13), predominant Green River facies are distributary channel-fill sandstone deposits.[17] Measured dimensions at Parley Canyon are shown in **Table 3**.[17]

Table 3—Facies dimensions measured at Parley Canyon.[17]

a) Isolated Lenticular Distributary Channels					
Width (m)			Thickness (m)		
Max	Mean	Min	Max	Mean	Min
41	29	8	3	N/A	N/A
b) Amalgamated Lenticular Distributary Channels					
Width (m)			Thickness (m)		
Max	Mean	Min	Max	Mean	Min
75	54	27	9	5	N/A
c) Amalgamated Undulatory Distributary Channels					
Width (m)			Thickness (m)		
Max	Mean	Min	Max	Mean	Min
205	193	180	11	6	N/A
d) Distributary Mouth Bar Deposits					
Width (m)			Thickness (m)		
Max	Mean	Min	Max	Mean	Min
247	164	45	10	5	<1

Reservoir Model Classification

In an effort to standardize reservoir characterization guidelines required to adequately model clastic reservoirs, Weber and Geuns[59] proposed a simple classification system that categorizes all clastic reservoirs into three basic types. These are layer-cake, jigsaw-puzzle, and labyrinth reservoir types. Our review of geology, outcrop analogs, and well correlations suggests that the Green River sandstone reservoirs fall under the jigsaw-puzzle category (**Figs. 25 and 26**). Thus, the reservoir characterization procedure in this study is applicable to reservoirs that fit into the jigsaw-puzzle category.

	Terrestrial	Coastal	Marine
Layer cake	Sheet flood deposits Lacustrine sheet sand Aeolian dunes	Barrier bars Chenier deposits Transgressive sands	Shallow marine sheet sands Offshore bars Outer-fan turbidites
Jigsaw puzzle	Braided river deposits Point bars Mixed lacustrine/fluvial Mixed aeolian/wadi	Combined facies complexes, e.g., barrier bar plus tidal channel-fill channel-fill/mouth bar combinations with high NGR	Storm sand lenses Mid-fan turbidites
Labyrinth	Fluvioglacial deposits with low NGR Low-sinuosity channel-fills	Low-sinuosity distributary channel-fills	Upper fan turbidites Slumps Storm deposits with low NGR

*NGR = net/gross ratio.

Fig. 25—Model types for reservoir characterization in clastic depositional environments (Weber and Geuns[12]). The Green River sandstone reservoirs fall under the jigsaw-puzzle category.

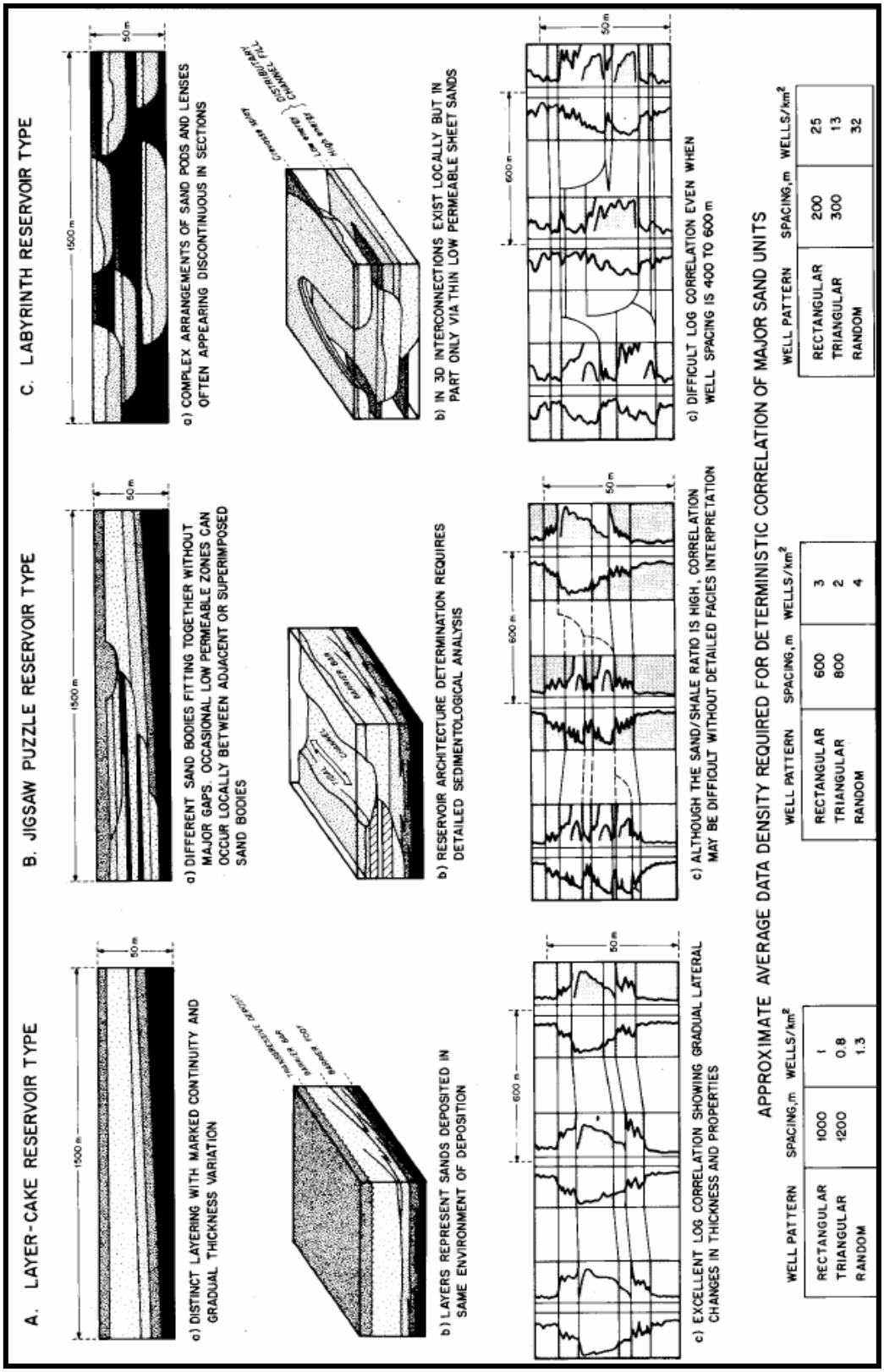

Fig. 26—Characteristic reservoir architecture, connectivity trends and approximate well density required for deterministic sand correlation (after Weber and Geuns[12]).

CHAPTER III

STATIC RESERVOIR CHARACTERIZATION

Structural and Stratigraphic Framework

The major structural and stratigraphic features delineate the reservoir geometry and architecture and constitute the framework for static reservoir characterization.[31,59] About 33 sandstone layers (**Figs. 27 and 28**) were delineated by well correlation of 68 markers horizons from the base of Castle Peak interval to the top of Garden Gulch interval in the Wells Draw study area. Since no faults were identified in the Wells Draw study area, structural maps of the correlated horizon markers constituted the reservoir framework (Fig. 5). Generally, the structure dips northeastward (**Fig. 29**).

Preliminary Investigations of Reservoir Connectivity

Ainsworth[23] reported that connectivity trends can be related directly to depositional trends and suggested that depositional connectivity should be understood prior to investigations into reservoir connectivity. Preliminary investigations focused on identifying the axis of depositional connectivity, as this would parallel the axis of reservoir connectivity. A simple approach employing mostly well data was used, since it is the most populous data type available. The approach assumes that a single vertically continuous, thick sandstone is likely to be more laterally continuous compared to a sequence of thin sandstones interrupted by shale beds. In other words, the direction of alignment of a series of continuously thick sandstones identified at well locations by the density-porosity log cutoff is inferred as the axis of primary or depositional

connectivity.[23] The approach was first tested in the D1 sandstone because of its lateral continuity and homogeneous lithology.[2] A density-porosity log cut-off (DPHI≥10%) was initially used to discriminate between reservoir and non-reservoir quality. **Fig. 30** illustrates how the numbers of sand isopleths were computed.

The number of sand isopleths is inversely related to proximity to the inferred axis of depositional connectivity. Simply stated, the smaller the number of sand isopleths, the closer it is to the inferred axis of depositional connectivity. The sand isopleths are aligned in a northwest direction and located in the central portion (**Fig. 31**). Looking at the larger region, it is observed that the inferred axis of depositional connectivity for the D1 sandstone agrees with the aligned direction of the sand isopleths values of unity in the study area (**Fig. 32**).[60] Similar trends in the axis of depositional connectivity were obtained for the D2 and C sandstones (**Figs. 33** and **34**). Due to general poor reservoir quality in the D3 sandstone, no trend was identified.

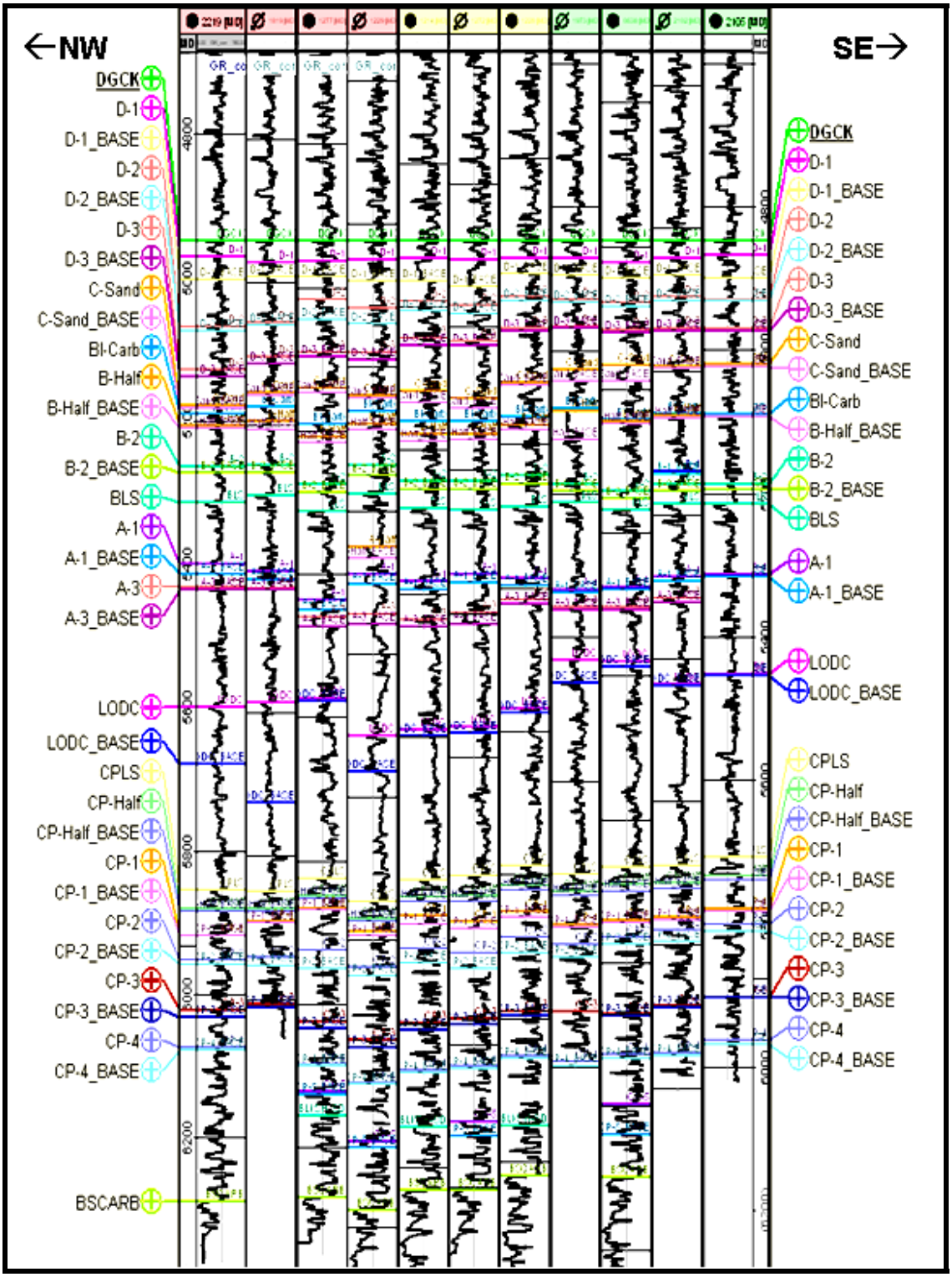

Fig. 27—Stratigraphic section along the northwest-southeast axis. It shows all correlated sand tops and bases below the Douglas Creek marker datum (see Fig. 3 for location).

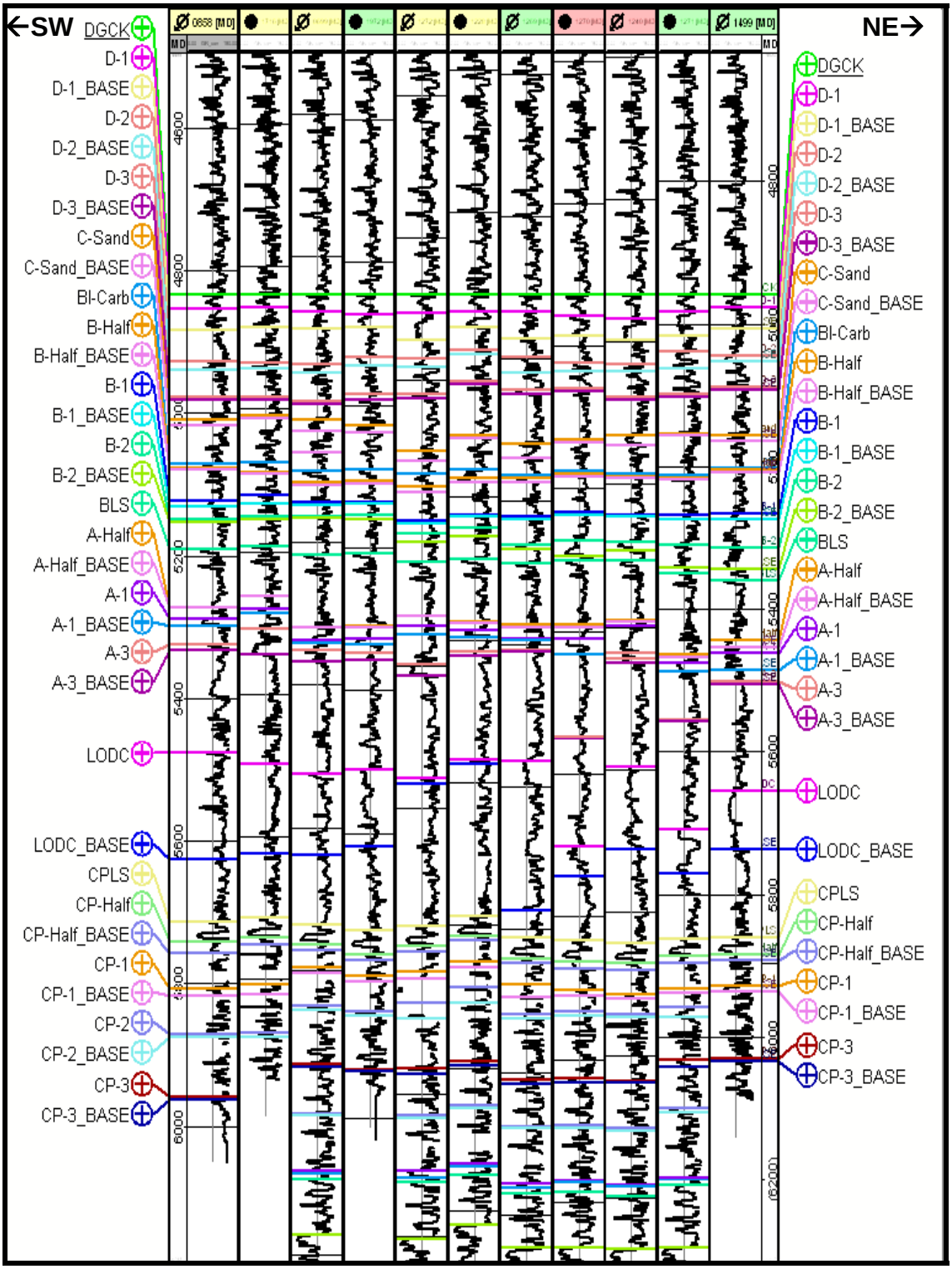

Fig. 28—Stratigraphic section along the southwest-northeast axis. It shows all correlated sand tops and bases below the Douglas Creek marker datum (see Fig. 3 for location).

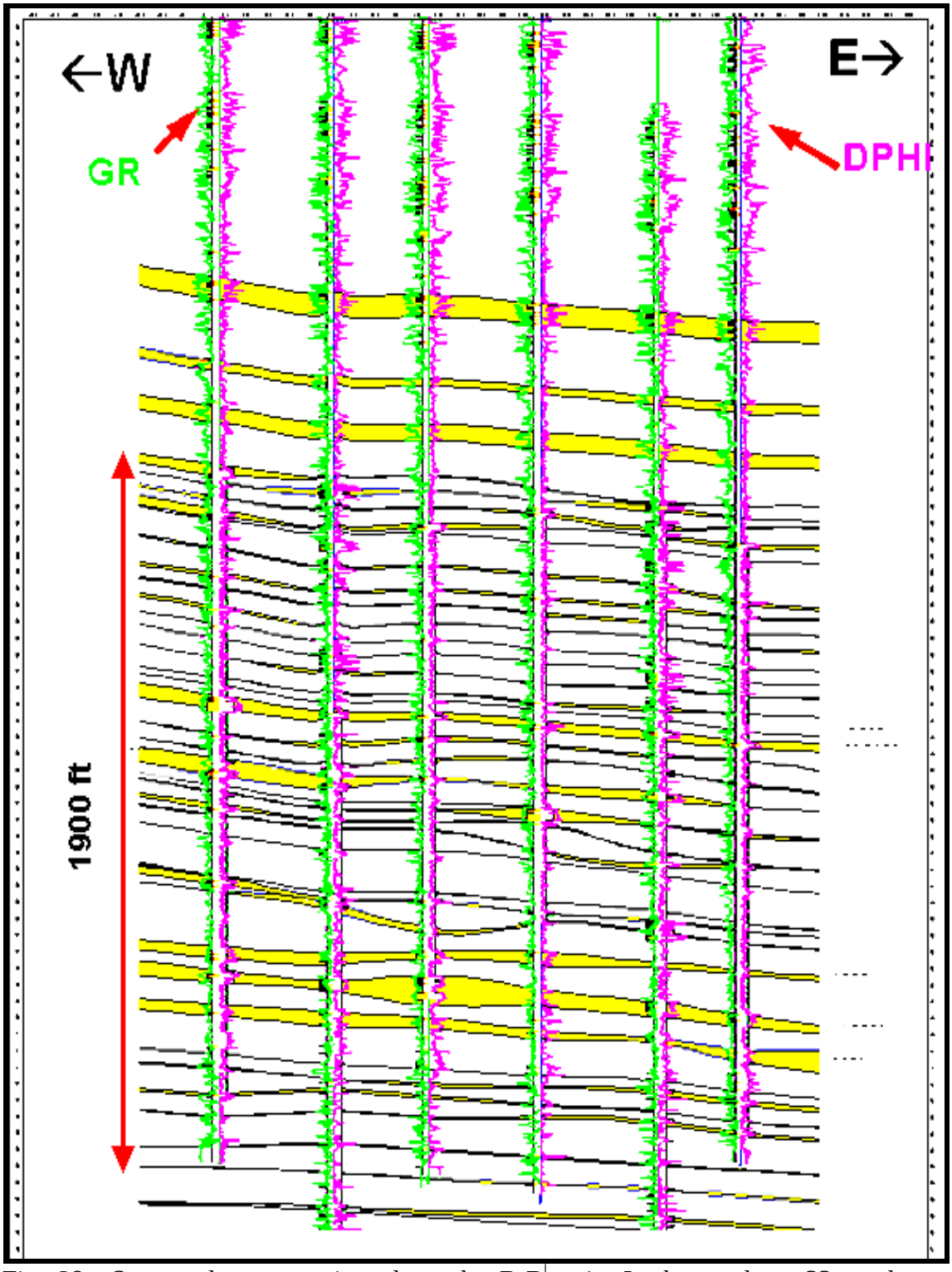

Fig. 29—Structural cross-section along the B-B' axis. It shows about 33 sandstone intervals delineated by well correlation of 68 markers horizon that constitute the reservoir framework (see Fig. 3 for location).

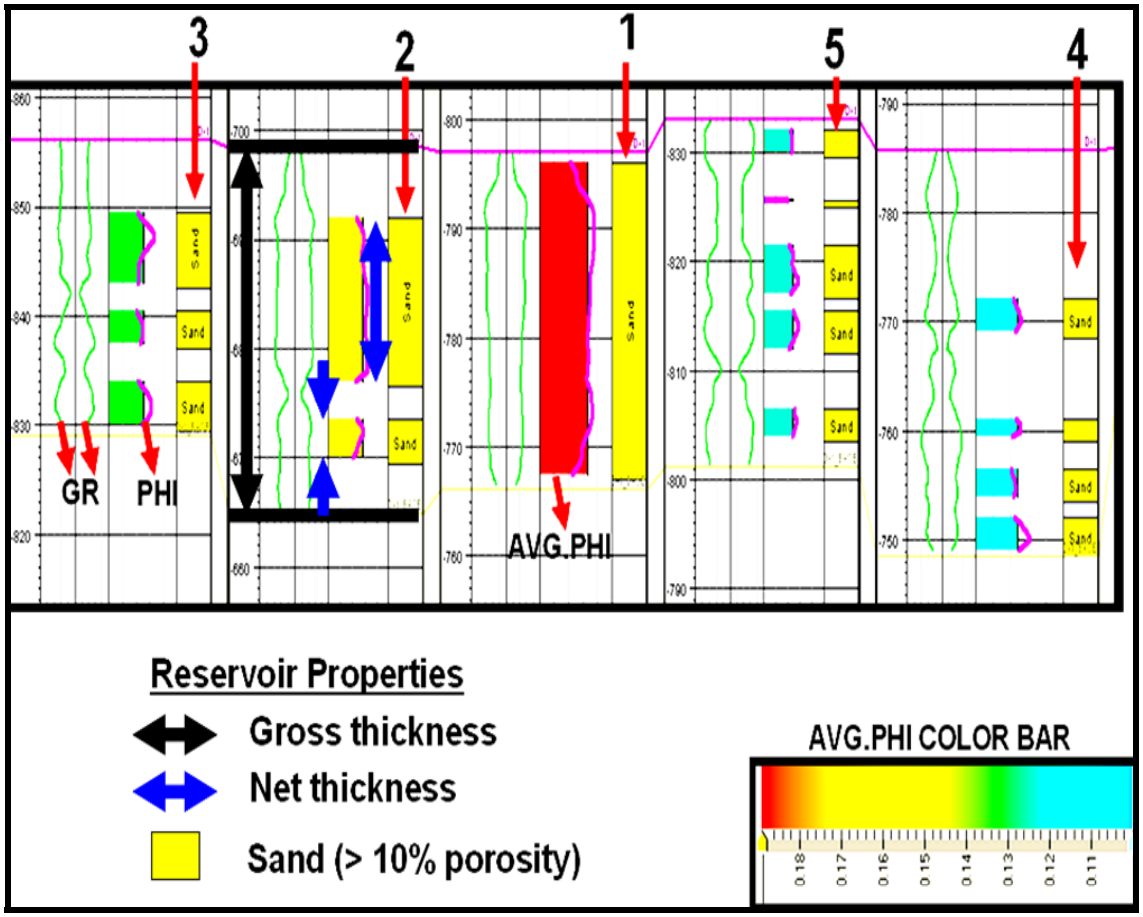

Fig. 30— Illustration of how the numbers of sand isopleths were computed.

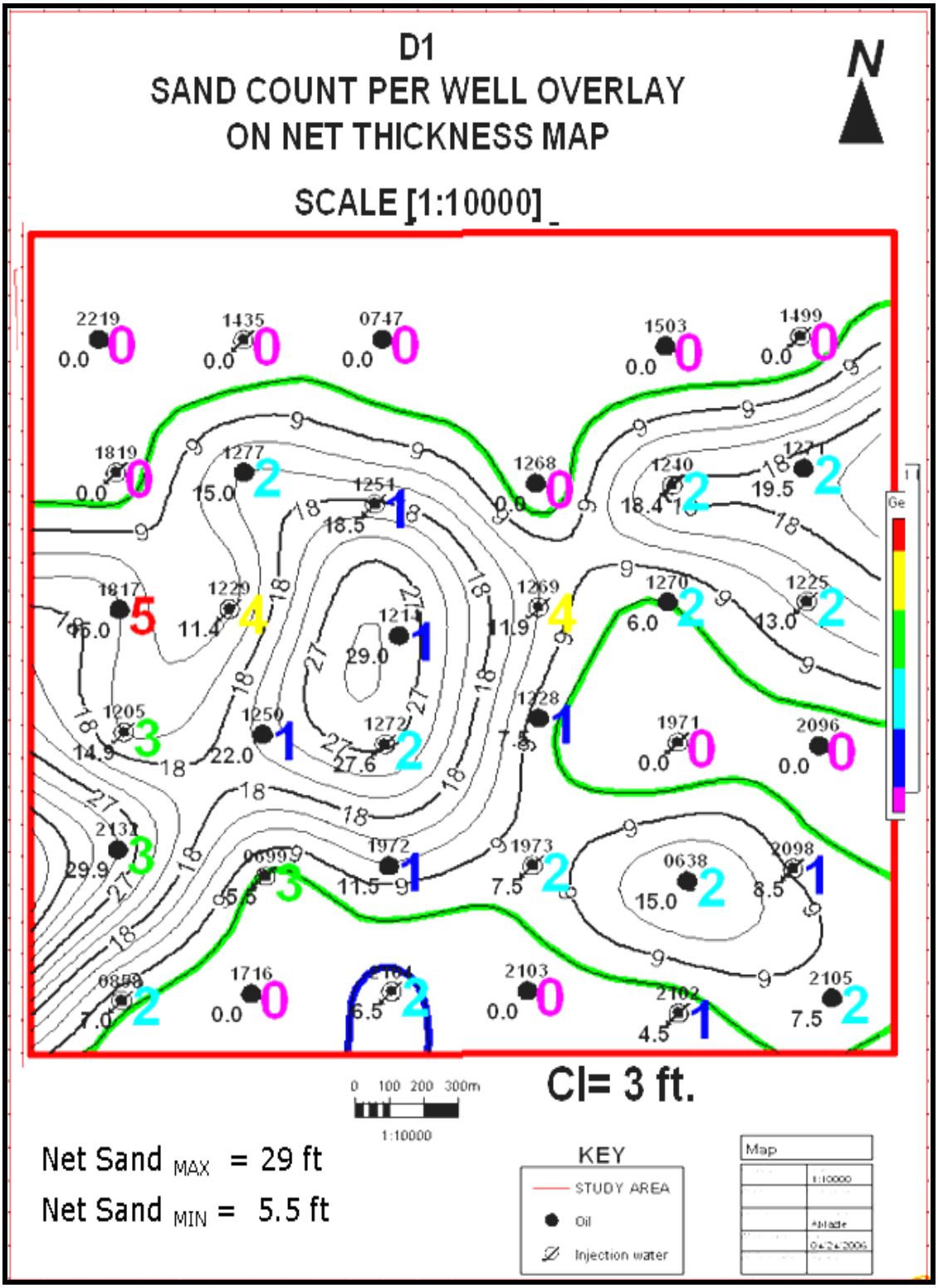

Fig. 31—D1 sand isopleths overlay on net thickness map.

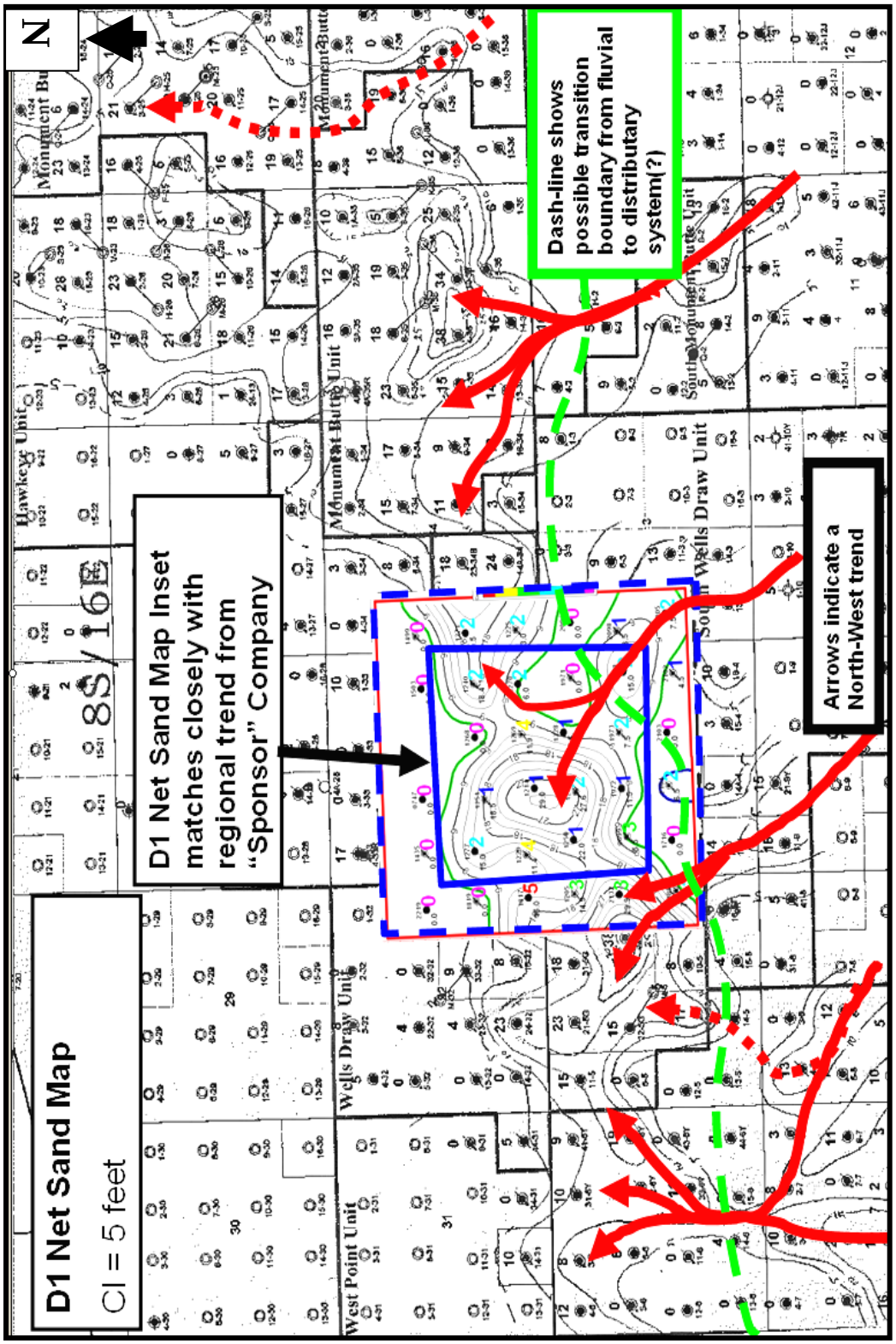

Fig. 32—Interpreted axis of deposition for the D1 sandstone agrees with the aligned direction of the sand isopleths values of unity in the Wells Draw study area.[60]

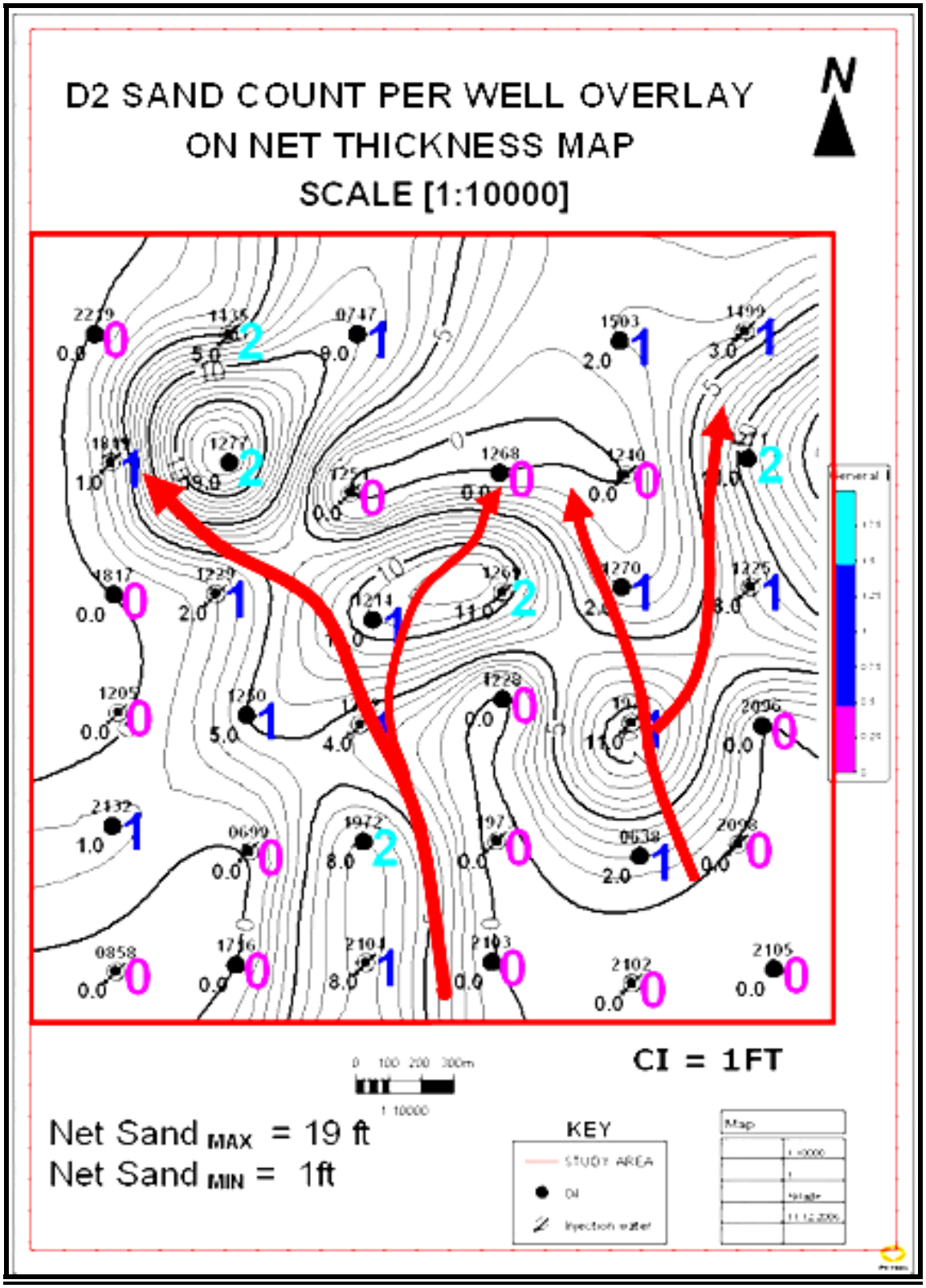

Fig. 33—D2 sand isopleths overlay on net thickness map.

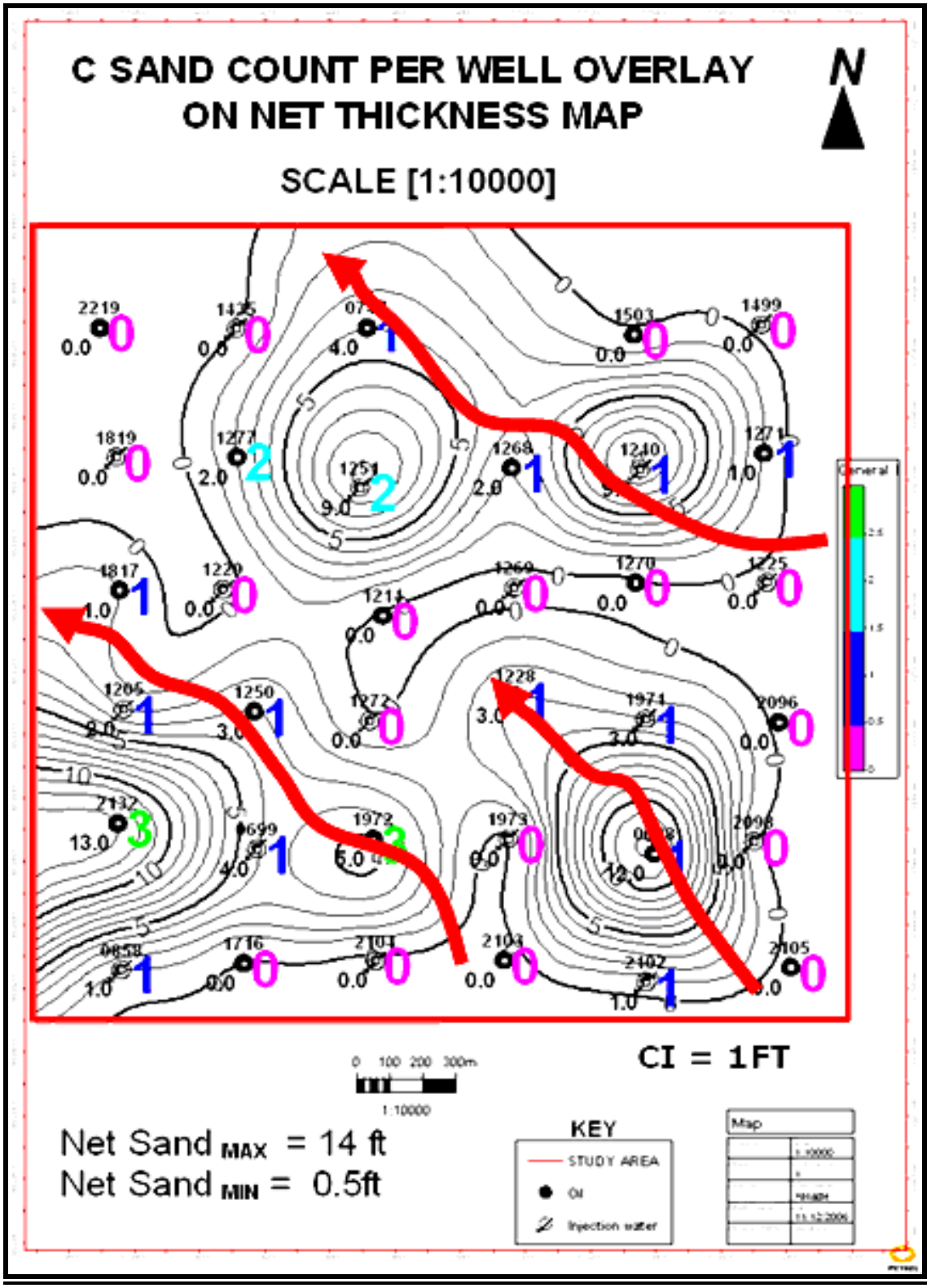

Fig. 34—C sand isopleths overlay on net thickness map.

Reservoir Model Simplifications

Reservoir models can only mimic reality.[21] They are simplified representations of subsurface reservoirs customized for addressing a particular reservoir engineering question. To create a model suitable for set objectives, certain simplifications to the representation of the reservoirs are applied. These include grouping of sand layers into zones, discretization of the model volume into manageable grid cell sizes, and averaging reservoir property in grid cells at well locations. A brief discussion of each simplification is provided.

Sand Layer Zonation

About 33 sandstone layers were delineated by well correlation of 68 marker horizons from the base of Castle Peak to the top of Garden Gulch (Fig. 29). Assigning a zone to each sandstone layer would result in a model with a cumbersome number of zones, especially since the sandstone intervals are separated by thin shales. The zoning was simplified by grouping the 33 sandstone layers into 13 sand zones separated by 9 significant shale zones (**Fig. 35**).

Volume Discretization

Volume discretization of the reservoir framework into a suitable number of grid cells is necessary to model both large- and small-scale heterogeneities observed from all available data. **Table 4** shows the grid cell statistics. The gross rock volume was discretized into a total of 33,462 grid cells. The area of each grid cell is approximately

one acre (1.11 acre), while the thickness varies according to zone thickness. From Table 4, we observe that each grid cell represents a large rock volume.

Averaging Reservoir Properties

For purpose of clarity, it is important to first note that the grid cells referred to in this section are those grid cells penetrated by the well paths. The account for only 2.23% of the gross rock volume characterized (Table 4). The values of reservoir properties assigned to these grid cells remain preserved because they are computed directly from well data. Each of the well-path grid cells represents a large rock volume with variations in reservoir properties. However, a grid cell can have only one value for a given reservoir property.[36] The arithmetic average for net-to-gross ratio and net-porosity are calculated from density-porosity logs for each grid cell penetrated by the well paths. The average values are the initial model input and are used in constructing histograms, semivariograms and correlations for subsequent estimation of reservoir properties at the interwell locations.

Table 4—Grid cell statistics

Cells (nI x nJ x nK)	**39 x 39 x 22**
Nodes (nI x nJ x nK)	**40 x 40 x 23**
No. of 3D cells / nodes	**33,462 / 36,800**
Xinc, Yinc, Zinc	**66 m, 68 m, variable (ft)**
Grid orientation	**0^{o} North**
No. of well-path cells	**749**
Percentage of well-path cells	**2.23 %**
Percentage of interwell cells	**97.77 %**

Zone #	Model Zones	HORIZONS	K
	GB-2	GB-2	1
		GB-2_BASE	2
Zone 1		GB-3	3
		GB-3_BASE	4
		GB-4	5
		GB_4_BASE	6
		GB-6	7
	GB-6_BASE	GB-6_BASE	8
		Pt-3-MKR	9
		GB_Base	10
	PB-7	PB-7	11
		PB-7_BASE	12
		PB-8	13
Zone 3		PB-8_BASE	14
		PB-10	15
		PB-10_BASE	16
		PB-11	17
	PB-11_BASE	PB-11_BASE	18
		X_MKR	19
		Y_MKR	20
Zone 5	D-S2	D-S2	21
		D-S2_BASE	22
		D-S3	23
	D-S3_BASE	D-S3_BASE	24
		DGCK	25
Zone 7	D-1	D-1	26
	D-1_BASE	D-1_BASE	27
Zone 9	D-2	D-2	28
		D-2_BASE	29
		D-3	30
	D-3_BASE	D-3_BASE	31
Zone 11	C-Sand	C-Sand	32
		C-Sand_BASE	33
		BI-Carb	34
		B-Half	35
	B-Half_BASE	B-Half_BASE	36
Zone 13	B-1	B-1	37
		B-1_BASE	38
		B-2	39
	B-2_BASE	B-2_BASE	40
		BLS	41
		BLS_BASE	42
Zone 15	A-Half	A-Half	43
		A-Half_BASE	44
		A-1	45
		A-1_BASE	46
		A-3	47
	A-3_BASE	A-3_BASE	48
Zone 17	LODC	LODC	49
		LODC_BASE	50
		LODC2	51
	LODC2_BASE	LODC2_BASE	52
Zone 19	LODC3	LODC3	53
Zone 20	LODC3_BASE	LODC3_BASE	54
Zone 21	CPLS	CPLS	55
		CP-Half	56
		CP-Half_BASE	57
		CP-1	58
		CP-1_BASE	59
		CP-2	60
		CP-2_BASE	61
		CP-3	62
		CP-3_BASE	63
		CP-4	64
Zone 22	CP-4_BASE	CP-4_BASE	65
		CP-5	66
		CP-5_BASE	67
		BSCARB	

Fig. 35—Zonation of the 33 sandstone layers into 13 sand zones (yellow) separated by 9 significant shale zones (green).

Geostatistical Data Analysis

I conducted geostatistical analysis of the blocked reservoir properties in the 13 sand zones to identify the representative statistics necessary for reservoir characterization. An underlying concept in the use of representative statistics for estimation or simulation is the assumption of stationarity[19] (local independence of moments of mean, variance, skewness and kurtosis). A major implication of stationarity is that the spatial continuity model (semivariogram) is valid at any simulated spatial location. Further discussion of the geostatistical analysis is provided in the following sections.

Histograms, Distributions and Normal Scores

A histogram is created from the blocked values for each reservoir property using the following basic steps. For each reservoir property, the data set is sorted in increasing order and the interval between the largest and smallest value is divided into classes with equal class intervals. The classes are displayed as a function of the number of values belonging to each class. The histograms provided the basis for modeling the probability distribution function (PDF) and the cumulative distribution function (CDF) for each reservoir property. Histograms of the averaged net-to-gross ratio and net-porosity for the combined 13 sand zones (**Figs. 36** and **37**) and the D1 sand zone (**Figs. 38** and **39**) are shown. Also, CDFs for net-porosity in each sand zone were normalized to have a mean of zero and standard deviation of unity. **Fig. 40** shows CDFs of net-porosity (raw score) and transformed net-porosity (normal score) for zones 7, 11, 15 and 17.

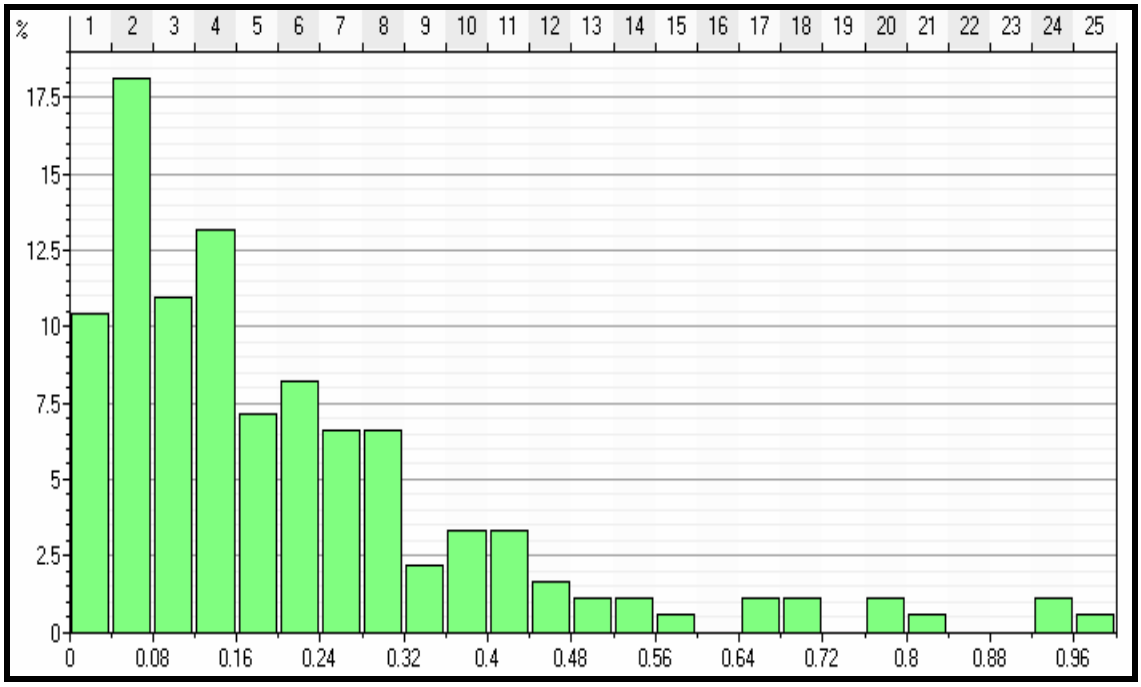

Fig. 36—Histogram of the averaged net-to-gross ratio values for the combined 13 sand zones.

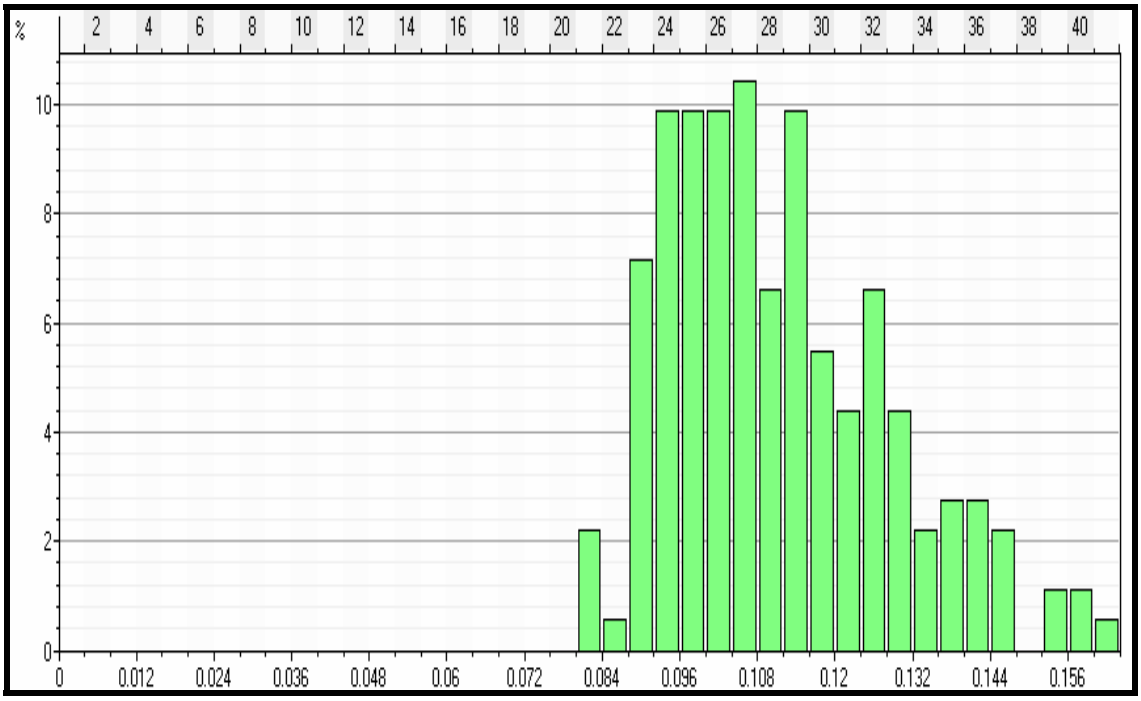

Fig. 37—Histogram of the averaged net-porosity values for the combined 13 sand zones.

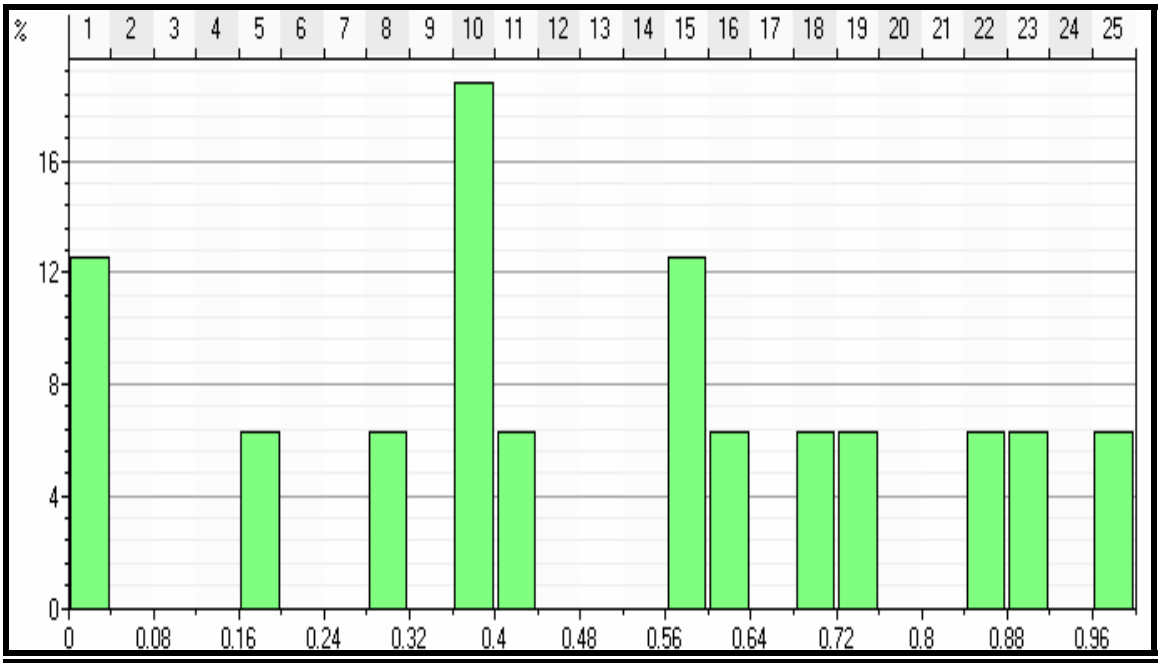

Fig. 38—Histogram of the averaged net-to-gross ratio values for the D1 sand.

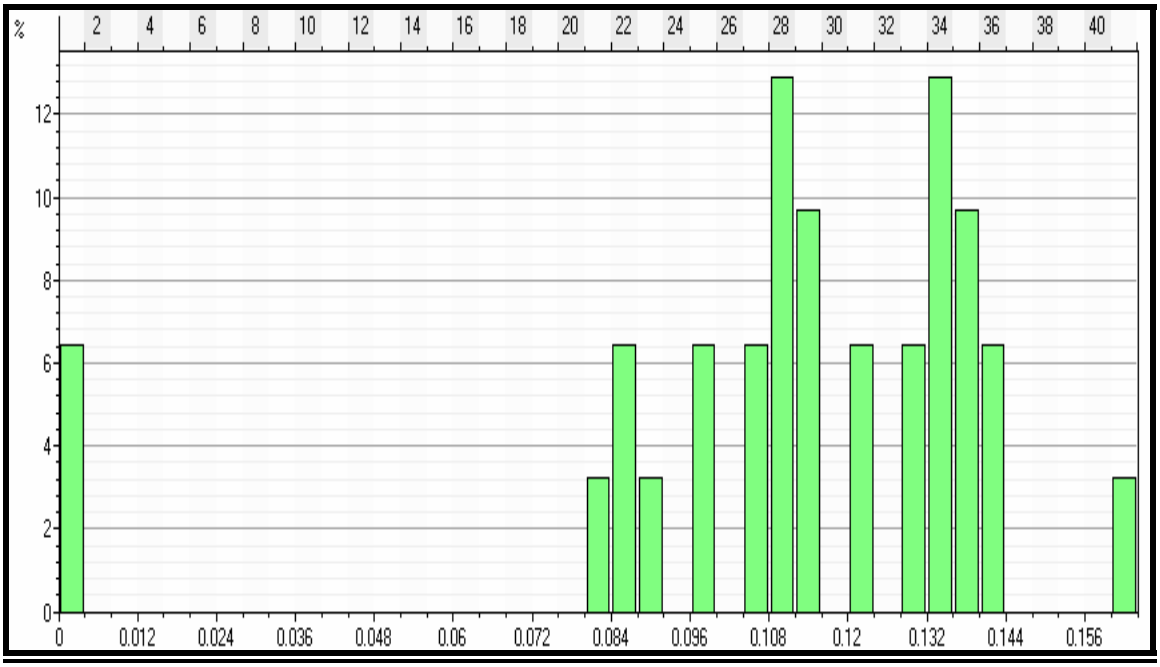

Fig. 39—Histogram of the net-porosity values for the D1 sand.

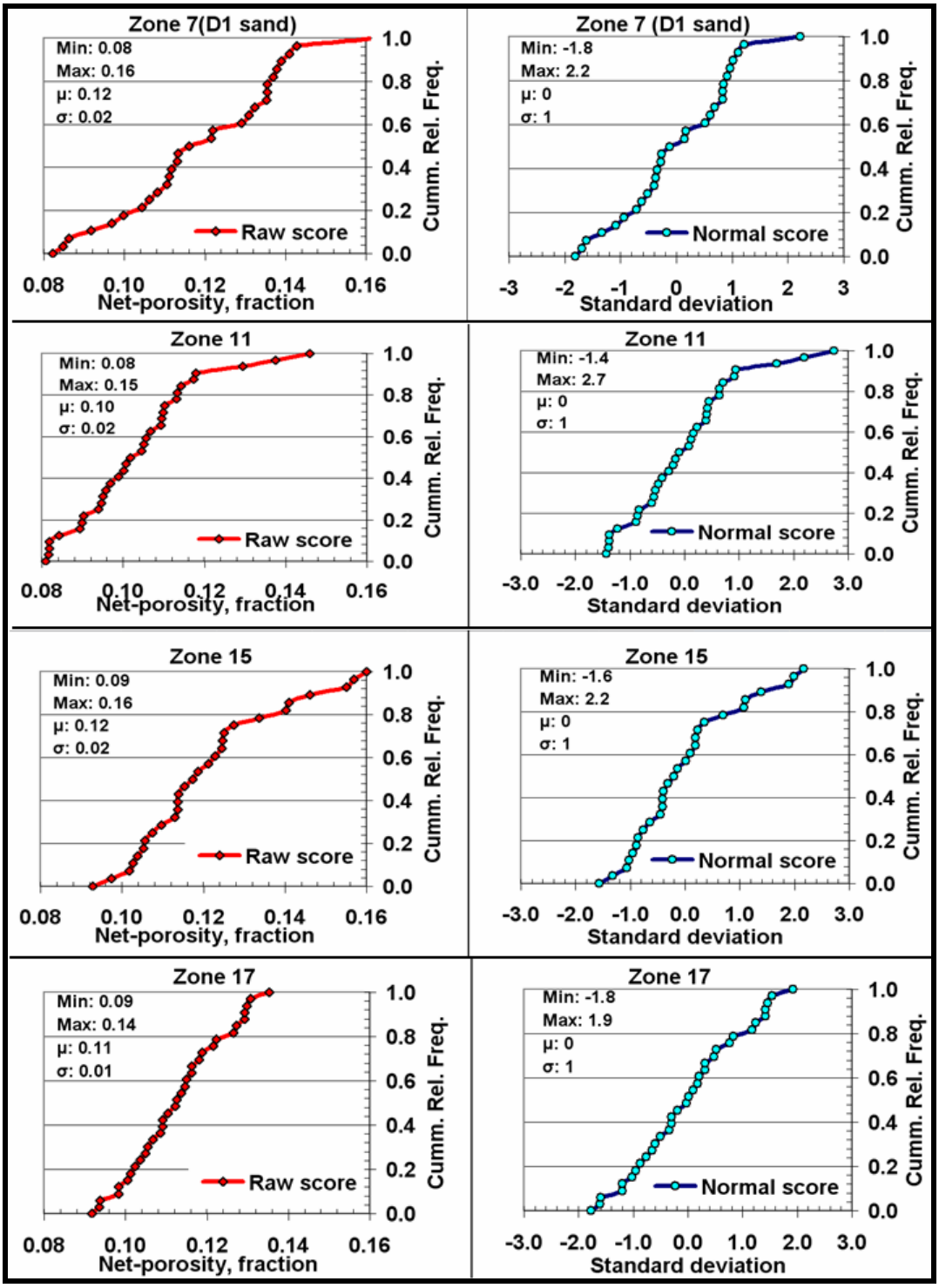

Fig. 40—CDFs of net-porosity (raw score) and transformed net-porosity (normal score) for zones 7, 11, 15 and 17.

Semivariograms and Anisotropy

A semivariogram shows the dissimilarity or semivariance between data points as a function of separation distance along a specified direction in a sample data set.[19,27,31] Semivariance is defined as one-half of the averaged squared difference between data pairs. A semivariogram is used to split the overall sample variance into a spatially related variance. Semivariogram analysis was performed on normal score transforms of net-porosity for each sand zone (Fig. 40). **Fig. 41** shows sample and modeled semivariograms along major axes of net-porosity in zones 7, 11, 15 and 17. The semivariance is plotted on the y-axis as a function of the separation distance on the x-axis. The sill or plateau is the largest semivariance between data pairs and represents the statistical variance of the sample data. The nugget is the semivariance between data points that are very close to each other with a near-zero separation distance. The range or correlation length is the distance to the sill for which data points have some degree of similarity and beyond which the variogram model reaches its plateau where no change or transition in degree of correlation between data pairs is observed. A range that changes with direction indicates anisotropy in spatial continuity. The range is characteristically shorter in the vertical or depth direction compared to the horizontal direction in most reservoirs due to cyclicity resulting from geological stratification and layering. When calculated in several 3D directions, the variation of the range typically displays an ellipsoidal behavior. Such an ellipsoid can be quantified in terms of five parameters namely: the ranges along major, minor and vertical axis; and the rotation parameters

defining its 3D orientation in terms of dip and azimuth. I used the spherical variogram model to determine anisotropy parameters for net-porosity in each sand zone (**Table 5**).

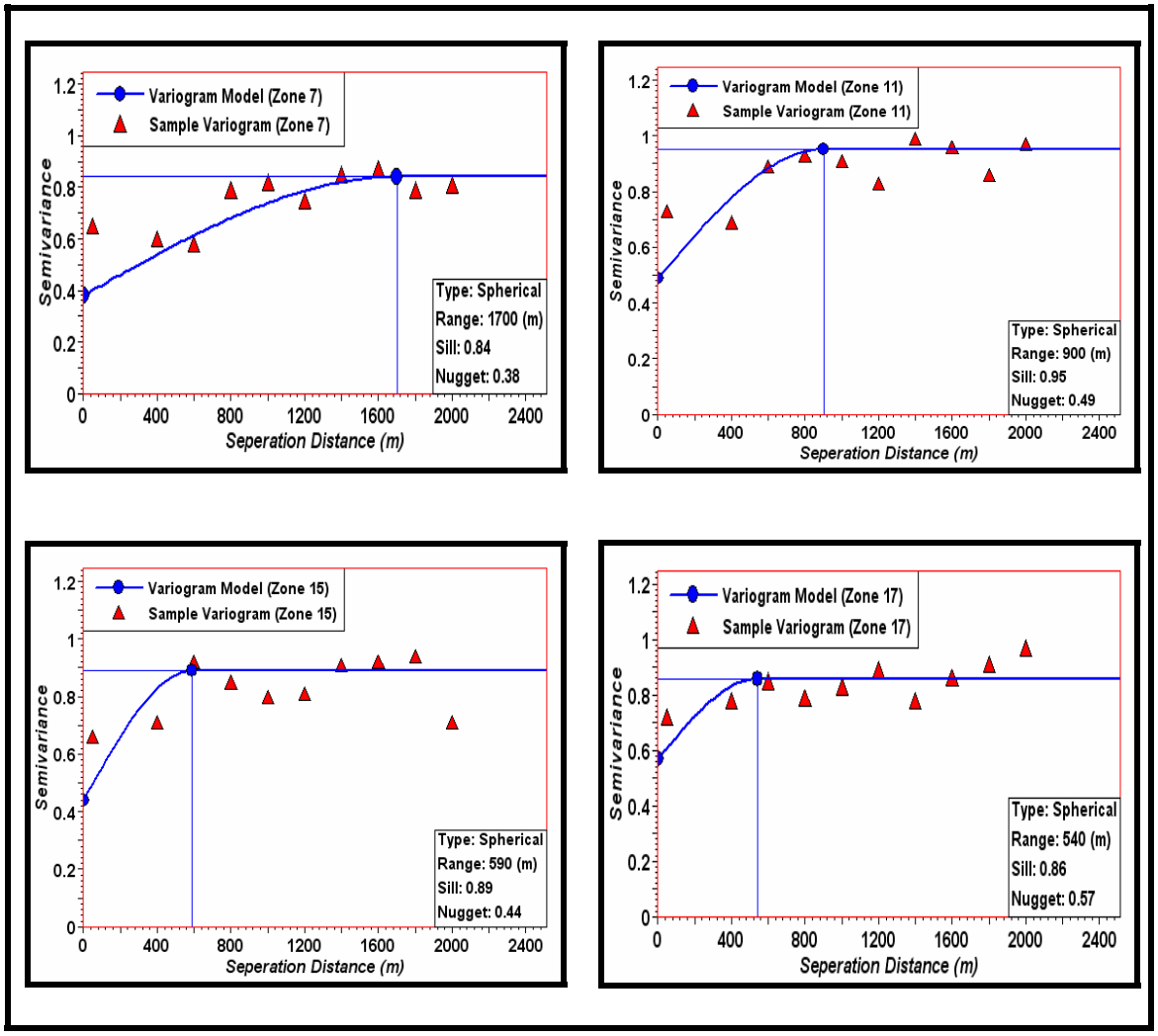

Fig. 41—Sample and modeled semivariograms along major axes of net-porosity in zones 7, 11, 15 and 17.

Table 5—Net-porosity anisotropy models for the 13 sand zones.

Zone #	Major Axis (m)	Minor Axis (m)	Vertical Axis (m)	Dip (deg.)	Azimuth (deg.)
1	1050	500	11	0	80
3	300	200	10	0	-30
5	350	170	6	0	7
7	1700	600	12	0	75
9	900	350	6	0	5
11	900	590	5	0	93
13	800	300	7	0	-3
15	590	430	13	0	2
17	540	350	37	0	129
19	520	310	15	0	105
20	410	370	12	0	15
21	380	220	13	0	23
22	280	150	9	0	21

Crossplots and Correlations

Since, I applied a density porosity log cutoff (≥8%) to identify net sandstones within the reservoirs, a relationship exists between the two. Crossplots were used to determine the correlation coefficients between net-to-gross ratio and net-porosity for the 13 sand zones. **Fig. 42** shows the correlation between net-to-gross ratio and net-porosity for sand zones 7, 11, 15 and 17

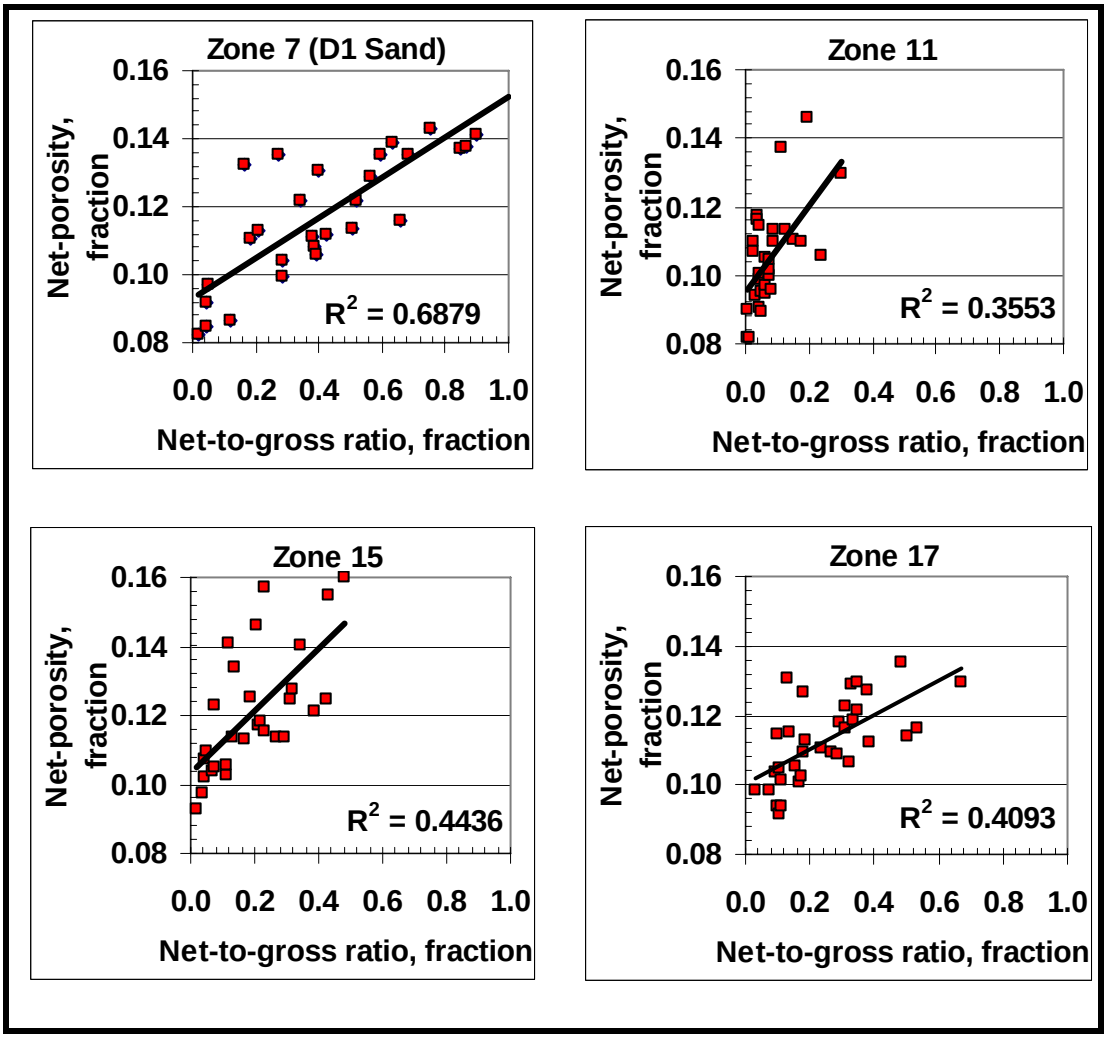

Fig. 42—Correlation between net-to-gross ratio and net-porosity for sand zones 7, 11, 15 and 17.

Characterization Techniques

The deterministic and geostatistical techniques used are presented.

Deterministic Technique

The moving average algorithm[34,38] was used to create a deterministic net-to-gross ratio model. This algorithm uses the square of inverse distance in a search radius neighborhood in weighting data points to determine average value at interwell locations. Thus, distant points have lesser influence on the determined average.

Geostatistical Technique

I used an established geostatistical technique that combines the sequential simulation of net-porosity conditional to a net-to-gross ratio co-variable. This technique is referred to as the sequential Gaussian simulation (SGS) algorithm with collocated cokriging.[21,31,32] The purpose of this technique is to generate several realizations of net-porosity models that reflect the continuity quantified in the porosity semivariogram, have the observed correlation with the net-to-gross ratio model, and honor the average net-porosity values in the well-path grid cells. The SGS algorithm is widely used and highly recommended in the literature because the ease of establishing conditional distributions. [21,31,32]

The SGS algorithm requires the sample data be transformed to have a mean of zero and a variance of unity. Thus, the first step involved the transformation of averaged net-porosity distribution to a normal distribution (Fig. 40). Secondly, a net-porosity value for an interwell location was randomly selected from the transformed net-porosity

distribution. Thirdly, conditional distributions were calculated by kriging and constrained by the normalized CDFs (Fig. 40), semivariograms (Fig. 41), correlation coefficients (Fig. 42) and a covariable net-gross model. Finally, the simulation results are back-transformed to the original data distribution. The simulation process was repeated until 21 net-porosity realizations were simulated for the 13 sand zones. Through out the simulation process, net-porosity values at the well-path grid cells were honored and unchanged.

Estimated and Simulated Properties

The estimated and simulated reservoir properties for the 13 sand zones are:

1. one estimated net-to-gross ratio model using the moving average algorithm
2. 21 simulated net-porosity realizations using the SGS algorithm with collocated cokriging
3. 21 permeability models each derived from 21 net-porosity realizations by a correlation obtained from core porosity-permeability analysis (Fig. 8).

Fig. 43 is the map of net-to-gross ratio for the D1 sandstone determined using the moving average algorithm. The output range for estimated net-to-gross ratio (0 to 1) corresponds to the input range (Fig. 38). **Fig. 44a-d** shows four of 21 net-porosity realizations simulated for the D1 sandstone. **Figs. 45a-d** shows the horizontal permeability models derived from the net-porosity realizations for the D1 sandstone using the correlation from core porosity-permeability analysis (Fig. 8). The horizontal permeability range (1 to 13 md) for all 21 models fall within the permeability range from the core analysis data (1 to 21 md). Vertical permeability models are derived using a horizontal to vertical permeability ratio of 0.1.

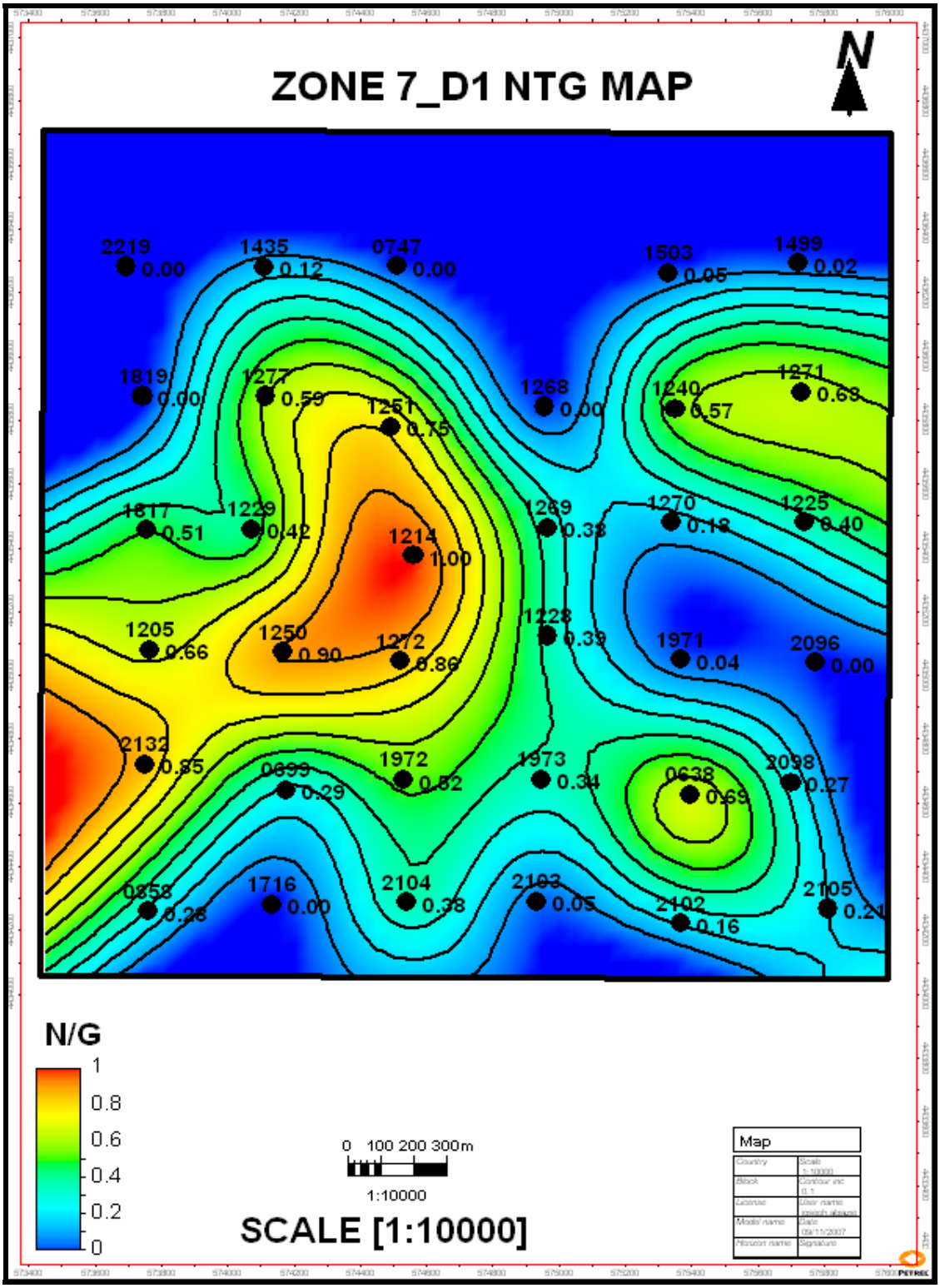

Fig. 43—Map of net-to-gross ratio for the D1 sandstone determined using the moving average algorithm.

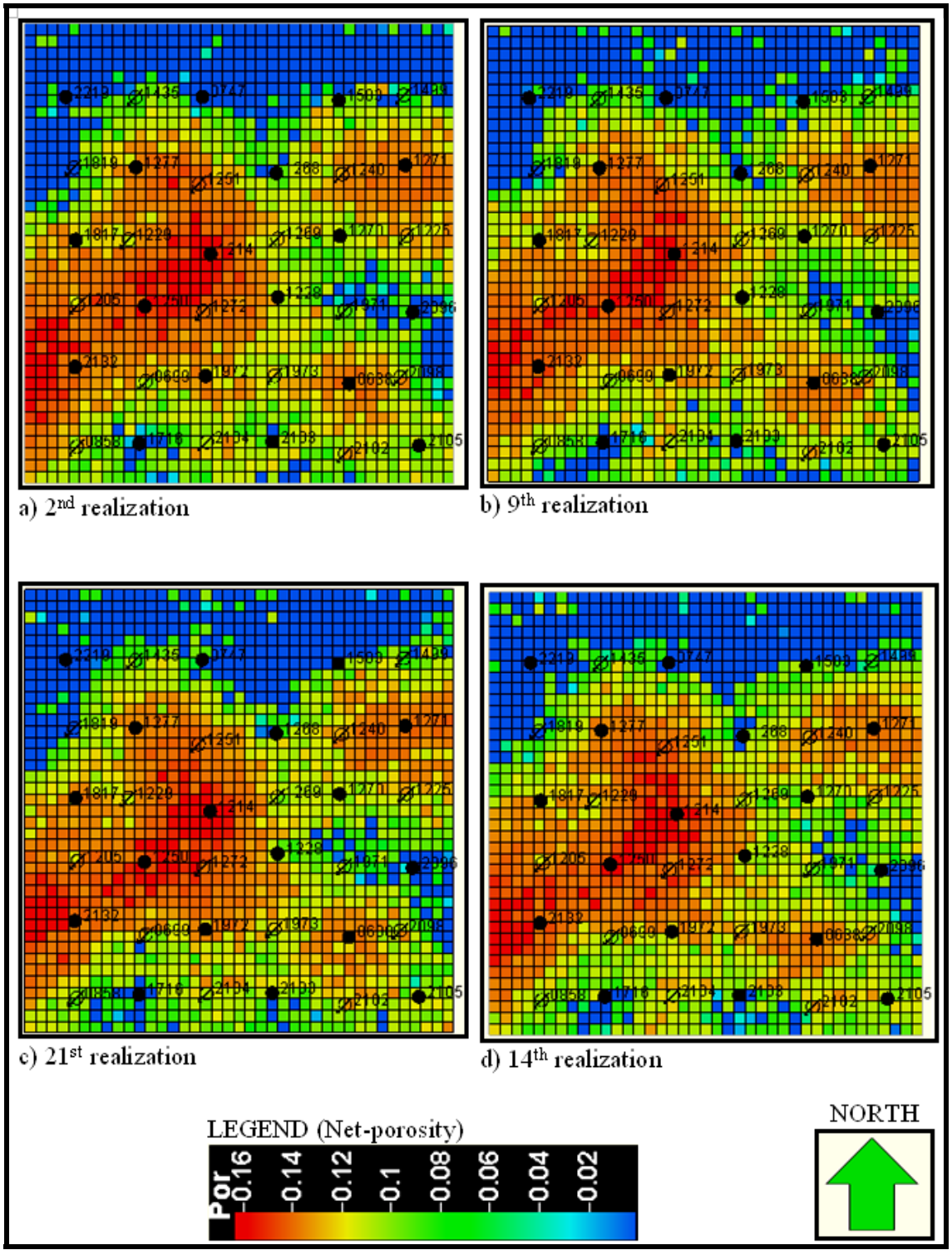

Fig. 44—Four realizations of net-porosity distribution in the D1 sandstone.

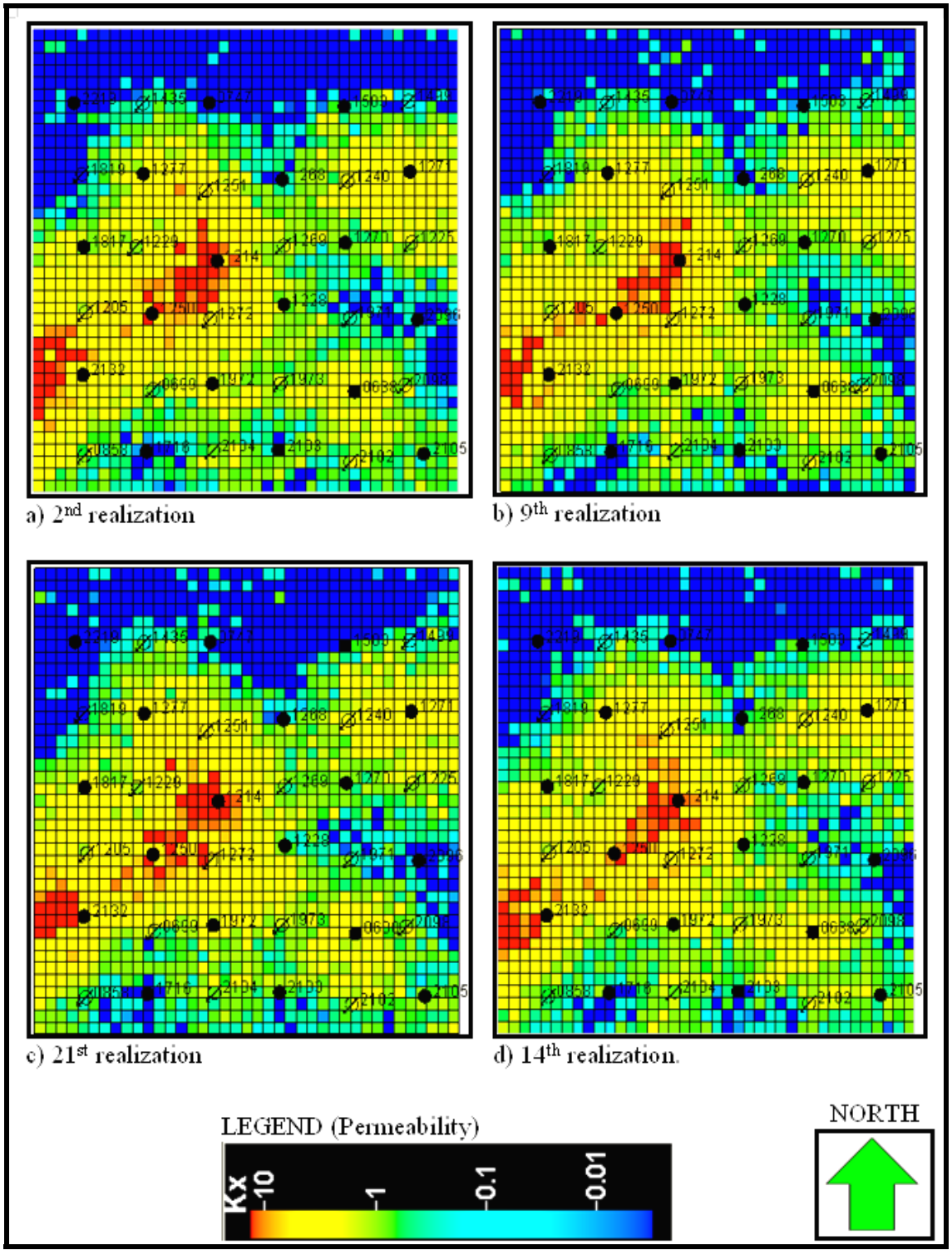

Fig. 45—Four realizations of permeability distribution in the D1 sandstone.

Pore Volume Ranking

Deutsch and Srinivasan[40] assessed the applicability of the pore volume ranking index. In line with the above, I selected the mean pore volume ranking parameter to weight the net-porosity with the product of net-to-gross ratio and cell bulk volume models. Firstly, pore volume is calculated for each grid cell in the reservoir model from a product of three other properties namely cell bulk volume, net-to-gross ratio ratio, and net-porosity. Since, we have one bulk-volume model from the volume discretization of the reservoir framework, one deterministic net-to-gross ratio model and 21 porosity realizations, the resulting pore volume models reflect only the uncertainty in porosity distribution. The pore volume of the sand zones for each realization was used to construct a cumulative relative frequency curve (**Fig. 46**). From Fig. 46, I selected the low case (P_{25}), base case (P_{50}) and high case (P_{75}) and recommended them for reservoir simulation assessments.

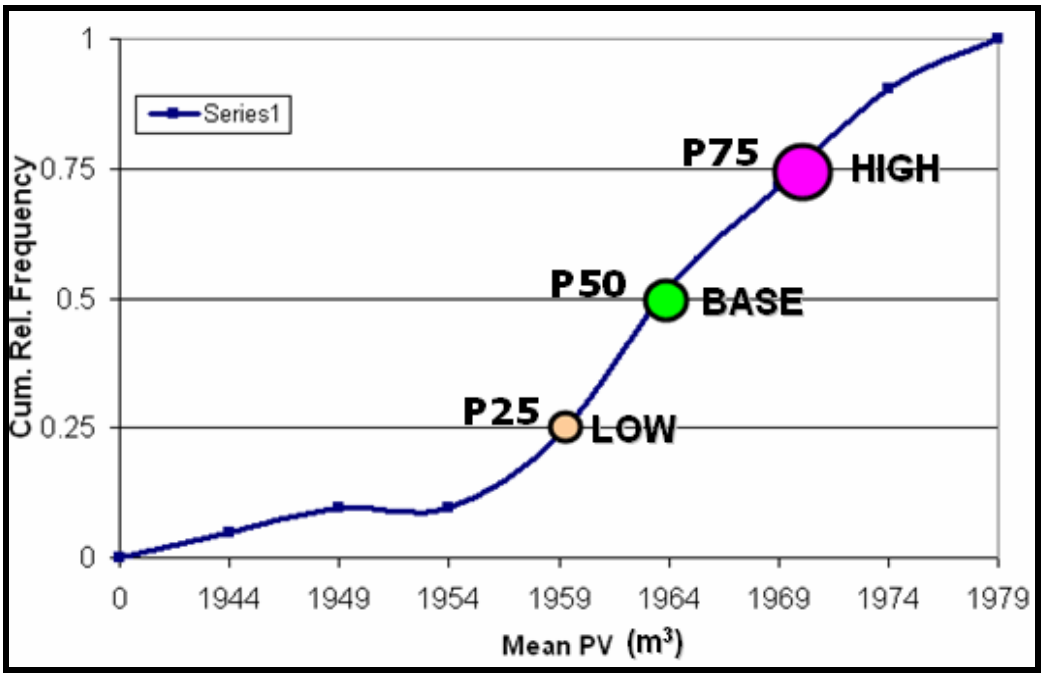

Fig. 46—Static ranking of average pore volume for the 21 realizations.

CHAPTER IV

INTERWELL CONNECTIVITY EVALUATION

Details of the interwell connectivity evaluation are presented. The spreadsheet application developed for the evaluation is henceforth referred to as interwell connectivity analysis program (ICAP).

ICAP Input Spreadsheet

The program requires three spreadsheet input:

1. A spreadsheet containing all 35 study wells in column-one and all the wells adjacent to each well in subsequent columns (**Fig. 47**).

2. A second spreadsheet containing the net sandstone thickness arranged by layer rows by well columns (**Fig. 48)**.

3. A third spreadsheet containing the perforated thickness arranged by layer rows by well columns (**Fig. 49)**.

How ICAP Works

ICAP links the three input spreadsheets and returns a number to indicate the presence of static or hydraulic connectivity between each well-pair penetrating a gross unit or zero where static or hydraulic connectivity is absent. **Fig. 50** shows two visualizations: (1) ICAP simulation model zone-based results for three adjacent wells and (2) Flow barrier assignment in simulation model based on ICAP visualization.

The flow barriers constrain fluid movement between wells in the simulation process. The constraint is due to zoning of the sand layers in the simulation model.

WELLS	ADJACENT WELLS			
0858	2132	0699	1716	
2132	1205	1250	0699	1716
1205	1817	1229	1250	0699
1817	1819	1277	1229	1250
1819	2219	1435	1277	1229
2219	1435	1277		
1716	0699	1972	2104	
0699	1250	1272	1972	2104
1250	1229	1214	1272	1972
1229	1277	1251	1214	1272
1277	1435	0747	1251	1214
1435	0747	1251		
2104	1972	1973	2103	
1972	1272	1228	1973	2103
1272	1214	1269	1228	1973
1214	1251	1268	1269	1228
1251	0747	1268	1269	
0747	1268			
2103	1973	0638	2102	
1973	1228	1971	0638	2102
1228	1269	1270	1971	0638
1269	1268	1240	1270	1971
1268	1503	1240	1270	
2102	0638	2098	2105	
0638	1971	2096	2098	2105
1971	1270	1225	2096	2098
1270	1240	1271	1225	2096
1240	1503	1499	1271	1225
1503	1499	1271		
2105	2098			
2098	2096			
2096	1225			
1225	1271			
1271	1499			
1499				

Net_thickness / Perf_thickness \ **Adjwells** / Chart / Z21H

Fig. 47— Input adjacent wells spreadsheet for ICAP.

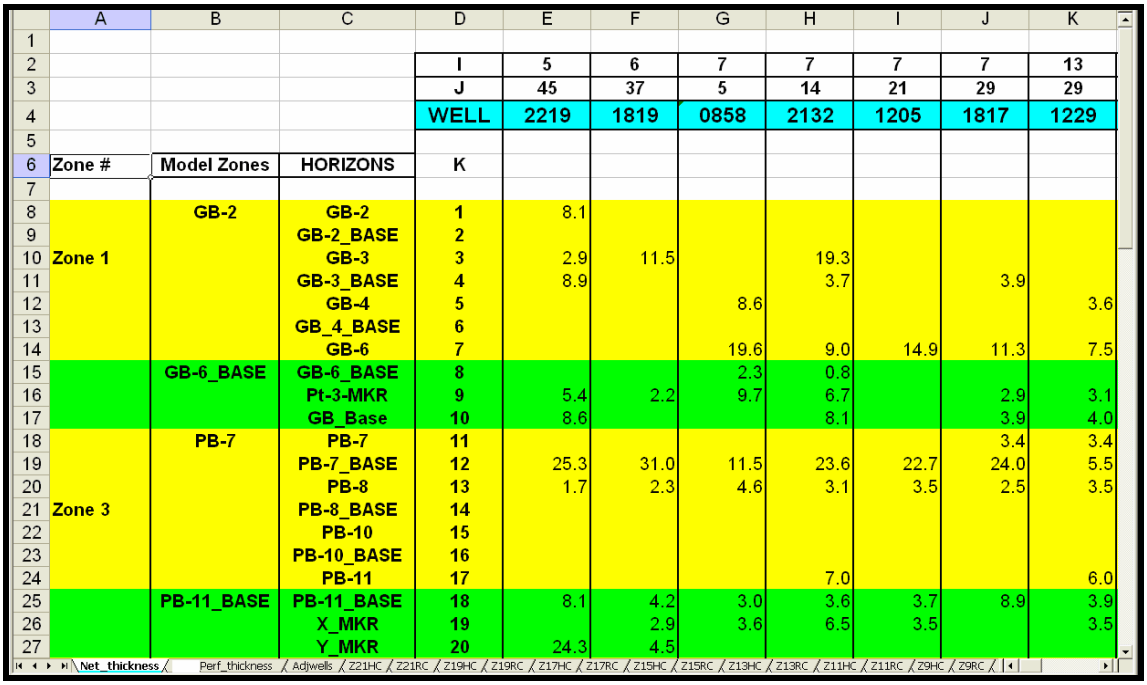

	A	B	C	D	E	F	G	H	I	J	K
1											
2				I	5	6	7	7	7	7	13
3				J	45	37	5	14	21	29	29
4				WELL	2219	1819	0858	2132	1205	1817	1229
5											
6	Zone #	Model Zones	HORIZONS	K							
7											
8		GB-2	GB-2	1	8.1						
9			GB-2_BASE	2							
10	Zone 1		GB-3	3	2.9	11.5		19.3			
11			GB-3_BASE	4	8.9			3.7		3.9	
12			GB-4	5			8.6				3.6
13			GB_4_BASE	6							
14			GB-6	7			19.6	9.0	14.9	11.3	7.5
15		GB-6_BASE	GB-6_BASE	8			2.3	0.8			
16			Pt-3-MKR	9	5.4	2.2	9.7	6.7		2.9	3.1
17			GB_Base	10	8.6			8.1		3.9	4.0
18		PB-7	PB-7	11						3.4	3.4
19			PB-7_BASE	12	25.3	31.0	11.5	23.6	22.7	24.0	5.5
20			PB-8	13	1.7	2.3	4.6	3.1	3.5	2.5	3.5
21	Zone 3		PB-8_BASE	14							
22			PB-10	15							
23			PB-10_BASE	16							
24			PB-11	17				7.0			6.0
25		PB-11_BASE	PB-11_BASE	18	8.1	4.2	3.0	3.6	3.7	8.9	3.9
26			X_MKR	19		2.9	3.6	6.5	3.5		3.5
27			Y_MKR	20	24.3	4.5					

Net_thickness | Perf_thickness | Adjwells | Z21HC | Z21RC | Z19HC | Z19RC | Z17HC | Z17RC | Z15HC | Z15RC | Z13HC | Z13RC | Z11HC | Z11RC | Z9HC | Z9RC

Fig. 48— Input **Net thickness** spreadsheet for ICAP.

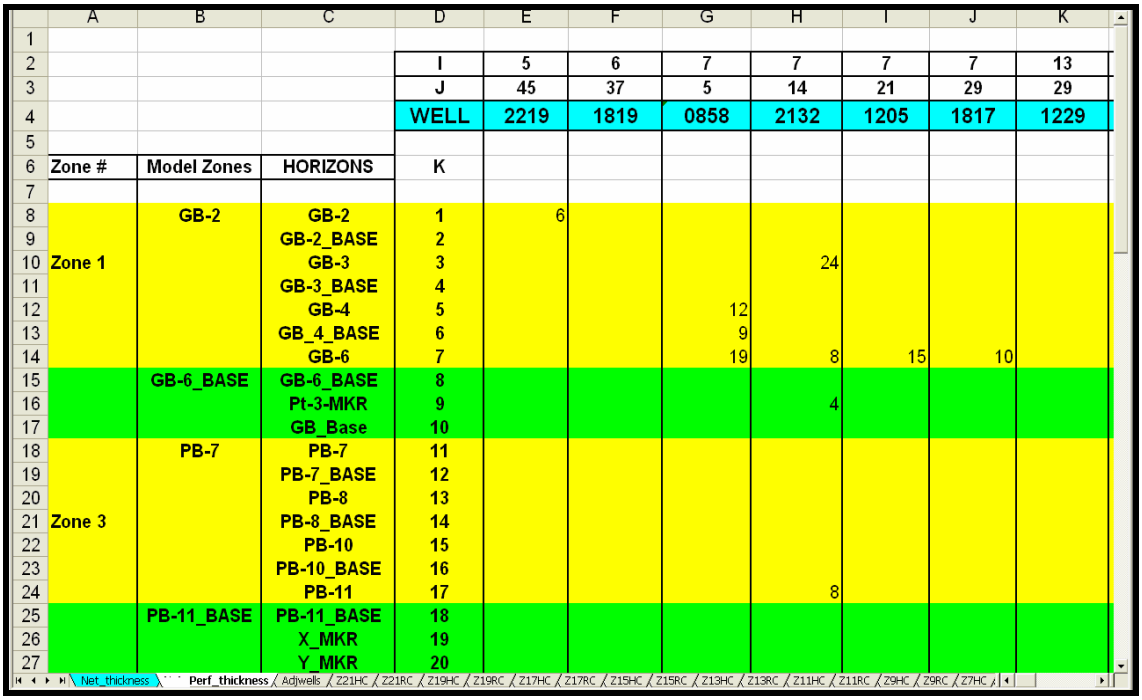

	A	B	C	D	E	F	G	H	I	J	K
1											
2				I	5	6	7	7	7	7	13
3				J	45	37	5	14	21	29	29
4				WELL	2219	1819	0858	2132	1205	1817	1229
5											
6	Zone #	Model Zones	HORIZONS	K							
7											
8		GB-2	GB-2	1	6						
9			GB-2_BASE	2							
10	Zone 1		GB-3	3				24			
11			GB-3_BASE	4							
12			GB-4	5			12				
13			GB_4_BASE	6			9				
14			GB-6	7			19	8	15	10	
15		GB-6_BASE	GB-6_BASE	8							
16			Pt-3-MKR	9				4			
17			GB_Base	10							
18		PB-7	PB-7	11							
19			PB-7_BASE	12							
20			PB-8	13							
21	Zone 3		PB-8_BASE	14							
22			PB-10	15							
23			PB-10_BASE	16							
24			PB-11	17				8			
25		PB-11_BASE	PB-11_BASE	18							
26			X_MKR	19							
27			Y_MKR	20							

Net_thickness | Perf_thickness | Adjwells | Z21HC | Z21RC | Z19HC | Z19RC | Z17HC | Z17RC | Z15HC | Z15RC | Z13HC | Z13RC | Z11HC | Z11RC | Z9HC | Z9RC | Z7HC

Fig. 49— Input **perforated thickness** spreadsheet for ICAP.

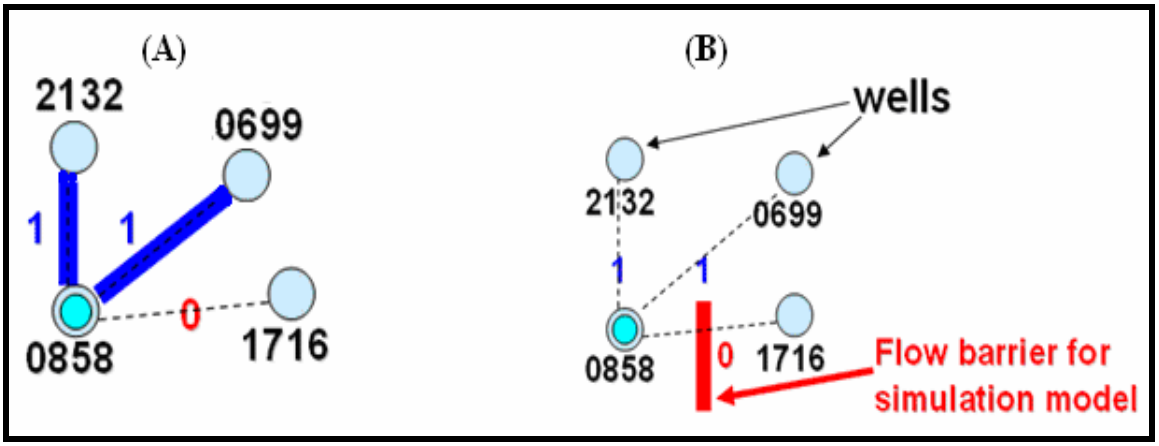

Fig. 50— ICAP connectivity visualization (A) for flow barrier indication (B).

How ICAP Calculates Static Connectivity

Fig. 51 shows an example net thickness spreadsheet used to illustrate the logic of how ICAP calculates static connectivity. For the purpose of illustration, calculation of static connectivity for wells 0858 and 2132 in zone 1 is used as an example. In Fig. 51, seven layers or identified by a porosity log cutoff (≥8%DPHI) and correlated across the 35 wells have been grouped together as zone 1 in the simulation model. For zone 1, using the porosity cutoff, two net thickness values were identified for layers GB-4 and GB-6 in well 0858 while three net thickness values were identified for layers GB-3, GB-3_BASE and GB-6 in well 2132 (focus is within the red square in Fig. 51). In zone 1 net thickness values were identified for both wells 0858 and 2132 only in layer GB-6. Thus ICAP will return an initial value of unity for both wells 0858 and 2132 in layer GB-6 and a value of zero for each of the other six layers in zone 1. Summing up the initial values yields a static connectivity value of unity for wells 0858 and 2132 in zone 1 for this example (see Fig. 50 for the visualization). In the same manner, ICAP will return a

static connectivity value of 2 for wells 0858 and 2132 in zone 3 (focus is within the blue square in Fig. 51). There are cases where the porosity cutoff identifies net thickness values in the thin shale layers within the larger reservoir zones in the 3D model. For example, in zone 1 the porosity cutoff identified a net thickness value for layer GB-3_BASE in well 2132. Layer GB-3_BASE represents a thin shale layer between two sand layers namely GB-3 and GB-4 within the larger zone 1 in the 3D model. This is the situation in some zones but these cases are not significant.

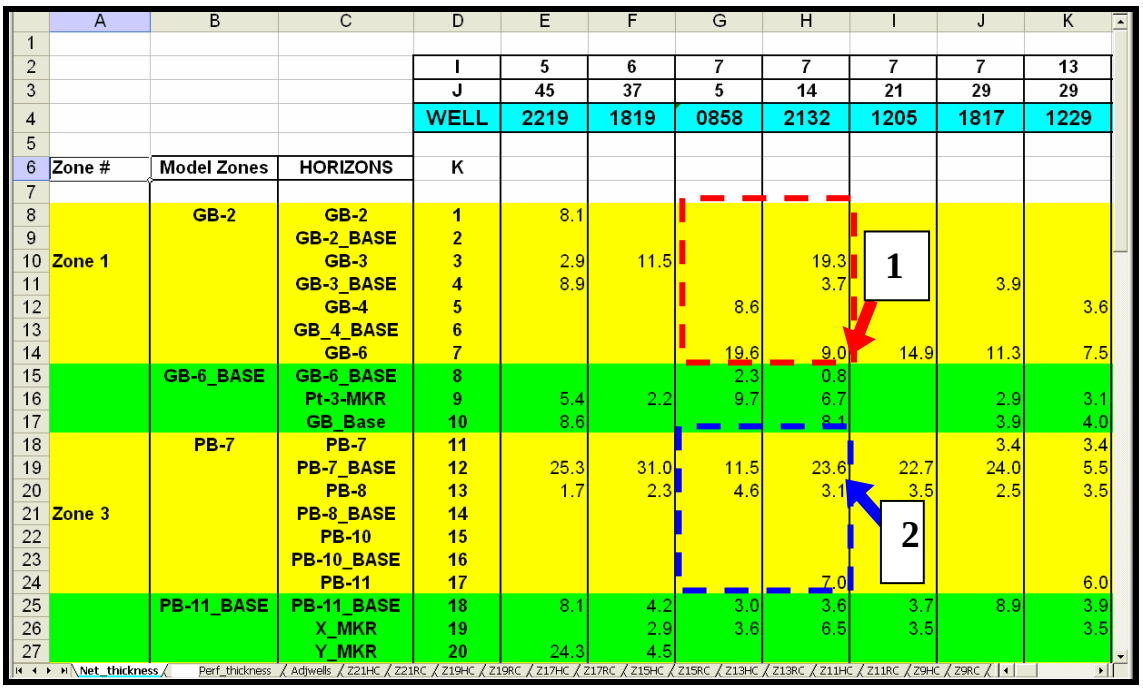

	A	B	C	D	E	F	G	H	I	J	K
1											
2				I	5	6	7	7	7	7	13
3				J	45	37	5	14	21	29	29
4				WELL	2219	1819	0858	2132	1205	1817	1229
5											
6	Zone #	Model Zones	HORIZONS	K							
7											
8		GB-2	GB-2	1	8.1						
9			GB-2_BASE	2							
10	Zone 1		GB-3	3	2.9	11.5		19.3			
11			GB-3_BASE	4	8.9			3.7		3.9	
12			GB-4	5			8.6				3.6
13			GB_4_BASE	6							
14			GB-6	7			19.6	9.0	14.9	11.3	7.5
15		GB-6_BASE	GB-6_BASE	8			2.3	0.8			
16			Pt-3-MKR	9	5.4	2.2	9.7	6.7		2.9	3.1
17			GB_Base	10	8.6			8.1		3.9	4.0
18		PB-7	PB-7	11						3.4	3.4
19			PB-7_BASE	12	25.3	31.0	11.5	23.6	22.7	24.0	5.5
20			PB-8	13	1.7	2.3	4.6	3.1	3.5	2.5	3.5
21	Zone 3		PB-8_BASE	14							
22			PB-10	15							
23			PB-10_BASE	16							
24			PB-11	17				7.0			6.0
25		PB-11_BASE	PB-11_BASE	18	8.1	4.2	3.0	3.6	3.7	8.9	3.9
26			X_MKR	19		2.9	3.6	6.5	3.5		3.5
27			Y_MKR	20	24.3	4.5					

Net_thickness | Perf_thickness | Adjwells | Z21HC | Z21RC | Z19HC | Z19RC | Z17HC | Z17RC | Z15HC | Z15RC | Z13HC | Z13RC | Z11HC | Z11RC | Z9HC | Z9RC

Fig. 51—Static connectivity calculation in ICAP.

How ICAP Calculates Hydraulic Connectivity

For any well pair, the hydraulic connectivity calculated for any simulation model zone is conditioned to the static connectivity calculated for that same zone. This procedure ensures that only those perforated intervals that are located in the intervals with net thickness get a value greater than zero for hydraulic connectivity.

Fig. 52 shows an example perforated thickness spreadsheet used to illustrate the logic of how ICAP calculates hydraulic connectivity. For the purpose of illustration, calculation of hydraulic connectivity for wells 0858 and 2132 in zone 1 is used as an example. In Fig. 52, seven layers identified by a porosity log cutoff (≥8%DPHI) and correlated across the 35 wells have been grouped together as zone 1 in the simulation model. For zone 1, using the perforation data, three perforated thickness values were identified for layers GB-4, GB-4_BASE and GB-6 in well 0858 while two net perforated thickness values were identified for layers GB-3 and GB-6 in well 2132 (focus is within the red square in Fig. 52). Within zone 1 perforated thickness values were identified for both wells 0858 and 2132 only in layer GB-6. Thus ICAP will return an initial value of unity for both wells 0858 and 2132 in layer GB-6 and a value of zero for each of the other six layers in zone 1. Summing up the initial values yields a perforated thickness value of unity in zone 1. An “if” logic statement is used to condition the perforated thickness value of unity in zone 1 to the static connectivity value previously calculated to be unity. Thus, in this case a hydraulic connectivity value of unity is obtained for wells 0858 and 2132 in zone 1 for this example (see Fig. 50 for the visualization). A further illustration of how hydraulic connectivity is conditioned to static connectivity using an “if” logic

statement is provided. By keeping the calculated perforated thickness value of unity in zone 1 but changing the previously calculated static connectivity value of unity to zero, the “if” logic statement yields a hydraulic connectivity value of zero instead of unity in zone 1. This illustration shows that the procedure for conditioning hydraulic connectivity to static connectivity ensures that only those perforated intervals that are located in the intervals with net thickness get a value greater than zero for hydraulic connectivity. In another example using zone 3, the static connectivity was previously calculated to be 2. However, no perforated interval is found in well 0858 in Zone 3 and only layer PB-11 is perforated in well 2132 in the same zone. Thus a perforated thickness value of zero conditioned by an “if” logic statement to a static connectivity value of 2 results in a hydraulic connectivity value of zero for wells 0858 and 2132 in zone 3 (focus is within the blue square in Fig. 52). Notice that there are cases where the perforation data identifies perforation thickness values in the thin shale layers within the larger reservoir zones in the 3D model. For example, in zone 1, the perforation data identified a perforated thickness value for layer GB-4_BASE in well 0858. Layer GB-4_BASE represents a thin shale layer between two sand layers namely GB-4 and GB-6 within the larger zone 1 in the 3D model. This is the situation in some zones but these cases are not significant.

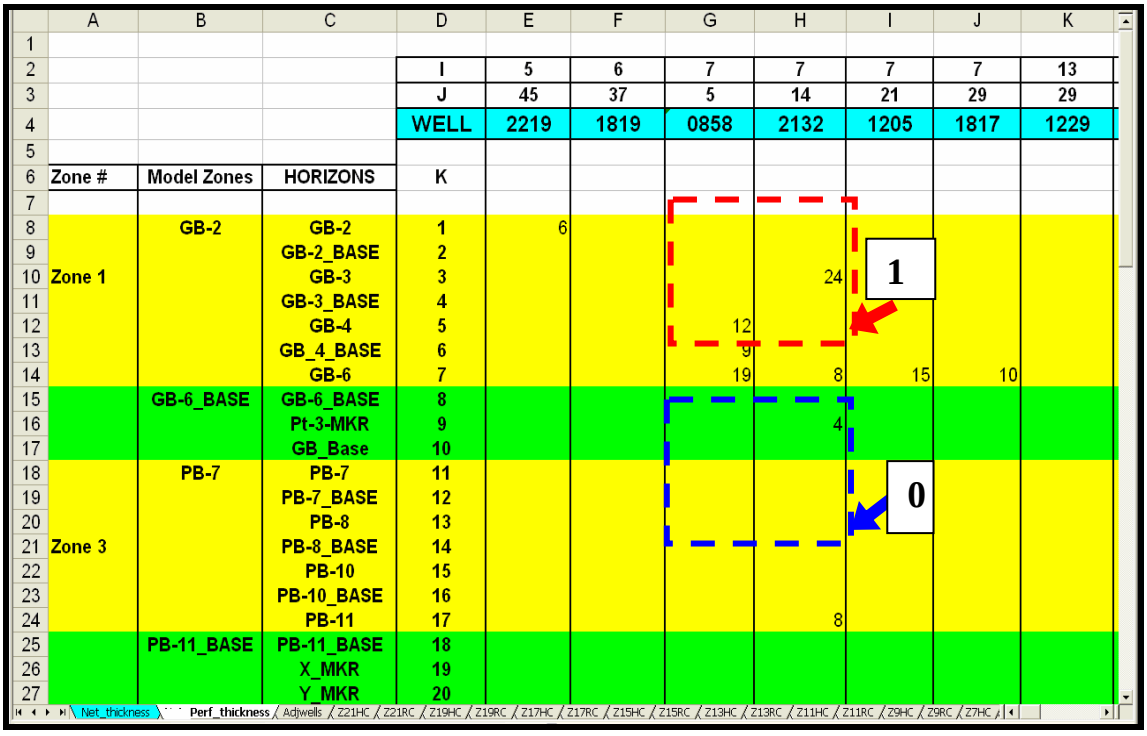

Fig. 52—Hydraulic connectivity calculation in ICAP.

Simplifying Assumptions

Three basic assumptions made for calculating connectivity in ICAP are:

1. Continuity is assumed if there is reservoir-quality sand in each well of the pair.
2. The wells are closely spaced—a sandstone layer is more likely than not to be connected between two adjacent wells spaced at 10 acres than 40 acres.
3. The sand interval within a layer is not inter-fingered by thin shales but exists as a continuous vertical section.

Based on these assumptions, ICAP establishes that a sand interval in the 3D model layer is connected between two adjacent wells if a net thickness value is identified at the location of the adjacent wells within the layer. The implication of these simplifying assumptions is that the connectivity predictions represent the upper limit of connectivity. Thus, the predictions should be more accurate at higher well densities.

Static Connectivity Visualizations

Fig. 53 shows static connectivity visualizations for D1, D2 and D3 sandstone layers. These were generated for comparison with the percolation model. For each layer, the maximum possible number of well-pair connections is 105. In the D1 sandstone layer, the number of well-pair connections is 78. 78 divided by 105 gives the static connectivity of 0.74 for the D1 sandstone layer. In a similar manner, static connectivity for the D2 and D3 sandstone layers were obtained. The D1 sandstone is the most connected (0.74) of the D sandstones. This agrees with Deo *et al.*[2] which reports that the D1 sandstone is laterally continuous. The D2 and D3 sandstones have poor static connectivity (<0.3). In the 3D model, the D1 sandstone layer is in zone 7 while D2 and D3 sandstones layers are in zone 9 (Fig. 35).

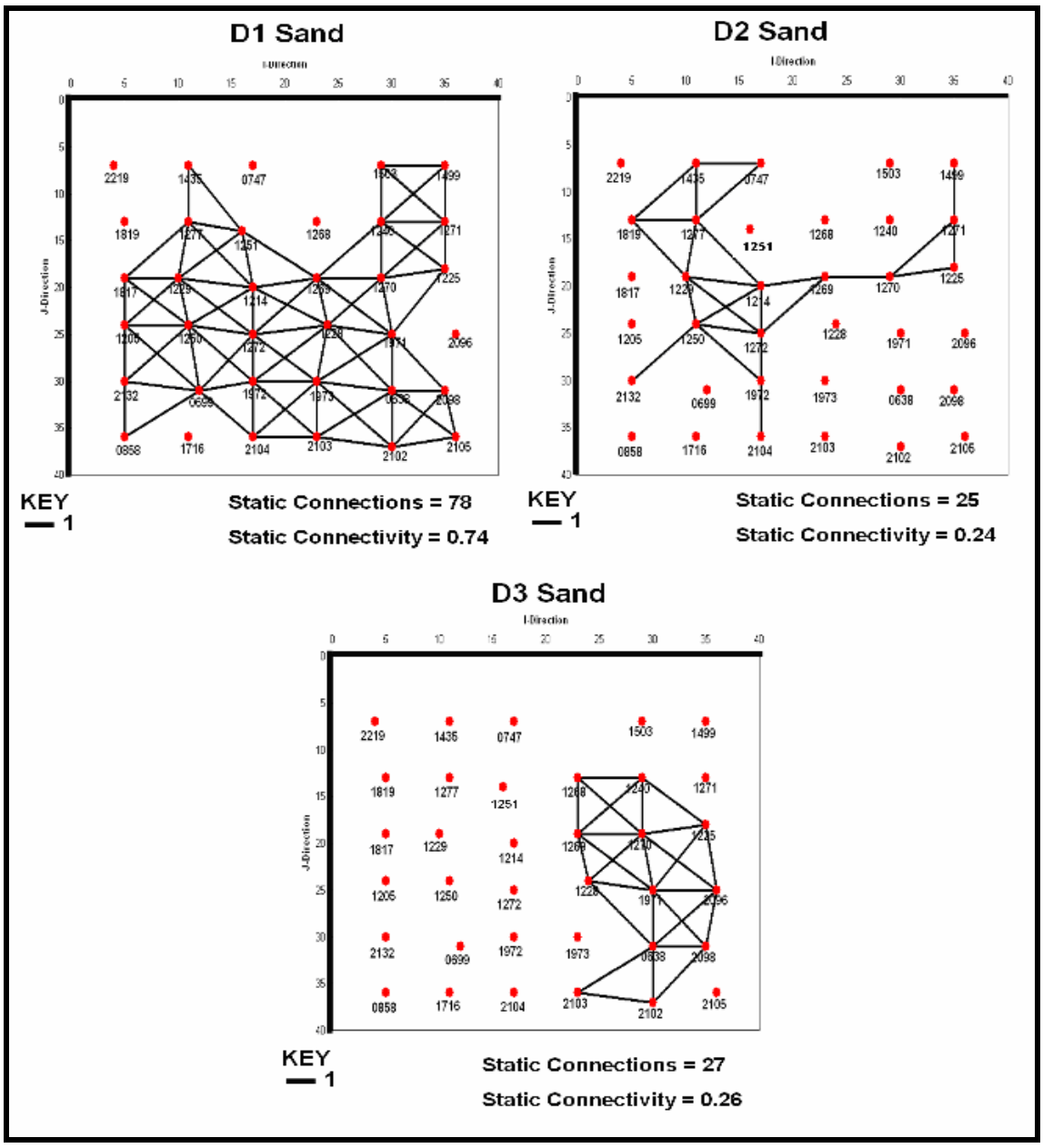

Fig. 53—Static connectivity visualization in the D1, D2 and D3 sands. These were generated for comparison with the percolation model.

Hydraulic Connectivity Visualizations

Fig. 54 shows hydraulic connectivity visualizations for four out of the 13 sand zones in the 3D model. Results of hydraulic connectivity visualizations show that 10 sand zones in the 3D model have hydraulic connectivity. They include zones 1, 5, 7, 9, 11, 13, 15, 17, 19 and 21. The D1 layer (Zone 7) has the highest hydraulic connectivity (0.63). For each layer, the maximum possible number of well-pair connections is 105. In the D1 layer, the number of well-pair connections is 66. 66 divided by 105 gives the hydraulic connectivity of 0.63 for the D1 layer. 12 zones have zero hydraulic connectivity and include 3 sand zones: 3, 20 and 22. It is important to note that zero hydraulic connectivity in a zone does not indicate the absence of perforations. Rather, it shows that there are no perforations between any two adjacent well-pairs for the layers in that zone.

I also evaluated hydraulic connectivity as a function of well spacing (40, 80, 160 and 360 acres per well) for the combined 22 zones. **Fig. 55** shows that the hydraulic connectivity for the combined 22 zones reduces as well spacing increases from 40 acres to 360 acres.

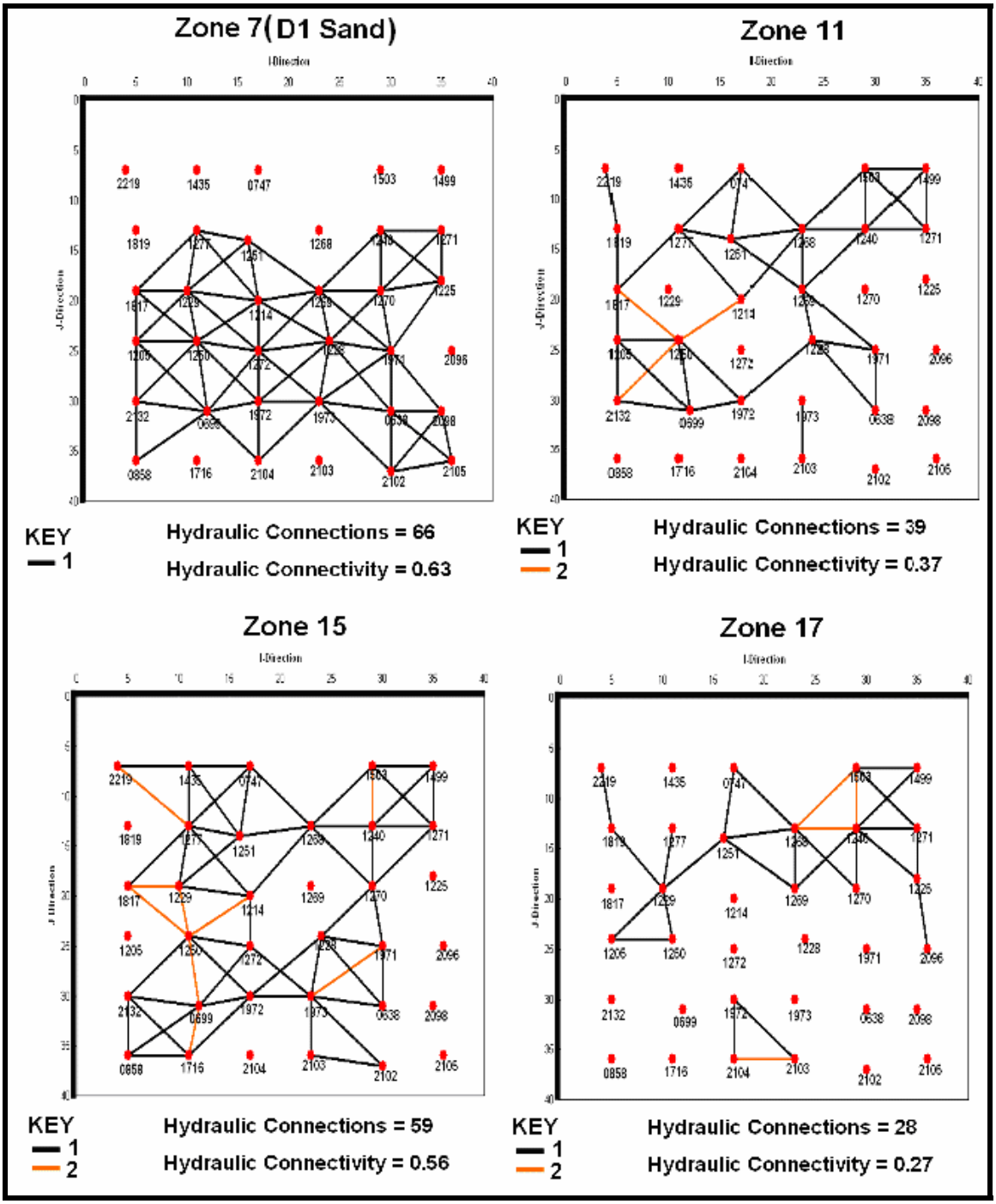

Fig. 54—Hydraulic connectivity visualization of four zones in the 3D model.

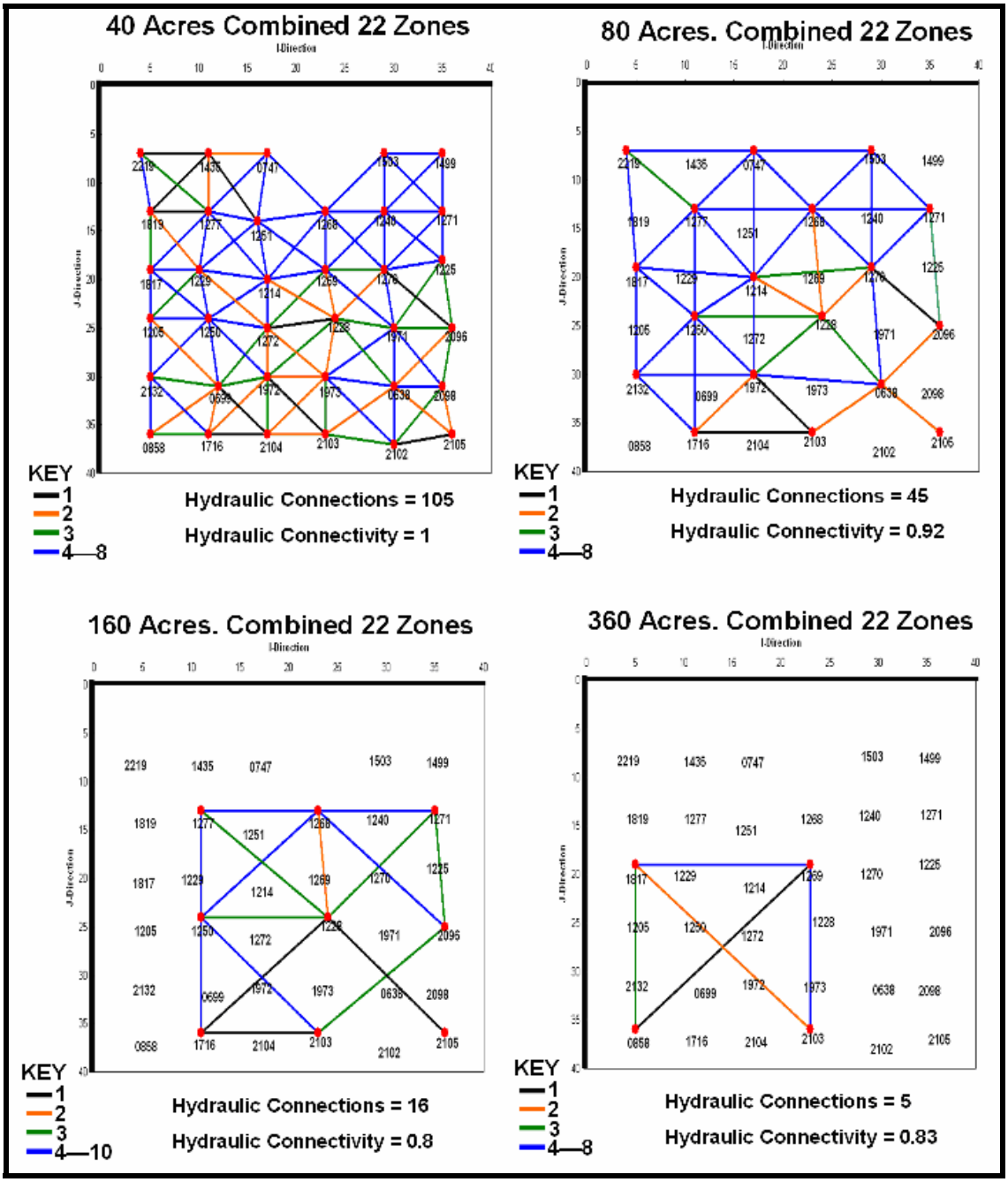

Fig. 55—Hydraulic connectivity visualization of the combined 22 zones for 40, 80, 160 and 360 acres well spacing.

Connectivity Plots

Table 6 summarizes results of the evaluation for D1 and D2 sandstones and the combined 22 zones at 40, 80, 160 and 360 acres well spacing. The connectivity values were calculated by dividing the sum connections from all evaluated layers by a product of the number of layers evaluated and total well-pair connections considered. 66 layers were evaluated for the combined 22 zones while the D1 and D2 sandstones were separately evaluated as single layers. **Fig. 56** shows plots of static and hydraulic connectivity versus well spacing for the three cases. For the D1 sandstone and the combined 22 zones, there is a strong negative correlation (R^2>0.89) between well density and connectivity—static and hydraulic connectivity increase as well spacing decreases. This relationship is not observed in the D2 sandstone because of its poor connectivity.

Fig. 56 (A and C) shows that at current well spacing of 40 acres, static connectivity in the D1 sandstone is very good (>0.7) compared to the combined 22 zones where it is poor (<0.3). Also, hydraulic connectivity in the D1 sandstone (0.629) is ten times more than hydraulic connectivity for the combined 22 zones (0.056). The curves of static connectivity represent the hypothetical limit for which hydraulic connectivity can be improved for the three cases. Thus, where sandstone layers are connected by well-pairs, increasing the perforations in the sandstone layers will improve the hydraulic connectivity. However, it is recognized that drilling new infill wells may be necessary to access those commercial oil accumulations in isolated or lense-like sandstone reservoirs.

Table 6—Summary of connectivity evaluation for three cases.

			Combined 22 Zones		D1 sand (Zone 7)		D2 sand (in Zone 9)	
Area (ac.)	Dist (ft.)	Total * Connections	HC	SC	HC	SC	HC	SC
40	1320	105	0.056	0.266	0.629	0.743	0.162	0.238
80	1867	94	0.053	0.256	0.606	0.723	0.170	0.245
160	2640	78	0.049	0.247	0.564	0.718	0.205	0.282
360	3960	39	0.042	0.233	0.513	0.615	0.179	0.231
Key: Hydraulic Connectivity (HC) and Static Connectivity (SC) Total Connections*= Total well-pair connections considered								

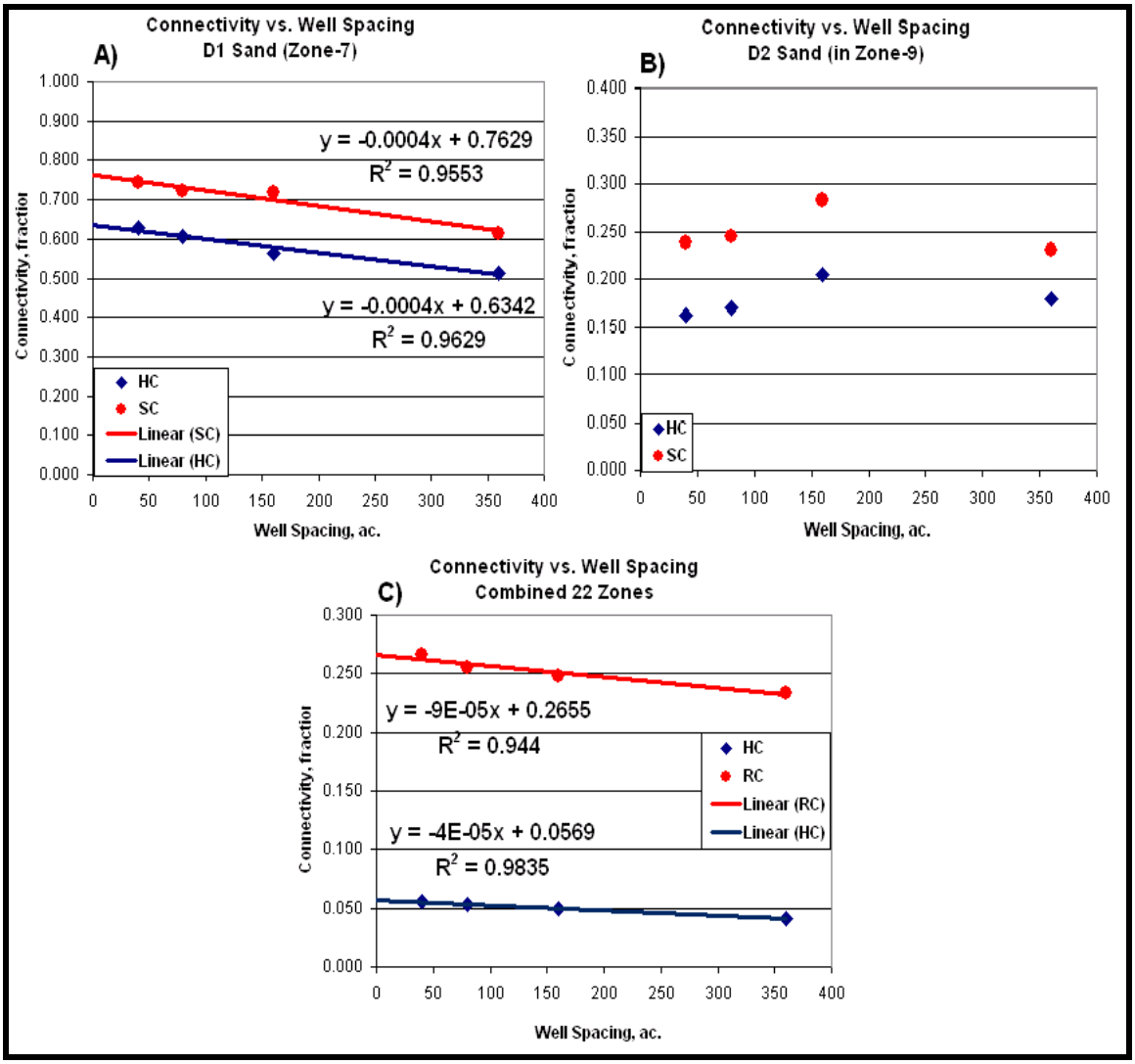

Fig. 56—Static and hydraulic connectivity versus well spacing for three cases.

Limitations of Connectivity Predictions

The assumptions for calculating connectivity mean that the connectivity predictions represent the upper limit of connectivity in the Wells Draw study area and therefore are optimistic. Thus, this approach to connectivity prediction is more suited to fields where infill drilling has resulted in smaller well spacing ($\leq$40 acres per well). Since the approach also assumes that wells are regularly spaced, it may not be suitable for fields in the initial stages of development where few wells are sparsely located.

Comparison with Capacitance Models

The capacitance model[26] (hereafter CM) infers interwell connectivity based on fluctuations in production and injection rates. It uses a nonlinear signal processing model that includes compressibility and transmissibility effects to infer transmissibility trends and flow barriers. The CM quantifies interwell connectivity by coefficients or weights.[26] However, the underlying assumptions of the CM limit its use for connectivity prediction in the Wells Draw study area. One CM limitation is the assumption of absence of producer extended shut-in periods during the assessment interval.[26] Therefore, time intervals dominated by extended production shut-in periods should be avoided in CM interwell connectivity assessments as strong correlation between injection rates may result in negative coefficients or weights. **Fig. 57** shows several shut-in periods in oil production in the Wells Draw study area from 1982 to 2005. Though water injection commenced on January 1, 1995, there is only a short period (2002 – 2005) of uninterrupted injection and production data for all 35 wells in the Wells Draw study area. Also the CM is sensitive to injection and production data quality and works better

with relatively smooth data.[26] **Figs. 58** and **59** show the GOR and water cut data in the Wells Draw study area which feature abrupt changes and several spikes. Furthermore, CM performance is weak in low permeability as found in the Wells Draw study area because most of the pressures induced by an injector will be dissipated before it reaches the producer. Due to the discussed limiting assumptions, the CM interwell connectivity assessment resulted in questionable weights (**Fig. 60**).[61] Thus, comparison between CM and ICAP results is not feasible and CM is not considered reliable for interwell connectivity evaluation in the Wells Draw study area.

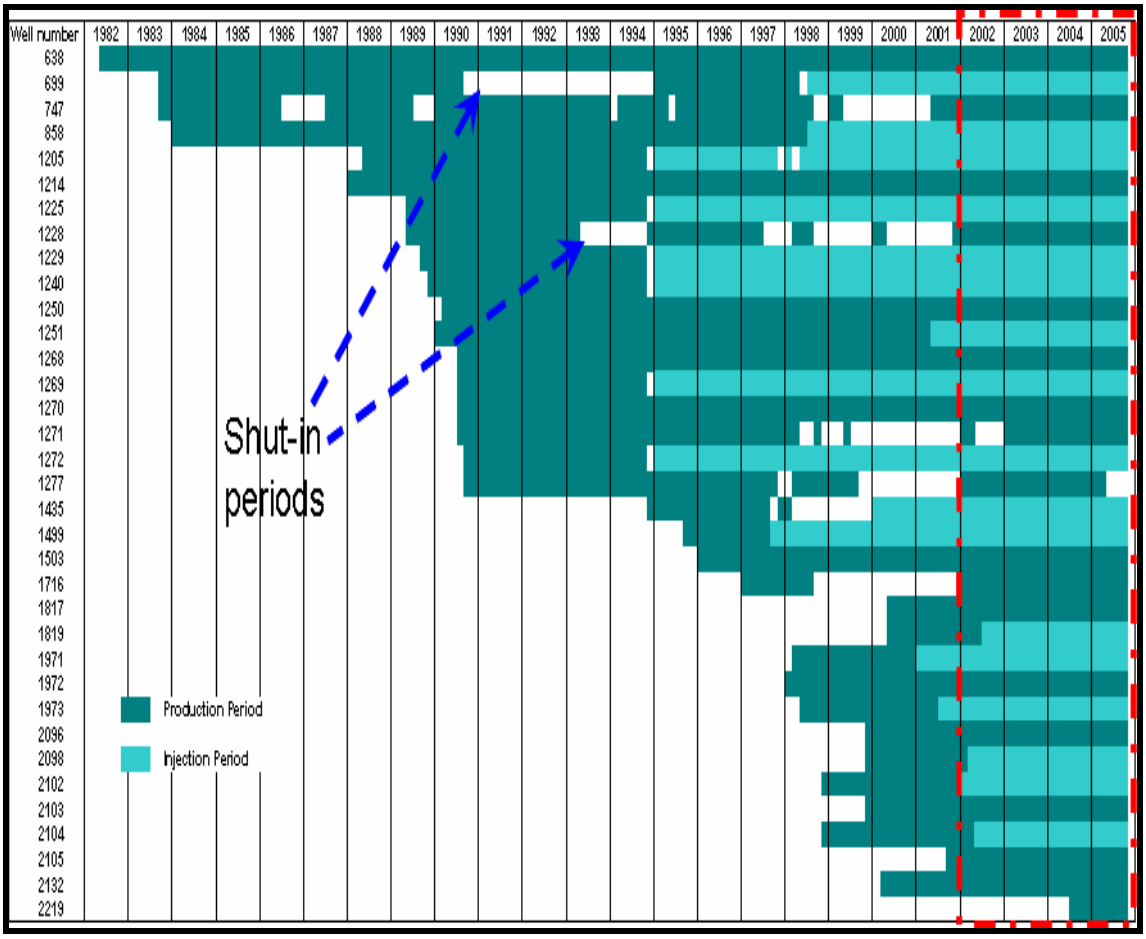

Fig. 57—Shut-in periods in oil production in Wells Draw study area from 1982 to 2005.

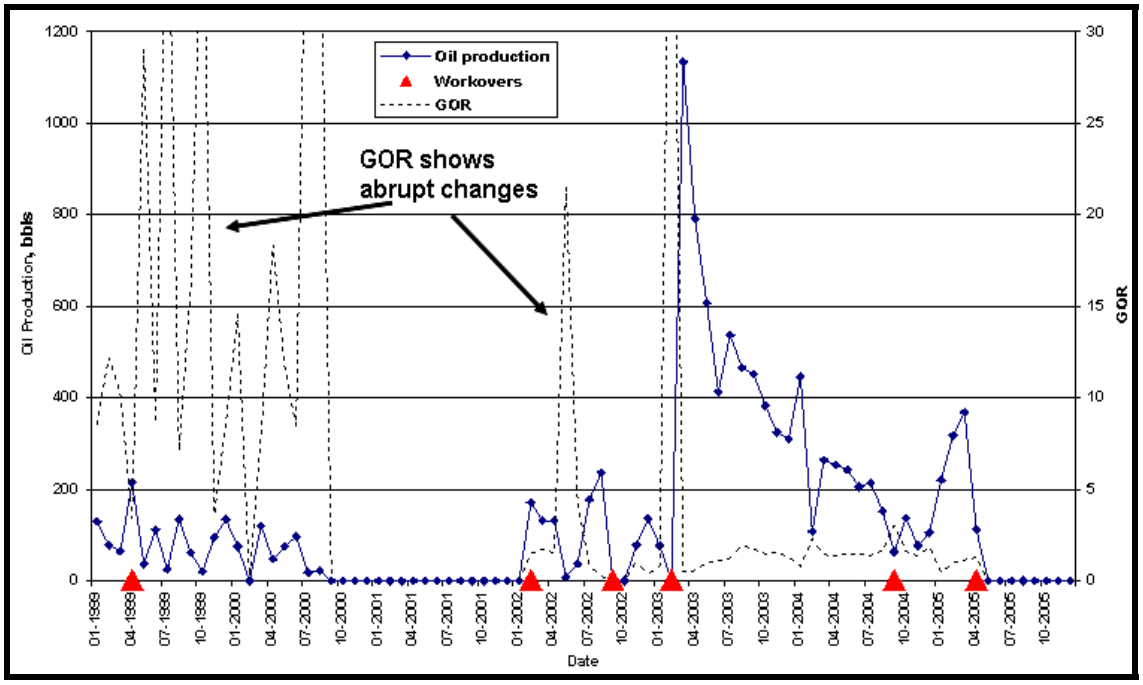

Fig. 58— Abrupt changes in gas production data (well 1277). Well is located in Fig. 3.

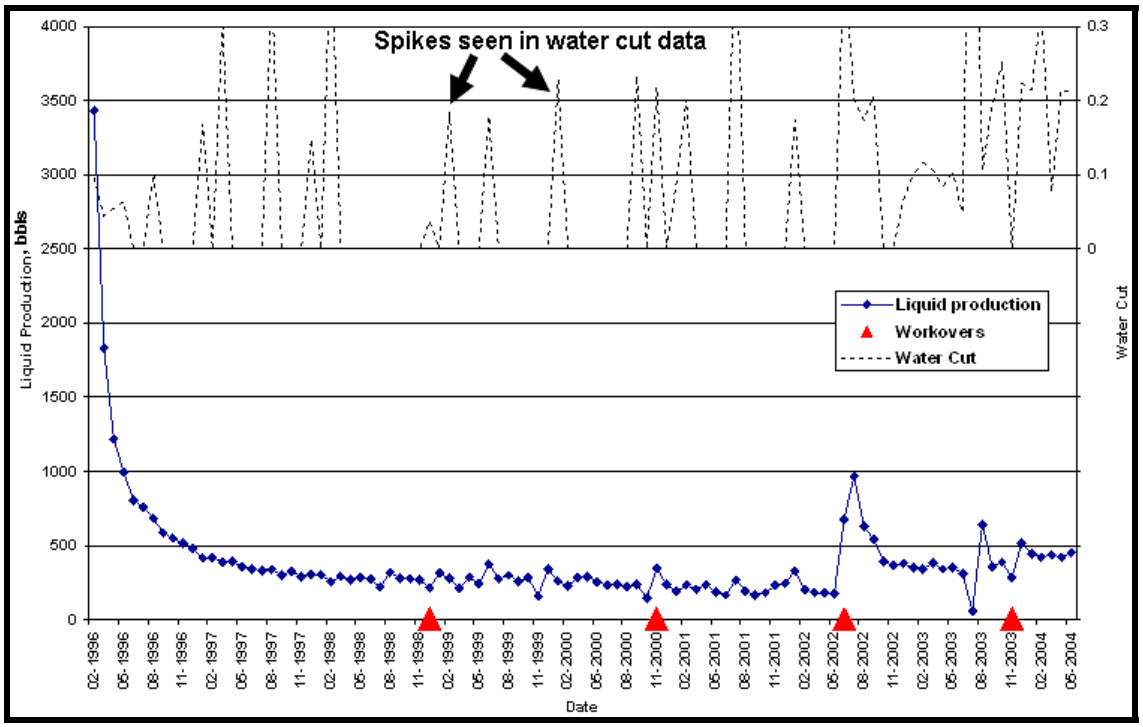

Fig. 59— Spike seen in water production data (well 1503). Well is located in Fig. 3.

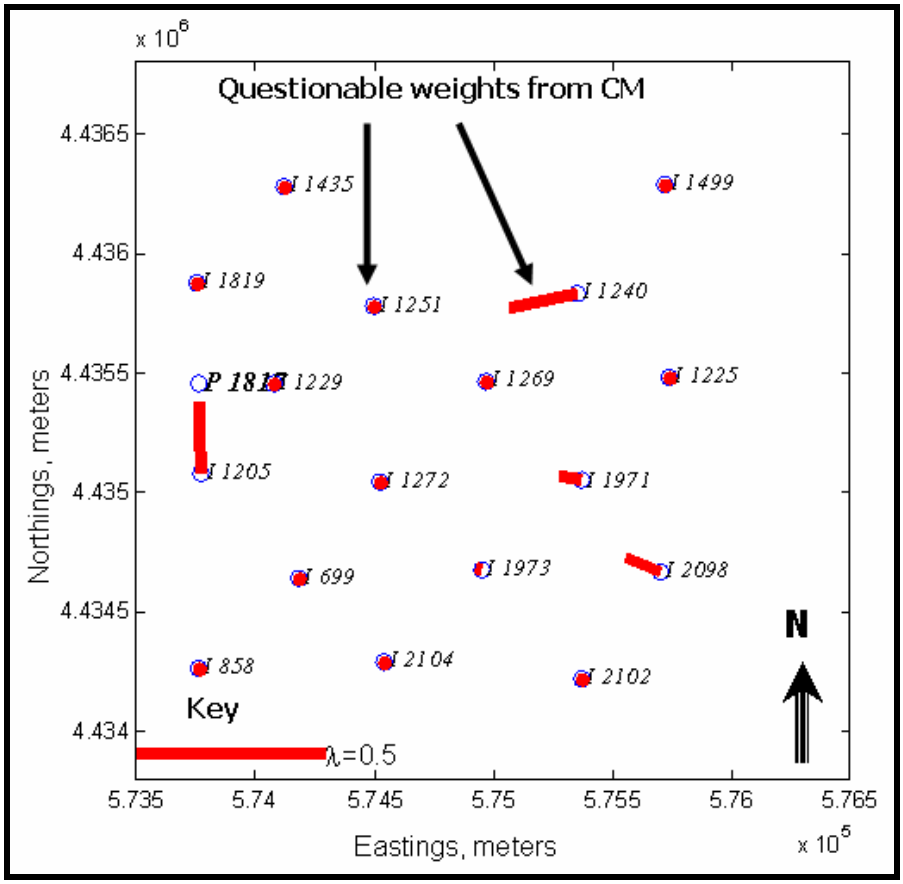

Fig. 60—Questionable interwell connectivity weights from CM assessments. Injectors (I1240, I1971 and I2098) farther away from analyzed producer (P1817) show relatively larger weights compared to the injectors closer to P1817. Wells are located in Fig. 3.

Comparison with Percolation Models

The percolation model is a simple 2D based model that has been used to estimate reservoir connectivity by assuming simple geometrical systems.[24, 25] The 2D model requires four parameters for evaluating interwell connectivity: 2D net-to-gross ratio ratio, typical sandbody size, reservoir length and well spacing.[24, 25] The percolation model assumes the sandbody geometry to be square-shaped and randomly distributed and requires the reservoir interval for evaluation to be sufficiently thin to approximate a 2D plane so that 2D percolation results can be applied. Because percolation model does not consider sandbody locations but assumes them to be distributed randomly in 2D space, it is more likely to predict a high connectivity value for a sandbody with high 2D net-to-gross ratio or large typical sandbody size (**Fig. 61**).[62] Since 2D percolation model is only applicable to thin reservoirs, it was used to estimate the mean static interwell connectivity and associated standard deviation in D1 and D2 sandstones at different well spacing in the Wells Draw study area.[62] The percolation model predictions were then compared to the predictions of the ICAP model in the Wells Draw study area (**Figs. 62** and **63**). The percolation model predicts higher connectivity in the D2 sandstone compared to the D1 at 40 acre (1320 ft) well spacing in the Wells Draw study area. The prediction is contrary to the connectivity visualized by the net sandstone thickness maps which show the D1 sandstone (Fig. 31) as non-reservoir quality in 11 wells and the D2 sandstone (**Fig. 64**) as non-reservoir quality in 16 wells. This contradiction is because of high 2D net-to-gross ratio and large typical sandbody size input combined with the assumption of random distribution of sandbodies in the percolation model.[62] It was also

observed from **Figs. 62** and **63** that while ICAP model predictions fall within the range predicted by percolation model in the poorly connected D2 sandstone, it predicts higher connectivity than the percolation model in the well connected D1 sandstone. Thus, the observations show that the percolation model is more likely than not to predict lower connectivity compared to the ICAP model. Furthermore, compared to the percolation model, the predictions of the ICAP model in the D1 and D2 sandstone reservoirs at 40 acre well spacing are more consistent with previous studies by Deo *et al.*[2] at the same well spacing that concluded that the D1 sandstone has a higher connectivity compared to the other D sandstone reservoirs.

From these comparisons, I conclude that ICAP and percolation model are both reliable tools for assessing interwell connectivity. Also, the percolation model is more likely than not to predict lower connectivity compared to the ICAP model (Fig. 63).

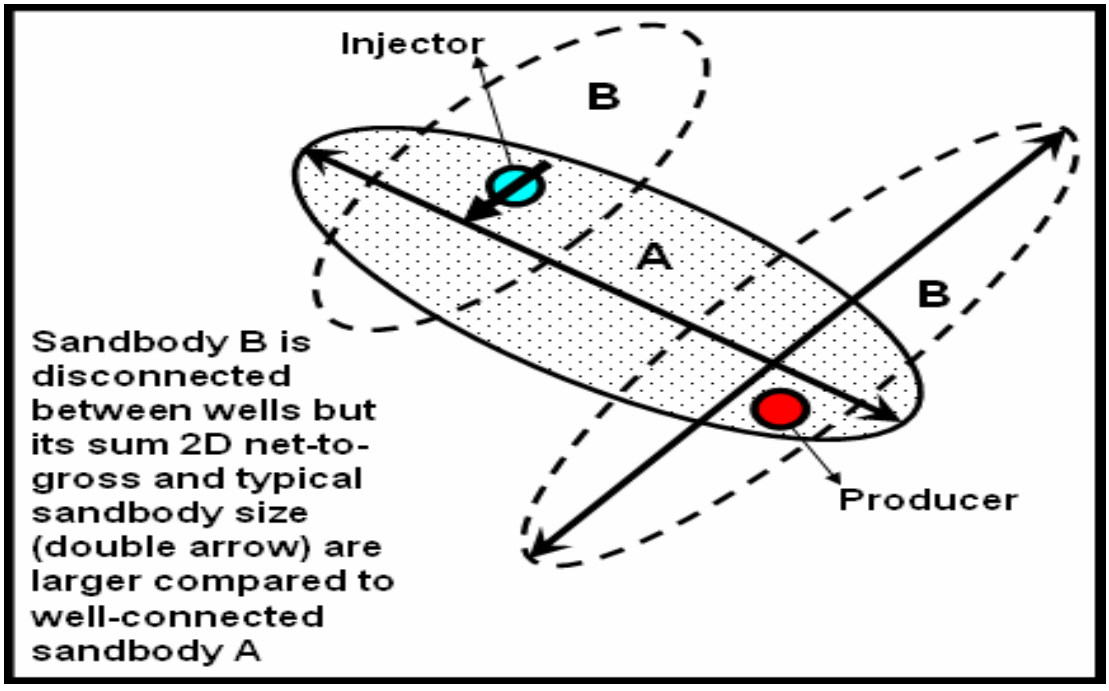

Fig. 61—Connectivity scenarios with relevant percolation model inputs.

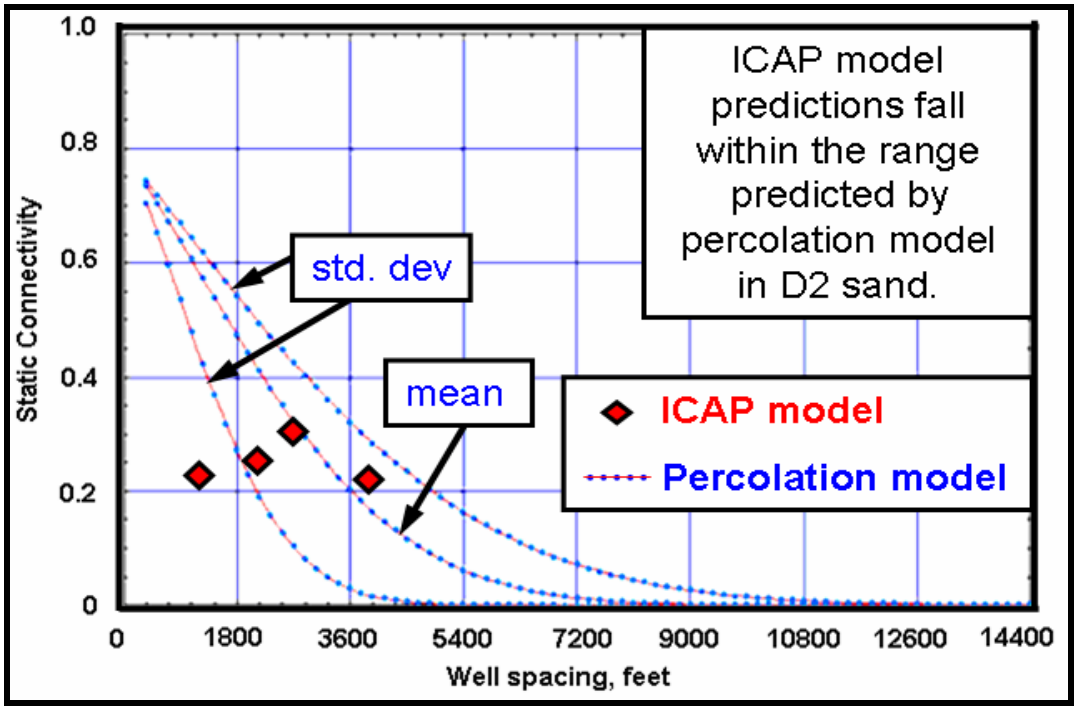

Fig. 62—ICAP versus percolation model [62] predictions in D2 sandstone.

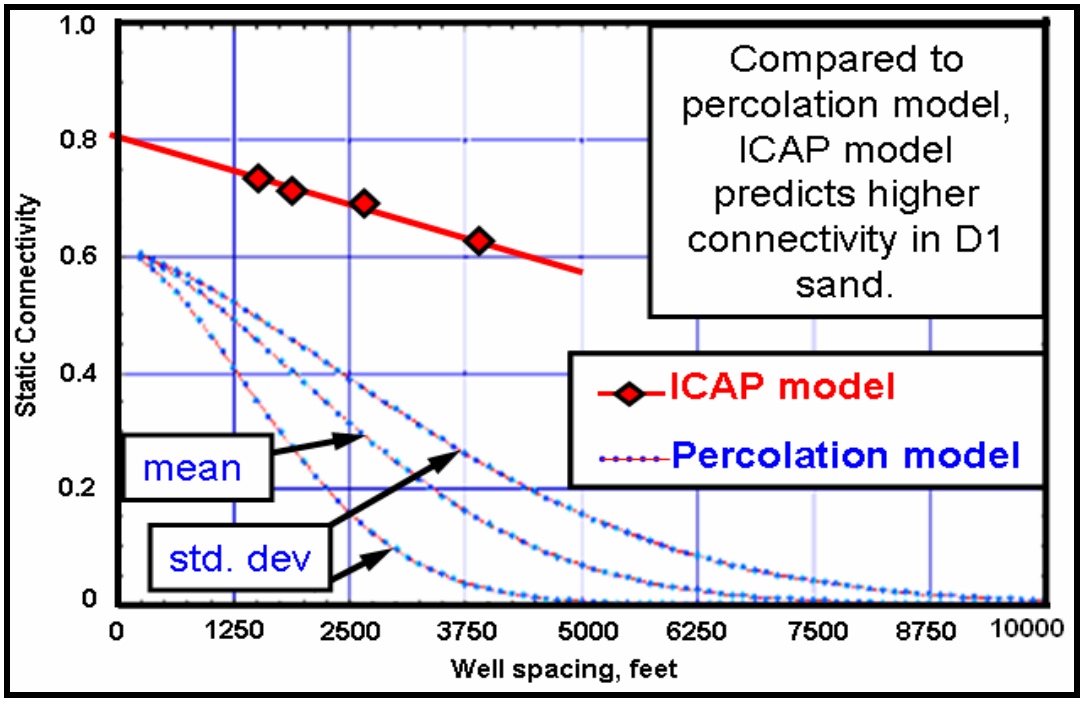

Fig. 63—ICAP versus percolation model [62] predictions in D1 sandstone.

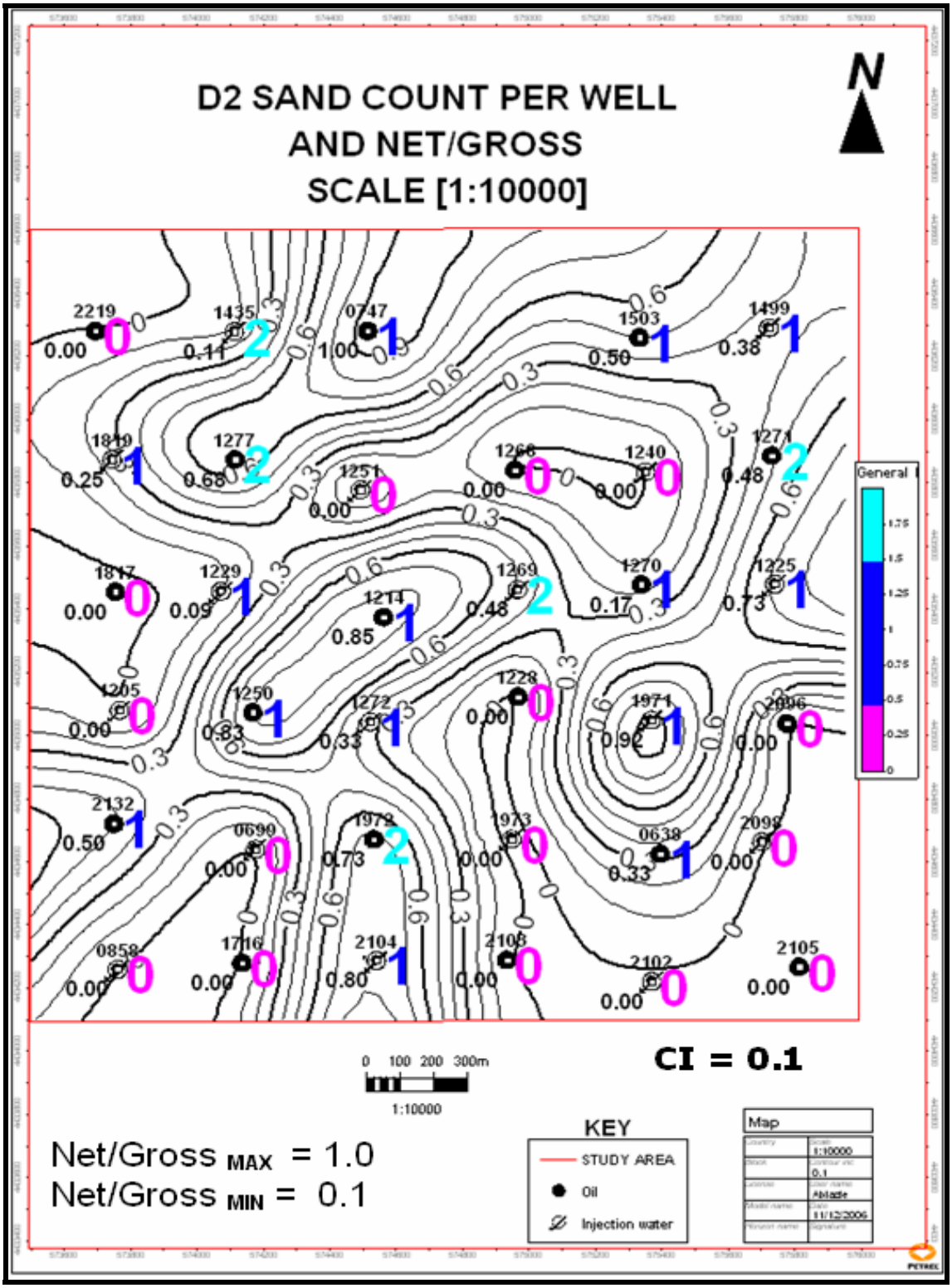

Fig. 64—D2 sand isopleths overlay on net thickness map.

CHAPTER V

CONCLUSIONS AND RECOMMENDATIONS

Conclusions from Static Characterization

A major conclusion from this static reservoir characterization study is that the Green River sandstone reservoirs fall under the jigsaw-puzzle category of the Weber and Geuns[59] reservoir model classification system. Thus, the reservoir characterization methodology (Chapter III) in this study is applicable to reservoirs that fit into the jigsaw-puzzle category.

Conclusions from Connectivity Evaluation

Regarding the interwell connectivity evaluation in the Wells Draw study area, the following is a summary of some key conclusions reached.

1. D1 sandstone has the highest static connectivity (0.74) among the D sandstones. This agrees with Deo *et al.*[2] which reports that the D1 sandstone is laterally continuous.
2. The D2 and D3 sands have poor static connectivity (<0.3). Static connectivity in the D3 sandstone is restricted to the southwestern part of the Wells Draw study area.
3. 10 out of 13 sand zones in the 3D model have non-zero hydraulic connectivity. They include zones 1, 5, 7, 9, 11, 13, 15, 17, 19 and 21.
4. At current well spacing of 40 acres, zone 7 (D1 sandstone) has the highest hydraulic connectivity (0.63).

5. 12 zones have zero hydraulic connectivity and include 3 sand zones which are zones 3, 20 and 22.
6. At current well spacing of 40 acres, the combined 22 zones have a very poor hydraulic connectivity of 0.056.
7. There is a strong negative correlation (R^2>0.89) between well density and connectivity for D1 sandstone and the combined 22 zones—static and hydraulic connectivity increase as well spacing decreases. This relationship is not observed in the D2 sandstone because of its poor connectivity.
8. Finally, the connectivity results we show represent the upper limit of connectivity in the Well Draw area. We can say that the hydraulic connectivity is less than 0.63 in the D1 sandstone and less than 0.056 for the combined 22 zones.

Conclusions from Comparative Analysis

The following is a summary of some key conclusions drawn from comparing our connectivity results with those of capacitance and percolation models in the Wells Draw study area.

1. Due to CM limiting assumptions, the CM interwell connectivity assessments resulted in questionable weights (Fig. 60). Thus, comparison between CM and ICAP results is not feasible and CM is not considered reliable for interwell connectivity evaluation in the Wells Draw study area.
2. The percolation model predicts higher connectivity in the D2 sandstone compared to the D1 sandstone at 40 acre (1320 ft) well spacing in the Wells Draw study area. This is because of a high 2D net-to-gross ratio input combined

with the assumption of random distribution of sandbodies in the percolation model.[62]

3. While ICAP model predictions fall within the range predicted by percolation model in the poorly connected D2 sandstone, it predicts higher connectivity than the percolation model in the well connected D1 sandstone.
4. The percolation model is more likely than not to predict lower connectivity compared to the ICAP model and is considered reliable for interwell connectivity evaluation in the Wells Draw study area.
5. Compared to the percolation model, the predictions of the ICAP model in the D1 and D2 sandstone reservoirs at 40 acre well spacing are more consistent with previous studies by Deo *et al.*[2] at the same well spacing that concluded that the D1 sandstone has a higher connectivity compared to the other D sandstone reservoirs.
6. Based on these comparisons, I conclude that ICAP and percolation model are both reliable tools for assessing interwell connectivity. Also, the percolation model is more likely than not to predict lower connectivity compared to the ICAP model (Fig. 63).

Recommendations

Based on the conclusions presented above, the following recommendations are provided for simulation assessments in the Wells Draw study area.

1. The base case, low case and high case models of reservoir connectivity in the Wells Draw study area from Castle Peak to Garden Gulch intervals are recommended for history matching and simulations assessments for enhanced oil recovery.
2. The map visualizations of hydraulic connectivity in 10 sand zones are recommended as an initial guide for flow barrier indication in the simulation model. Since the maps visualize the upper limit of interwell connectivity in the Wells Draw study area, they can also serve as justification for establishing additional flow barriers.

NOMENCLATURE

SYMBOL		Description
V_{Pm}	=	Mean pore volume
ϕ	=	Porosity
A	=	Area
h_n	=	Thickness
GRFM	=	Green River Formation
GR	=	Gamma Ray
DPHI	=	Density Porosity
NPHI	=	Neutron Porosity
LLD	=	Laterolog-Deep Resistivity
LLS	=	Laterolog-Shallow Resistivity
X_{inc}	=	Increment in X-direction
Y_{inc}	=	Increment in Y-direction
Z_{inc}	=	Increment in Z-direction
q_o	=	Oil production rate, Stb/mon.
q_w	=	Water production rate, Stb/mon.
I_w	=	Water injection rate, Stb/mon.
q_g	=	Gas production rate, Mscf/mon.
GOR	=	Gas-oil ratio, Mscf/Stb

REFERENCES

1. Deo, M.D., Sarkar, A., Nielson, D.L., Lomax, J.D., and Pennington, B.I. 1994. "Monument Butte Unit Case Study: Demonstration of A Successful Waterflood In A Fluvial Deltaic Reservoir," *Proc.,* SPE/DOE Ninth Symposium on Improved Oil Recovery, Tulsa, Oklahoma 143.

2. Deo, M.D., Nielson, D.L., Lomax, J.D., Dyer, J.E., and Lutz, S.J. 1996. "Green River Formation Waterflood Demonstration Project" Utah Geological Survey, Unpublished final report to the U.S. Department of Energy for the period 10/01/92 - 12/31/95, Contract DE/BC/14958-15 (November).

3. Pawar, R.J., Deo, M.D., and Dyer, J.E. 1996. "Effect of Reservoir Connectivity on Primary and Secondary Recovery," *Proc.*, SPE/DOE Tenth Symposium on Improved Oil Recovery, Tulsa, Oklahoma 147.

4. Morgan, C.D., Chidsey, T.C., Jr., Hanson, J.A., McClure, K.P., Weller, K., Bereskin, S.R., Deo, M.D., and Yeager, R. 1999. "Reservoir Characterization of the Lower Green River Formation, Southwest Uinta Basin, Utah," Utah Geological Survey, Unpublished biannual technical progress report to the U.S. Department of Energy for the period 10/1/98 - 3/31/99, Contract DE-AC26-98BC15103 (April).

5. Morgan, C.D., Chidsey, T.C., Jr., McClure, K.P., Bereskin, S.R., Deo, M.D., Weller, K., and Yeager, R. 1999. "Reservoir Characterization of the Lower Green River Formation, Southwest Uinta Basin, Utah" Utah Geological Survey, Unpublished biannual technical progress report to the U.S. Department of Energy for the period 04/01/99 - 09/30/99, Contract DE-AC26-98BC15103 (November).

6. Morgan, C.D., McClure, K.P., Bereskin, S.R., Deo, M.D., and Weller, K. 2000. "Reservoir Characterization of the Lower Green River Formation, Southwest Uinta Basin, Utah" Utah Geological Survey, Unpublished biannual technical progress report to the U.S. Department of Energy for the period 10/01/99 - 03/31/00, Contract DE-AC26-98BC15103 (June).

7. Morgan, C.D., McClure, K.P., Bereskin, S.R., Deo, M.D., and Weller, K. 2001. "Reservoir Characterization of the Lower Green River Formation, Southwest Uinta Basin, Utah" Utah Geological Survey, Unpublished biannual technical progress report to the U.S. Department of Energy for the period 04/01/00 - 09/30/00, Contract DE-AC26-98BC15103 (February).

8. C. D. Morgan. 2001. "Reservoir Characterization of the Lower Green River Formation, Southwest Uinta Basin, Utah" Utah Geological Survey, Unpublished biannual technical progress report to the U.S. Department of Energy for the period 10/01/00 - 03/31/01, Contract DE-AC26-98BC15103 (May).

9. Morgan, C.D., McClure, K.P., Bereskin, S.R., Deo, M.D., and Weller, K. 2001. "Reservoir Characterization of the Lower Green River Formation, Southwest Uinta Basin, Utah" Utah Geological Survey, Unpublished biannual technical progress report to the U.S. Department of Energy for the period 04/01/01 - 09/31/01, Contract DE-AC26-98BC15103 (October).

10. Morgan, C.D., McClure, K.P., Bereskin, S.R., and Deo, M.D. 2002. "Reservoir Characterization of the Lower Green River Formation, Southwest Uinta Basin, Utah" Utah Geological Survey, Unpublished biannual technical progress report to the U.S. Department of Energy for the period 10/01/01 - 03/31/02, Contract DE-AC26-98BC15103 (May).

11. Morgan, C.D., Chidsey, T.C., Jr., Hanson, J.A., McClure, K.P., Weller, K., Bereskin, S.R., Deo, M.D., and Yeager, R. 2003. "Reservoir Characterization of the Lower Green River Formation, Southwest Uinta Basin, Utah" Utah Geological Survey Open-File Report 411, CD-ROM.

12. Morgan, C.D., Chidsey, T.C., Jr., and Bereskin, S.R. 2002. "Characterization of Oil Reservoirs in the Lower and Middle members of Green River Formation, Southwest Uinta Basin, Utah," Utah Geological Survey slideshow presented at the AAPG Rocky Mountain Section Meeting, Laramie, Wyoming. http://geology.utah.gov/emp/greenriver/poster02/slideshow.pdf accessed June 1, 2007.

13. Morgan, C.D. and McClure K. P. 2004. "Basin-wide correlation of Petroleum Plays and Subplays in the Green River Petroleum System, Uinta Basin, Utah" Utah Geological Survey poster presented at the AAPG Rocky Mountain Section Meeting, Denver, Colorado (August). Poster 4. http://geology.utah.gov/emp/pump/pdf/gr_river_poster3-6.pdf accessed June 1, 2007.

14. Chidsey, T.C., Jr., Morgan, C.D., and McClure, K.P. 2004. "Outcrop Analogs in Utah: Templates for Reservoir Characterization and Modeling," Utah Geological Survey poster presented at the AAPG Rocky Mountain Section Meeting, Denver, Colorado (August). Poster 5. http://geology.utah.gov/emp/pump/pdf/poster5.pdf accessed June 1, 2007.

15. Bereskin, S.R and Morgan, C.D. 2001. "Fluvial-Lacustrine Oil Reservoirs in the Middle Member of the Eocene Green River Formation, South-Central Uinta Basin, Utah," Utah Geological Survey poster presented at the AAPG National Convention, Denver, Colorado, (June). Poster 1. http://geology.utah.gov/emp/greenriver/pdf/greenr1_2001postr.pdf accessed June 1, 2007.

16. Bereskin, S.R., Morgan, C.D., and McClure, K.P. 2004. “Descriptions, Petrology, Photographs, and Photomicrographs of Core from the Green River Formation, South Central Uinta Basin, Utah,” Utah Geological Survey, Miscellaneous Publication **4.**

17. Taylor, A.W. and Ritts, B.D. 2004. “Mesoscale Heterogeneity of Fluvial Lacustrine Reservoir Analogues: Examples from the Eocene Green River and Colton Formations, Uinta Basin, Utah, USA” *JPT* (January), 3.

18. Chidsey, T.C., Jr., Morgan, C.D., McClure, K.P., Bon, R.L., Gwynn, J.W. Jarrard, R., and Curtice, R. 2004. “Major Oil plays In Utah and Vicinity,” Utah Geological Survey, unpublished quarterly technical progress report to the U.S. Department of Energy for the period 01/01/04 – 03/01/04, Contract DE-FC26-02NT15133 (June).

19. Kelkar, M. and Perez, G. 2002. *Applied Geostatistics for Reservoir Characterization*, SPE, Richardson, Texas.

20. “Reservoir Characterization Using Expert Knowledge, Data and Statistics,” *Oilfield Review* (January 1992) 25.

21. Caers, J. 2005. *Petroleum Geostatistics*, SPE, Richardson, Texas.

22. Serra, O. and Abbott, H.T. 1982. “The Contribution of Logging Data to Sedimentology and Stratigraphy,” *SPEJ* (February) 117–131.

23. Ainsworth, R.B. 2005. “Sequence Stratigraphic-based Analysis of Reservoir Connectivity: Influence of Depositional Architecture- A Case Study from a Marginal Marine Depositional Setting,” *Petroleum Geoscience* **11**, 257-276.

24. Stauffer, D. 1985. *Introduction to Percolation Theory*, London: Taylor and Francis Inc.

25. King, P.R. 1990. *The Connectivity and Conductivity of Overlapping Sand Bodies, North Sea Oil and Gas Reservoirs II,* A.T. Buller (ed.), The Norwegian Institute of Technology, London: Graham and Trotman, 353-362.

26. Yousef, A.A., Gentil, P., Jensen, J.L., and Lake, L.W. 2005. “A Capacitance Model to Infer Interwell Connectivity from Production and Injection Rate Fluctuations,” paper SPE 95322 presented at the SPE Annual Technical Conference and Exhibition, Dallas, Texas, 9–12 October.

27. Yuan, L. and Strobl, R. 1991. “Variograms and Reservoir Continuity,” *Proc.*, Third International Reservoir Characterization Technical Conference, Tulsa, Oklahoma, 3–5 November.

28. Haldorsen, H.H. and MacDonald, C.J. 1987. “Stochastic Modeling of Underground Reservoir Facies (SMURF),” paper SPE 16751 at the SPE Annual Technical Conference and Exhibition, Dallas, Texas, 27–30 September.

29. Ruijtenberg, P.A., Buchanan, R. and Marke, P. 1990. “Three Dimensional Data Improve Reservoir Mapping,” *JPT* (January) 22–25, 59–61.

30. Weber, K.J and van Geuns, L.C. 1990. “Framework for Constructing Clastic Reservoir Simulation Models,” *JPT* 1248.

31. Dubrule, O.R.F. 1998. “Geostatistics in Petroleum Geology,” *AAPG Continuing Education Course Note Series* **38**.

32. Haldorsen, H.H. and Damsleth, E. 1990. “Stochastic Modeling,” *JPT* (April) 404.

33. Journel, A.G. and Alabert, F.G. 1990. “New Method for Reservoir Mapping,” *JPT* (February) 212 – 218.

34. Chopra, A.K., Steverson, C.D. and Carhart, S.R. 1990. “Evaluation of Geostatistical Techniques for Reservoir Characterization,” paper SPE 20734 at the SPE Annual Technical Conference and Exhibition, New Orleans, Louisiana, 23 – 26 September.

35. Budding, M.C., Paardekam, A.H.M. and van Rossem, S.J. 1992. “3D Connectivity and Architecture in Sandstone Reservoirs,” paper SPE 22342 presented at the SPE International Meeting on Petroleum Engineering, Beijing, China, 24 – 27 March.

36. Mattax, C.C. and Dalton, R.L. 1990. *Reservoir Simulation*, Monograph Series, SPE, Richardson, Texas **13**.

37. Wolcott, D.S. and Chopra, A.K. 1991. “Investigating Infill Drilling Performance and Reservoir Continuity Using Geostatistics,” presented at the Third International Reservoir Characterization Technical Conference, Tulsa, Oklahoma, 3–5 November.

38. Haldorsen, H.H. and Damsleth, E. 1993. “Challenges in Reservoir Characterization,” *AAPG Bull.* 77, 541.

39. Cosentino, L. 2001. *Integrated Reservoir Studies*, TECHNIP, Paris, France.

40. Deutsch, C.V. and Srinivasan, S. 1996. “Improved Reservoir Management Through Ranking Stochastic Reservoir Models,” *Proc.*, SPE/DOE Tenth Symposium on Improved Oil Recovery, Tulsa, Oklahoma 105.

41. McLennan, J.A. and Deutsch, C.V. 2005. “Ranking Geostatistical Realizations by Measures of Connectivity,” paper SPE/PS-CIM/CHOA 98168 presented at the SPE International Thermal Operations and Heavy Oil Symposium, Calgary, Alberta, Canada, 1–3 November.

42. Tyler, K., Sandsdalen, C., Maeland, L., Aasen, J.O., Siring, E., and Barbieri, M. 1996. “Integrated Stochastic Modeling in Reservoir Evaluation for Project Evaluation and Risk Assessment,” paper SPE 36706 presented at the SPE Annual Technical Conference and Exhibition, Denver, Colorado, 6–9 October.

43. Corre, B., Thore, P., de Feraudy V. and Vincent G. 2000. “Integrated Uncertainty Assessment For Project Evaluation and Risk Analysis,” paper SPE 65205 presented at the SPE European Petroleum Conference, Paris, France, 24–25 October.

44. Bruhn, R.L., Picard, M.D., and Isby, J.S. 1986. “ Tectonics and Sedimentology of the Uinta Arch, Western Uinta Mountains, and Uinta Basin,” Paleotectonics and Sedimentation in Rocky Mountain Region, United States, J.A. Peterson (ed.), *AAPG Memoir* **41**, 333-352.

45. Chidsey, T.C., Jr., and Laine, M.D. 1992. “The fractured Green River and Wasatch Formations of the Uinta Basin, Utah – targets for horizontal drilling,” Hydrocarbon and mineral resources of the Uinta Basin, Utah and Colorado, T.D. Fouch, V.F. Nuccio, and T.C. Chidsey, Jr. (eds.), *Utah Geological Association Guidebook* **20**, 123-134.

46. Stearns, D.W., and Friedman, M. 1972. “Reservoirs in Fractured Rocks,” Stratigraphic Oil and Gas Fields—classification, exploration methods, and case histories, R.E. King (ed.), *AAPG Memoir* **16**, 82-106.

47. Narr, W., and Currie, J.B. 1982. 1982 “Origin of fracture porosity—example from Altamont field, Utah,” *AAPG Bull.* **66**, Chap. 9, 1231- 1247.

48. Ryder, R.T., Fouch, T.D., and Elison, J.H. 1976. “Early Tertiary Sedimentation in the Western Uinta Basin, Utah,” Geological Society of America Bulletin **87**, 496-512.

49. Fouch, T.D., Nuccio, V.F., Anders, D.E., Rice, D.D., Pitman, J.K., and Mast, R.F. 1994. “Green River Petroleum System, Uinta Basin, Utah, U.S.A,” The Petroleum System – From Source to Trap, L. B. Magoon and W. G. Dow (eds.), *AAPG Memoir* **60,** Chap. 25, 399 – 421.

50. Lucas, P.T., and Drexler, J.M. 1976. “Altamont-Bluebell—a major naturally fractured stratigraphic trap,” North American Oil and Gas Fields, J. Braunstein (ed.), *AAPG Memoir* **24**, 121-135.

51. Koesoemadinata, R.P. 1970. “Stratigraphy and Petroleum Occurrence, Green River Formation, Red Wash field, Utah,” Colorado School of Mines Quarterly **65**, 1.

52. Castle, J.W. 1990. “Sedimentation in Eocene Lake Uinta (Lower Green River Formation), Northeastern Uinta Basin, Utah,” Lacustrine Basin Exploration: Case Studies and Modern Analogs, B.J. Katz (ed.), *AAPG Memoir* **50**, Chap. 15, 243-263.

53. Bradley, W.H. 1931. “Origin and microfossils of the oil shale of the Green River Formation of Colorado and Utah,” *U.S.G.S Professional Paper* **168**, 56 p.

54. Picard, M.D. 1957a. “Criteria used for distinguishing lacustrine and fluvial sediments in Tertiary beds of Uinta Basin, Utah,” *Journal of Sedimentary Petrology* **27**, 373-377.

55. Picard, M.D. 1957b. “Green shale facies, lower Green River Formation, Utah,” *AAPG Bull.* **41**, 2373-2376.

56. Weiss, M.P., Witkind, I.J., and Cashion, W.B. 1990. “Geologic map of the Price 30'X60' quadrangle, Carbon, Duchesne, Uintah, Utah, and Wasatch Counties, Utah,” U.S. Geological Survey Miscellaneous Investigations Series Map I-1981 1 sheet, 1:100,000.

57. Remy, R.R. 1992. “Stratigraphy of the Eocene part of the Green River Formation in the south-central part of the Uinta Basin, Utah,” *USGS Bull.* **1787-BB**, 79 p.

58. Little, T.M. 1988. “Depositional environments, petrology, and diagenesis of the basal limestone facies, Green River Formation (Eocene), Uinta Basin, Utah” M.S. thesis, University of Utah, Salt Lake City, Utah 154.

59. Weber, K.J and van Geuns, L.C. 1990. “Framework for Constructing Clastic Reservoir Simulation Models,” *JPT* 1248.

60. Adams, S. 2007. “Personal Communication,” Newfield Exploration Company, (January).

61. Wang, J. 2008. “A Demonstration of Integrated Reservoir Characterization and Simulation Studies in Stripper Oil and Gas Fields,” Ph.D. dissertation in progress, Texas A&M University, College Station.

62. Li, W. 2007. “Using percolation techniques to estimate interwell connectivity probability,” M.S. thesis, Texas A&M University, College Station.

APPENDIX A

Net thickness spreadsheet for Wells Draw study area (page 1).

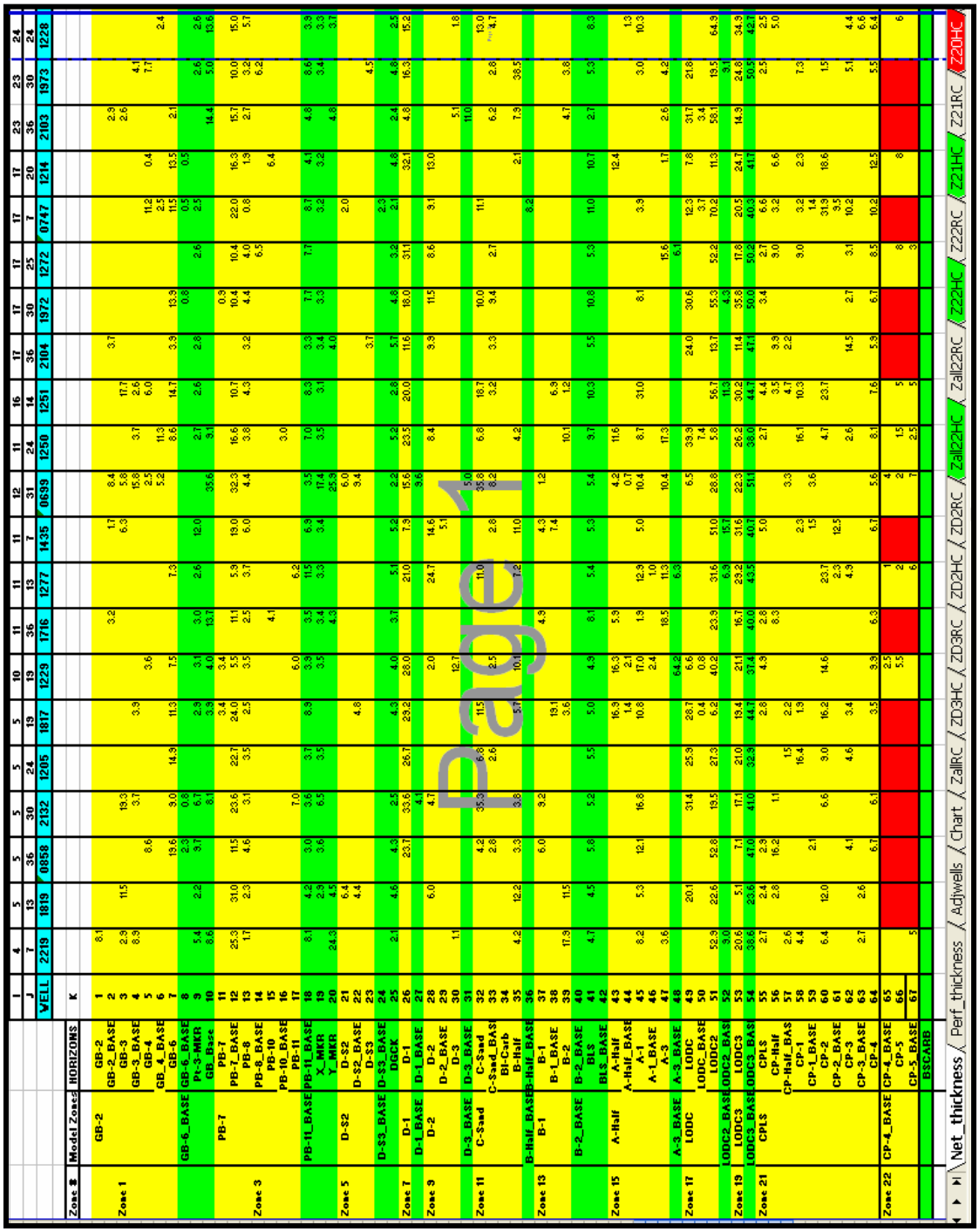

Net thickness spreadsheet for Wells Draw study area (page 2).

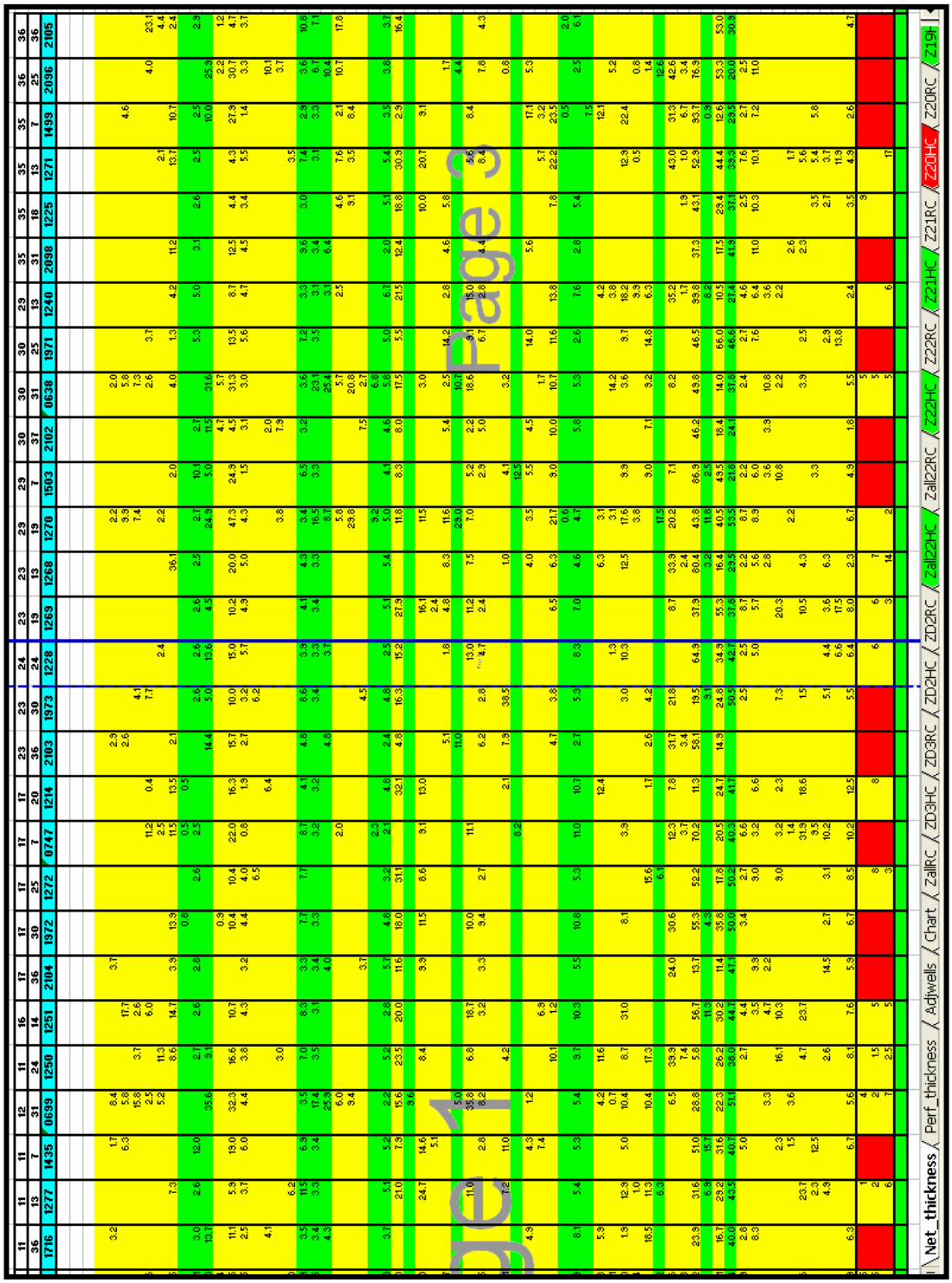

APPENDIX B

Perforated thickness spreadsheet for Wells Draw study area (page 1).

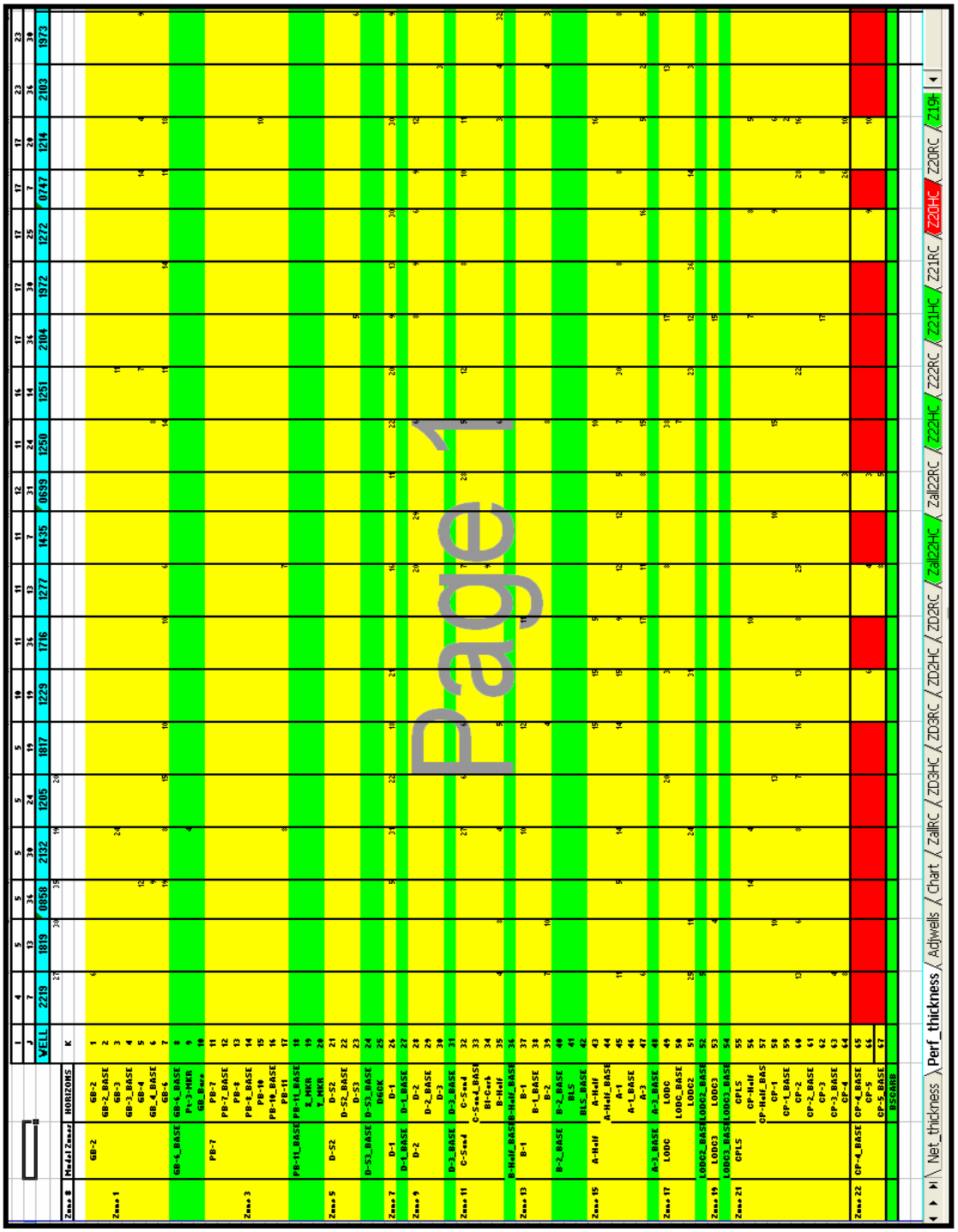

Perforated thickness spreadsheet for Wells Draw study area (page 2).

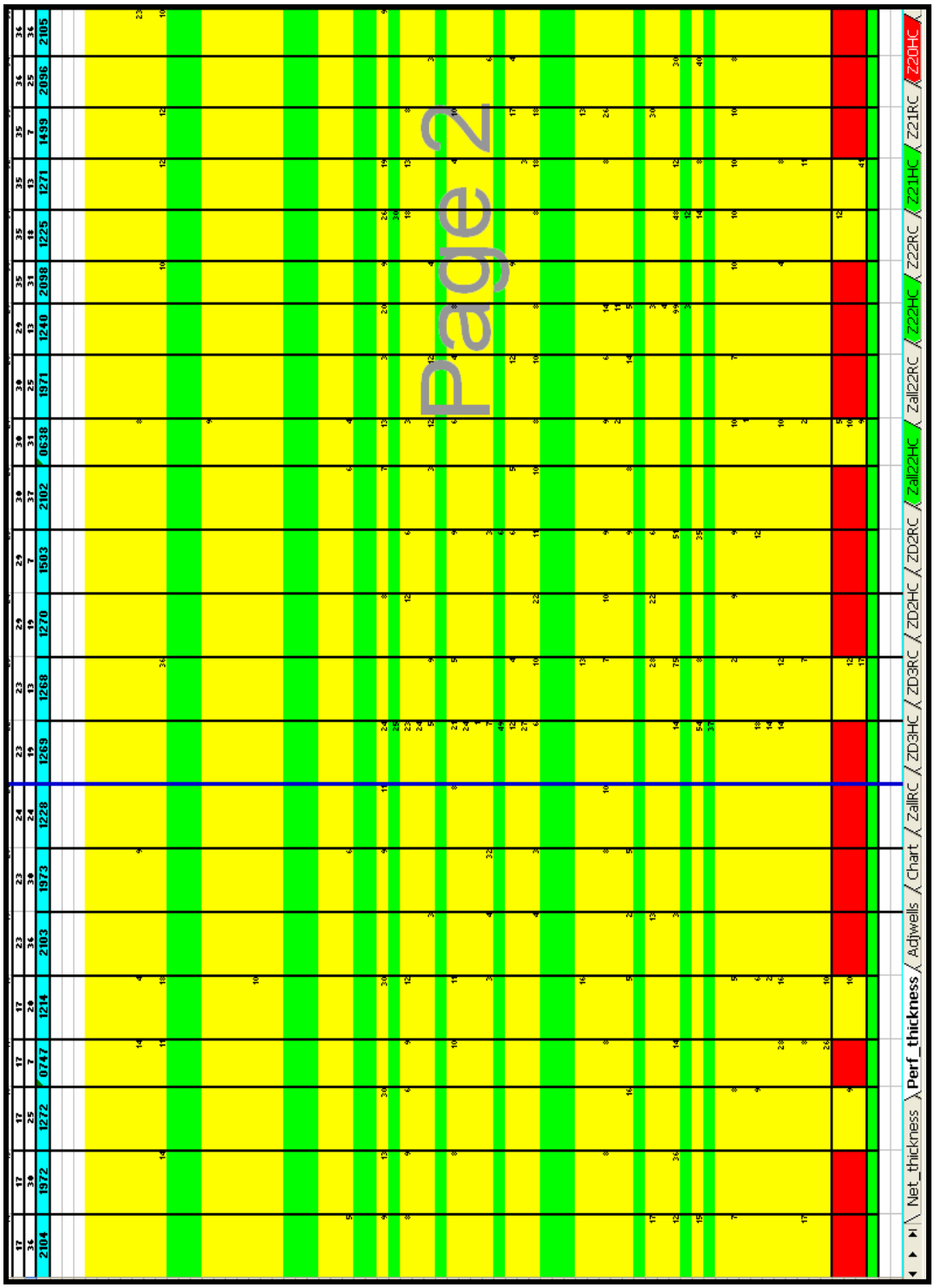

VITA

Joseph Uchechukwu Abiazie completed his Bachelor of Technology degree in Geology at the Federal University of Technology, Owerri, Nigeria, in December 2000. His permanent address is Hess Corporation, 500 Dallas Street, Houston, Texas, 77002, USA.